POST-FIRE STREAM CHANNEL PROCESSES: CHANGES IN RUNOFF RATES, SEDIMENT DELIVERY ACROSS SPATIAL SCALES, AND MITIGATION EFFECTIVENESS

By

JOSEPH WILLIAM WAGENBRENNER

A dissertation submitted in partial fulfillment of
the requirements for the degree of

DOCTOR OF PHILOSOPHY

WASHINGTON STATE UNIVERSITY
Biological and Agricultural Engineering

JULY 2013

To the Faculty of Washington State University:

The members of the Committee appointed to examine the dissertation of JOSEPH WILLIAM WAGENBRENNER find it satisfactory and recommend that it be accepted.

_____
Joan Q. Wu, Ph.D., Chair

_____
Markus Flury, Ph.D.

_____
Ray G. Huffaker, Ph.D.

_____
Claudio O. Stöckle, Ph.D.

_____
Peter Goodwin, Ph.D.

_____
Peter R. Robichaud, Ph.D.

ACKNOWLEDGMENTS

This work was supported in part by a National Needs Fellowship grant from the US Department of Agriculture, National Institute of Foods and Agriculture, under agreement no. 2008-38420-04761. The research projects were funded through the US Department of Agriculture Forest Service, Rocky Mountain Research Station, and part of this funding came from the Apache-Sitgreaves and the Pike-San Isabel National Forests. I greatly appreciate the contribution of each of my doctoral committee members to my education and professional training. I thank Lee MacDonald for discussions on these topics and for providing mentorship throughout my career and graduate programs. Bob Brown, Keenan Storrar, and Sierra Larson contributed to each of the projects and I am especially grateful for their help in the field, lab, and office. I also thank Natalie Wagenbrenner for sharing her love, perseverance, companionship, insights, and critical thoughts throughout our doctoral studies and beyond.

POST-FIRE STREAM CHANNEL PROCESSES: CHANGES IN RUNOFF RATES, SEDIMENT DELIVERY ACROSS SPATIAL SCALES, AND MITIGATION EFFECTIVENESS

ABSTRACT

by Joseph William Wagenbrenner, Ph.D.
Washington State University
July 2013

Chair: Joan Q. Wu

Wildfires dramatically affect hydrologic processes including runoff and erosion, which in turn can impact society. Disturbance by fire creates ecosystem heterogeneity, prompting many species to adapt to fire cycles. Human impacts have altered fire frequency and affected natural systems to the point that additional landscape-scale disturbances may cause a disruption in ecosystem form and function. The altered ecosystems and increased development in forests may exacerbate post-fire impacts, affecting more of the population in fire-prone regions.

The following three studies will improve our understanding and management of post-fire impacts on stream channel processes. A catchment in eastern Arizona where runoff data were collected between 1962 and 1983 was subsequently burned by a wildfire in 2011. The direct comparison of pre and post-fire runoff showed that the fire made runoff more rapid, increased peak discharge rates, and compressed the time scale of storm hydrographs. These results can help improve post-fire runoff modeling and management efforts.

The second topic addressed the scaling of sediment delivery across hillslope and small catchment scales. Erosion data used in this study were from the Arizona site and five other sites across the western US. Results from five of the six sites showed that sediment delivery significantly decreased with increasing spatial extent, while the lack of trend at the sixth site illustrates the variability in erosion responses across ecosystems. The relationships developed in this study will help improve estimates of sediment delivery rates at the small-catchment scale using more easily acquired data from small plots.

The third study addressed whether straw bale check dams reduce post-fire sediment yields or affect ephemeral stream channel morphology. A series of laboratory flume experiments based on measured post-fire field conditions showed that check dams can store sediment from initial runoff events, but that a large number of check dams would be needed to reduce post-fire sediment yields. The stored sediment reduced the local channel gradient, but the check dams did not otherwise affect the channel morphology. These data and field observations were used to develop a check dam classification system that can be applied in ephemeral streams in burned or unburned areas.

TABLE OF CONTENTS

LIST OF TABLES

LIST OF FIGURES

CHAPTER TWO:

CHAPTER THREE:

CHAPTER FOUR:

CHAPTER ONE: INTRODUCTION

Background and need

Wildfires change several parts of the hydrologic cycle, including interception, evapotranspiration, infiltration, and runoff (DeBano et al., 1998; Helvey, 1980; Lane et al., 2006; Mayor et al., 2007; Moody and Martin, 2001; Moody et al., 2008, 2013; Rowe et al., 1954; Shakesby and Doerr, 2006; Shakesby et al., 2003). These changes often result in substantial increases in runoff and erosion rates, which can affect human health and safety, infrastructure, property, and wildlife habitat within and downstream of the burned areas (Calkin et al., 2007; Dunham et al., 2003; Gresswell, 1999; Robichaud et al., 2000). Fires are becoming more frequent (Chmura et al., 2011; Flannigan et al., 2009; Westerling et al., 2006) and development in or near forests in the western US continues to increase (Theobald and Romme, 2007), often without acknowledgment of fire risks (McCaffrey, 2004). As a consequence a larger portion of society in fire-prone areas will be affected by post-fire flooding and sedimentation in the future. Increases in post-fire runoff rates of up to three orders of magnitude greater than unburned rates have been reported at several locations across the western US (Ffolliott et al., 2011; Helvey, 1980; Moody and Martin, 2001). A better understanding of the effects of fire on runoff will improve our predictions and management of post-fire events. Chapter two adds to our understanding of post-fire runoff processes by comparing pre-fire and post-fire runoff rates at the catchment scale.

Post-fire erosion rates often show even greater relative increases when compared to unburned rates and increases up to three or more orders of magnitude have been relatively widespread (Moody and Martin, 2009). Combined, these increases in runoff and erosion increase the sediment delivered to stream channels and downstream resources. While there

has been much work on hillslope erosion rates in burned forests (Benavides-Solorio and MacDonald, 2005; Blake et al., 2009; Larsen et al., 2009; Moody and Martin, 2001, 2009; Moody et al., 2008; Robichaud and Brown, 1999; Robichaud, 2000; Robichaud et al., 2010b; Shakesby, 2011; Sheridan et al., 2007; Smith and Dragovich, 2008; Spigel and Robichaud, 2007) and several studies have addressed sediment delivery at the small catchment scale (Brown, 1972; Desilets et al., 2007; Helvey, 1980; Kunze and Stednick, 2006; Lane et al., 2006; Malmon et al., 2007; Meyer et al., 1992; Moody and Martin, 2001; Noske et al., 2010; Reneau et al., 2007; Rowe et al., 1954; Scott, 1993; Silins et al., 2009; Troendle and Bevenger, 1996), very few studies address post-fire sediment delivery rates across spatial scales (Ferreira et al., 2008). This means there is little information available to apply measured erosion rates at smaller scales, which are relatively easy to obtain and therefore more prevalent, to larger catchments where the main concerns and detrimental impacts occur. Chapter three addresses this gap by relating hillslope erosion rates and catchment scale sediment delivery rates.

Attempts to mitigate post-fire flooding, erosion, and sediment delivery have had varying degrees of success (Robichaud et al., 2010a) and several studies have measured effectiveness of hillslope treatments at reducing erosion (Fernández et al., 2007, 2011; Prats et al., 2012; Robichaud et al., 2008, 2013a, 2013c; Wagenbrenner et al., 2006). Channel treatments are often used to reduce sediment delivery and maintain channel form and function. Straw bale check dams are the most commonly used channel treatment (Napper, 2006), and three studies have revealed somewhat contradictory results (Collins and Johnston, 1995; Fox, 2011; Miles et al., 1989). Chapter four relates the effectiveness of straw bale check dams at reducing sediment yields and maintaining channel morphology.

Social and economic considerations

While fires are natural disturbances, humans have dramatically impacted our ecosystems and have increased the occurrence and extent of wildfires in parts of the western US (Beschta et al., 2004). In some ecosystems, particularly in the American Southwest, fire suppression activities throughout the past century have resulted in forests with more fuels than would have occurred with more frequent fire cycles (Fule et al., 1997; Jensen and McPherson, 2008; Schoennagel et al., 2004; Swetnam and Baisan, 1996). The greater fuel loads in some cases, such as low elevation ponderosa pine forests, causes more severe fire behavior and impacts as measured in the heat release and effects on soils and vegetation (Schoennagel et al., 2004). Climate change will also lead to a greater number and extent of wildfires, especially in regions that are expected to become drier over time (Westerling et al., 2006).

These systemic changes have caused or will cause increases in wildfire impacts (Davis et al., 2013) to stream ecosystems, but humans have also disturbed most forested ecosystems. Development or resource extraction in or near forests has influenced the population dynamics of many species, and the effects on aquatic habitat have received much attention (e.g., Bisson et al., 1992; DeMaynadier and Hunter Jr., 1995). Sedimentation and chemical changes in aquatic resources, damming or diverting free-flowing rivers, and draining of wetlands all caused substantial changes in aquatic and riparian habitat in the western states. Fluvial erosion and sediment transport from disturbed forested catchments can lead to several issues that affect environmental sustainability. Broad categories of potential downstream problems include the destruction of aquatic habitat and sedimentation of lakes and rivers (Benda et al., 2003; Dunham et al., 2003; Reneau et al., 2007). When the past impacts on forested ecosystems and habitat are combined with additional disturbance such as wildfire, the

cumulative impact may be sufficient to eradicate isolated populations of sensitive species (Gresswell, 1999). Public resource managers are therefore compelled to attempt to mitigate post-fire effects, especially with respect to sedimentation, by applying hillslope and channel treatments and thereby enhance the viability of sensitive species (Dunham et al., 2003; Robichaud et al., 2000).

Development in or near forests also increases the risks to human safety and infrastructure (Calkin et al., 2007). Post-fire flooding and debris flows can directly affect human safety, but they can also damage infrastructure such as roads or water supplies that we rely upon, especially during emergencies, causing indirect threats to human safety. This is a major motivation for land and emergency managers to attempt to mitigate post-fire flooding and erosion (USDA Forest Service, 1995).

Society has an obligation to future generations to maintain the form and function of our ecosystems. Because of the legacy impacts on water resources and ecosystem components, some restoration and mitigation of future impacts must occur. Improving our understanding of the physical post-fire effects will lead to better post-fire management, including better techniques to mitigate post-fire effects and target key catchments.

Outline of subsequent chapters

Chapter Two compares pre-fire runoff responses from a 21-year record in eastern Arizona to the runoff responses in the first two years after the 2011 Wallow fire. This chapter has been formatted for future submission to the *Journal of Hydrology*.

Chapter Three relates post-fire sediment delivery rates across spatial scales. This study uses data from six sites: the Wallow fire in Arizona; a site in central Utah where straw

bale check dams are being evaluated as a channel treatment; and previously published data from four sites that were used to test post-fire hillslope mitigation treatments. This chapter has been submitted to *Earth Surface Processes and Landforms* and retains that journal's formatting.

Chapter Four presents a laboratory flume study used to evaluate the effects of straw bale check dams on post-fire channel morphology and sediment yields. This chapter has been submitted to the *Journal of Hydraulic Engineering* and retains that journal's formatting.

Peter Robichaud is a coauthor on each of the three following chapters. He helped design and interpret the experiments, arranged for funding and staff to carry out the experiments, and critically reviewed chapters three and four prior to submission to their respective journals. Peter Goodwin, a coauthor on the paper presented in chapter four, assisted in the interpretation of the results of the flume experiments, developed the initial design for the check dam classification system, and critically reviewed this chapter prior to submission to its journal.

References

Benavides-Solorio JD, MacDonald LH. 2005. Measurement and prediction of post-fire erosion at the hillslope scale, Colorado Front Range. International Journal of Wildland Fire **14**: 457–474. DOI: 10.1071/WF05042

Benda LE, Miller D, Bigelow P, Andras K. 2003. Effects of post-wildfire erosion on channel environments, Boise River, Idaho. Forest Ecology and Management **178** : 105–119.

Beschta RL, Rhodes JJ, Kauffman JB, Gresswell RE, Minshall GW, Karr JR, Perry DA, Hauer FR, Frissell CA. 2004. Postfire management on forested public lands of the western United States. Conservation Biology **18** : 957–967. DOI: 10.1111/j.1523–1739.2004.00495.x

Bisson PA, Quinn TP, Reeves GH, Gregory S V. 1992. Best management practices, cumulative effects, and long-term trends in fish abundance in Pacific Northwest river systems. In Watershed Management , Naiman RJ (ed). Springer: New York; 189–232.

Blake WH, Wallbrink PJ, Wilkinson SN, Humphreys GS, Doerr SH, Shakesby RA, Tomkins KM. 2009. Deriving hillslope sediment budgets in wildfire-affected forests using fallout radionuclide tracers. Geomorphology **104** : 105–116.

Brown JAH. 1972. Hydrologic effects of a bushfire in a catchment in south-eastern New South Wales. Journal of Hydrology **15** : 77–96.

Calkin DE, Hyde KD, Robichaud PR, Jones JG, Ashmun LE, Loeffler D. 2007. Assessing post-fire values-at-risk with a new calculation tool, General Technical Report RMRS-GTR-205 . USDA Forest Service, Rocky Mountain Research Station: Fort Collins, Colorado

Chmura DJ, Anderson PD, Howe GT, Harrington CA, Halofsky JE, Peterson DL, Shaw DC, Brad St.Clair J. 2011. Forest responses to climate change in the northwestern United States: Ecophysiological foundations for adaptive management. Forest Ecology and Management **261** : 1121–1142.

Collins LM, Johnston CE. 1995. Effectiveness of straw bale dams for erosion control in the Oakland Hills following the fire of 1991. In Brushfires in California Wildlands: Ecology and Resource Management , Keeley JE and Scott T (eds). International Association of Wildland Fire: Missoula, MT; 171–183.

Davis JM, Baxter C V., Rosi-Marshall EJ, Pierce JL, Crosby BT. 2013. Anticipating stream ecosystem responses to climate change: Toward predictions that incorporate effects via land–water linkages. Ecosystems : 14 pp. DOI: 10.1007/s10021-013-9653-4

DeBano LF, Neary DG, Ffolliott PF. 1998. Fire's Effects on Ecosystems . Wiley: New York

DeMaynadier PG, Hunter Jr. ML. 1995. The relationship between forest management and amphibian ecology: a review of the North American literature. Environmental Reviews **3**: 230–261. DOI: 10.1139/a95-012

Desilets SLE, Nijssen B, Ekwurzel B, Ferré TPA. 2007. Post-wildfire changes in suspended sediment rating curves: Sabino Canyon, Arizona. Hydrological Processes **21** : 1413–1423. DOI: 10.1002/hyp.6352

Dunham JB, Young MK, Gresswell RE, Rieman BE. 2003. Effects of fire on fish populations: landscape perspectives on persistence of native fishes and nonnative fish invasions. Forest Ecology and Management **178** : 183–196.

Fernández C, Vega JA, Fonturbel T, Pérez-Gorostiaga P, Jiménez E, Madrigal J. 2007. Effects of wildfire, salvage logging and slash treatments on soil degradation. Land Degradation & Development **18** : 591–607. DOI: 10.1002/ldr.797

Fernández C, Vega JA, Jiménez E, Fonturbel T. 2011. Effectiveness of three post-fire treatments at reducing soil erosion in Galicia (NW Spain). International Journal of Wildland Fire **20** : 104–114.

Ferreira AJD, Coelho C de OA, Ritsema CJ, Boulet A-K, Keizer JJ. 2008. Soil and water degradation processes in burned areas: Lessons learned from a nested approach. Catena **74**: 273–285. DOI: 10.1016/j.catena.2008.05.007

Ffolliott PF, Stropki CL, Chen H, Neary DG. 2011. The 2002 Rodeo-Chediski Wildfire's impacts on southwestern ponderosa pine ecosystems, hydrology, and fuels, Research Paper RMRS-RP-85 . U.S. Department of Agriculture, Forest Service, Rocky Mountain Research Station: Fort Collins, Colorado

Flannigan MD, Krawchuk MA, De Groot WJ, Wotton BM, Gowman LM. 2009. Implications of changing climate for global wildland fire. International Journal of Wildland Fire **18** : 483–507. DOI: 10.1071/WF08187

Fox DM. 2011. Evaluation of the efficiency of some sediment trapping methods after a Mediterranean forest fire. Journal of Environmental Management **92** : 258–265.

Fule PZ, Covington WW, Moore MM. 1997. Determining reference conditions for ecosystem management of southwestern ponderosa pine forests. Ecological Applications **7** : 895–908.

Gresswell RE. 1999. Fire and aquatic ecosystems in forested biomes of North America. Transactions of the American Fisheries Society **128** : 193–221.

Helvey JD. 1980. Effects of a north central Washington wildfire on runoff and sediment production. Journal of the American Water Resources Association **16** : 627–634. DOI: 10.1111/j.1752-1688.1980.tb02441.x

Jensen SE, McPherson GR. 2008. Living with Fire . University of California Press: Berkeley, California

Kunze MD, Stednick JD. 2006. Streamflow and suspended sediment yield following the 2000 Bobcat fire, Colorado. Hydrological Processes **20** : 1661–1681. DOI: 10.1002/hyp.5954

Lane PNJ, Sheridan GJ, Noske PJ. 2006. Changes in sediment loads and discharge from small mountain catchments following wildfire in south eastern Australia. Journal of Hydrology **331**: 495–510.

Larsen IJ, MacDonald LH, Brown E, Rough D, Welsh MJ, Pietraszek JH, Libohova Z, Benavides-Solorio JD, Schaffrath K. 2009. Causes of post-fire runoff and erosion; water repellency, cover, or soil sealing? Soil Science Society of America Journal **73** : 1393–1407. DOI: 10.2136/sssaj2007.0432

Malmon D V., Reneau SL, Katzman D, Lavine A, Lyman J. 2007. Suspended sediment transport in an ephemeral stream following wildfire. Journal of Geophysical Research **112**: F02006. DOI: 10.1029/2005jf000459

Mayor ÁG, Bautista S, Llovet J, Bellot J. 2007. Post-fire hydrological and erosional responses of a Mediterranean landscape: Seven years of catchment-scale dynamics. Catena **71** : 68–75.

McCaffrey S. 2004. Thinking of wildfire as a natural hazard. Society & Natural Resources **17**: 509–516. DOI: 10.1080/08941920490452445

Meyer GA, Wells SG, Balling Jr. RC, Jull AJT. 1992. Response of alluvial systems to fire and climate change in Yellowstone National Park. Nature **357** : 147–150.

Miles SR, Haskins DM, Ranken DQ. 1989. Emergency burn rehabilitation: cost, risk, and effectiveness. 97–102 pp.

Moody JA, Martin DA. 2001. Initial hydrologic and geomorphic response following a wildfire in the Colorado Front Range. Earth Surface Processes and Landforms **26** : 1049–1070. DOI: 10.1002/esp.253

Moody JA, Martin DA. 2009. Synthesis of sediment yields after wildland fire in different rainfall regimes in the western United States. International Journal of Wildland Fire **18** : 96–115. DOI: 10.1071/WF07162

Moody JA, Martin DA, Cannon SH. 2008. Post-wildfire erosion response in two geologic terrains in the western USA. Geomorphology **95** : 103–118.

Moody JA, Shakesby RA, Robichaud PR, Cannon SH, Martin DA. 2013. Current research issues related to post-wildfire runoff and erosion processes. Earth-Science Reviews **122** : 10–37. DOI: 10.1016/j.earscirev.2013.03.004

Napper C. 2006. Burned area emergency response treatments catalog . US Department of Agriculture, Forest Service, National Technology & Development Program: Washington, D.C.

Noske PJ, Lane PNJ, Sheridan GJ. 2010. Stream exports of coarse matter and phosphorus following wildfire in NE Victoria, Australia. Hydrological Processes **24** : 1514–1529. DOI: 10.1002/hyp.7616

Prats SA., MacDonald LH, Monteiro M, Ferreira AJD, Coelho COA., Keizer JJ. 2012. Effectiveness of forest residue mulching in reducing post-fire runoff and erosion in a pine and a eucalypt plantation in north-central Portugal. Geoderma DOI: 10.1016/j.geoderma.2012.02.009

Reneau SL, Katzman D, Kuyumjian GA, Lavine A, Malmon DV. 2007. Sediment delivery after a wildfire. Geology **35** : 151–154. DOI: 10.1130/g23288a.1

Robichaud PR. 2000. Fire effects on infiltration rates after prescribed fire in Northern Rocky Mountain forests, USA. Journal of Hydrology **231–232** : 220–229.

Robichaud PR, Ashmun LE, Sims BD. 2010a. Post-fire treatment effectiveness for hillslope stabilization, General Technical Report RMRS-GTR-240 . US Department of Agriculture, Forest Service, Rocky Mountain Research Station: Fort Collins, Colorado

Robichaud PR, Beyers JL, Neary DG. 2000. Evaluating the effectiveness of postfire rehabilitation treatments, General Technical Report RMRS–63 . USDA Forest Service, Rocky Mountain Research Station: Fort Collins, Colorado

Robichaud PR, Brown RE. 1999. What happened after the smoke cleared: Onsite erosion rates after a wildfire in eastern Oregon. 419–426 pp.

Robichaud PR, Lewis SA, Wagenbrenner JW, Ashmun LE, Brown RE. 2013a. Post-fire mulching for runoff and erosion mitigation Part I: Effectiveness at reducing hillslope erosion rates. Catena **105** : 75–92. DOI: 10.1016/j.catena.2012.11.015

Robichaud PR, Wagenbrenner JW, Brown RE. 2010b. Rill erosion in natural and disturbed forests: 1. Measurements. Water Resources Research **46** : W10506. DOI: 10.1029/2009wr008314

Robichaud PR, Wagenbrenner JW, Brown RE, Wohlgemuth PM, Beyers JL. 2008. Evaluating the effectiveness of contour-felled log erosion barriers as a post-fire runoff and erosion mitigation treatment in the western United States. International Journal of Wildland Fire **17**: 255–273. DOI: 10.1071/Wf07032

Robichaud PR, Wagenbrenner JW, Lewis SL, Brown RE, Wohlgemuth PM, Ashmun LE. 2013b. Post-fire mulching for runoff and erosion mitigation Part II: Effectiveness in reducing

runoff and sediment yields from small catchments. Catena **105** : 93–111. DOI: 10.1016/j.catena.2012.11.016

Rowe PB, Countryman CM, Storey HC. 1954. Hydrologic analysis used to determine effects of fire on peak discharges and erosion rates in southern California watersheds. USDA Forest Service, California Forest and Range Experiment Station: Berkeley, California

Schoennagel T, Veblen TT, Romme WH. 2004. The interaction of fire, fuels, and climate across Rocky Mountain forests. BioScience **54** : 661–667. DOI: 10.1641/0006-3568(2004)054[0661:TIOFFA]2.0.CO;2

Scott DF. 1993. The hydrological effects of fire in South African mountain catchments. Journal of Hydrology **150** : 409–432.

Shakesby RA. 2011. Post-wildfire soil erosion in the Mediterranean: Review and future research directions. Earth-Science Reviews **105** : 71–100.

Shakesby RA, Chafer CJ, Doerr SH, Blake WH, Wallbrink P, Humphreys GS, Harrington BA. 2003. Fire severity, water repellency characteristics and hydrogeomorphological changes following the Christmas 2001 Sydney forest fires. Australian Geographer **34** : 147–175. DOI: 10.1080/0004918032000108446

Shakesby RA, Doerr SH. 2006. Wildfire as a hydrological and geomorphological agent. Earth-Science Reviews **74** : 269–307.

Sheridan GJ, Lane PNJ, Noske PJ. 2007. Quantification of hillslope runoff and erosion processes before and after wildfire in a wet Eucalyptus forest. Journal of Hydrology **343**: 12–28.

Silins U, Stone M, Emelko MB, Bladon KD. 2009. Sediment production following severe wildfire and post-fire salvage logging in the Rocky Mountain headwaters of the Oldman River Basin, Alberta. Catena **79** : 189–197.

Smith HG, Dragovich D. 2008. Post-fire hillslope erosion response in a sub-alpine environment, south-eastern Australia. Catena **73** : 274–285. DOI: 10.1016/j.catena.2007.11.003

Spigel KM, Robichaud PR. 2007. First-year post-fire erosion rates in Bitterroot National Forest, Montana. Hydrological Processes **21** : 998–1005. DOI: 10.1002/Hyp.6295

Swetnam TW, Baisan CH. 1996. Historical fire regime patterns in the Southwestern United States since AD 1700. 11–32 pp.

Theobald DM, Romme WH. 2007. Expansion of the US wildland–urban interface. Landscape and Urban Planning **83** : 340–354.

Troendle CA, Bevenger GS. 1996. Effect of fire on streamflow and sediment transport in Shoshone National Forest, Wyoming. In The ecological implications of fire in greater Yellowstone , Greenlee JM (ed). International Association of Wildland Fire: Fairfield, Washington; 43–52.

USDA Forest Service. 1995. Forest Service Handbook 2509-13: burned-area emergency rehabilitation handbook . USDA Forest Service: Washington, D.C.

Wagenbrenner JW, MacDonald LH, Rough D. 2006. Effectiveness of three post-fire rehabilitation treatments in the Colorado Front Range. Hydrological Processes **20** : 2989–3006. DOI: 10.1002/Hyp.6146

Westerling AL, Hidalgo HG, Cayan DR, Swetnam TW. 2006. Warming and earlier spring increases western U.S. forest wildfire activity. Science **313** : 1–9. DOI: 10.1126/science.1128834

CHAPTER TWO: CHANGES IN RUNOFF FOLLOWING WILDFIRE IN AN EASTERN ARIZONA FORESTED CATCHMENT

Joseph W. Wagenbrenner [a,b*], Peter R. Robichaud [b]

[a] Department of Biological Systems Engineering, Washington State University, Pullman, Washington, 99164-6120, USA

[b] USDA Forest Service, Rocky Mountain Research Station, Moscow, Idaho, 83843, USA

*Correspondence: USDA Forest Service, Rocky Mountain Research Station, 1221 S. Main St., Moscow, Idaho, 83843, USA, jwagenbrenner@fs.fed.us, +1 208 883 2353

Abstract

The Wallow Fire burned over 217,000 ha in eastern Arizona in 2011, including a 117 ha catchment that had been used for water yield experiments between 1962 and 1983. We re-instrumented the catchment and compared the pre-fire and post-fire precipitation and runoff to assess changes in flow frequency, magnitude, timing, and hydrograph shape. The annual maximum instantaneous peak flow rates during the 21-year pre-fire record ranged from 0.0018 to 0.466 $m^3 s^{-1}$ and the annual hydrograph was dominated by snow melt. There was no change in runoff relative to the winter precipitation in either of the two post-fire melt periods. Thirty one rainfall-initiated storm flows were measured in 2011–2012, and 9 of these exceeded the pre-fire peak discharge rate by as much as 3.1 times. Each of the post-fire summer flows was caused by relatively ordinary rainfall events, as all of the storms' maximum 30-min rainfall intensities (4–26 mm hr^{-1}) were much less than the 2-yr return period intensity (45 mm hr^{-1}). Because of the shift from snow melt dominated hydrograph to

a bimodal hydrograph, the mean timing of the annual 24-hr peak discharge rate shifted from 8 June during the pre-fire period to 14 August after the fire. The post-fire storm flows had similar total runoff volumes as the pre-fire events, but because of the shorter storm durations, the mean slope of the hydrographs' rising and falling limbs increased by at least two orders of magnitude. Based on the time to peak and the peak discharge rates, the post-fire runoff was dominated by infiltration excess overland flow. Changes in the hydrographs for the summer storm flows were quantified and orders-of-magnitude increases in both the rising limb and receding limb slopes occurred after the fire. These results can be used to improve predictions of post-fire runoff using triangular unit hydrographs and other modeling approaches. The shift in timing as well as the dramatic increases in the magnitude of the peak flows may have implications for riparian or aquatic habitat, as shown through changes in several indicators of hydrologic alteration.

Keywords: post-fire, unit hydrograph, storm flow, peak discharge, hydrologic alteration, baseflow, watershed

Introduction

Background

Wildfires can have dramatic effects on forested landscapes. Burning of vegetation can greatly reduce interception and transpiration rates, resulting in large quantities of water available for runoff (Rowe et al., 1954; Helvey, 1980; Moody and Martin, 2001a; Lane et al., 2006; Shakesby and Doerr, 2006; Mayor et al., 2007; Moody et al., 2008, 2013). Removal of

the vegetative canopy and litter and duff layers, characterized by the degree of vegetation or soil burn severity (Keeley, 2009; Parsons et al., 2010), can enhance the soil sealing effect caused by raindrop splash (Benavides-Solorio and MacDonald, 2001; Johansen et al., 2001; Llovet et al., 2008; Larsen et al., 2009). High soil temperatures caused by wildfires can affect the soil structure (Giovannini and Lucchesi, 1997; Badía and Martí, 2003; Certini, 2005) and soil water repellency (DeBano, 2000; Robichaud, 2000; Huffman et al., 2001; Doerr et al., 2006), resulting in lower infiltration capacities and greater proportion of runoff by overland flow (Moody and Ebel, 2013). The residual ash layer can absorb rainfall, resulting in lower post-fire runoff rates (Cerdà and Doerr, 2008; Gabet and Sternberg, 2008; Woods and Balfour, 2008, 2010; Zavala et al., 2009; Bodí et al., 2012), but the ash is quickly removed by wind or rain events so this effect rapidly disappears. Burning can also reduce the hydraulic roughness of forested hillslopes and floodplains, resulting in greater hillslope (Robichaud et al., 2010) and channel runoff velocities. These effects combine to produce the capacity for much greater total runoff and peak discharge rates in burned areas as compared to unburned forests (Robichaud et al., 2013).

Most of the post-fire hydrologic catchment-scale research to date has been conducted using a reference reach design, where the responses in a burned catchment were compared to a nearby unburned catchment (e.g., Mayor et al., 2007; Owens et al., 2013). While this experimental design is very informative, this approach often leaves questions about the effects of unmeasured hydrologic differences on the responses in the study and reference reaches. A few studies from diverse fire-affected regions have reported both pre-fire and post-fire hydrologic data from the same catchment (Hoyt and Troxell, 1934; Rich, 1962; Brown, 1972; Anderson et al., 1976; Langford, 1976; Helvey, 1980; Scott and Van Wyk, 1990; Lavabre et

al., 1993; Veenhuis, 2002; Lane et al., 2006; Ffolliott et al., 2011; Chen et al., 2013), and these results have the benefit of the before/after fire analysis in the same catchment.

Two of the before/after studies occurred in Arizona, near where the current study was conducted (Rich, 1962; Ffolliott et al., 2011). An experimental catchment in central Arizona was partly burned in 1957 after partial harvest in 1953 (Rich, 1962). Despite the potential cumulative effect of the harvest operation, the study measured post-fire peak discharge rates that were 5 to 15 times greater than the expected value based on pre-fire calibration with an unburned control catchment. Two 24 ha catchments were instrumented from 1972–1977 and then re-instrumented after the 2002 Rodeo-Chediski fire in eastern Arizona (Ffolliott et al., 2011). One of the catchments was severely burned, and high intensity rainfall events produced peak discharge rates in this catchment of up to 2200 times the pre-fire values.

Advance knowledge of the timing and magnitude of the post-fire peak discharge rates can be vital in protecting human life and property from flooding (USDA Forest Service, 1995; Robichaud et al., 2000; Moody and Martin, 2001b). Accurately predictions of the hydrologic effects of wildfires make the efforts to mitigate post-fire effects more effective, as the most at-risk areas can be addressed. Targeted mitigation efforts may also be more economically efficient, resulting in cost savings to landowners and/or taxpayers. Because of these benefits, improving the ability to predict the magnitude and timing of post-fire peak discharge rates currently has much focus (Moody et al., 2013).

While the potential emergency of post-fire flooding is usually the highest concern, the changes in runoff rates after fires can also cause impacts to wildlife and their habitat. Biota in wildfire-prone ecosystems have adapted to the effects of fires (e.g., Dunham et al., 2003), but in some cases local populations have been reduced and additional disturbances such as from

post-fire flooding may lead to permanent loss of aquatic or terrestrial species that depend on riverine ecosystems. Changes in the magnitude or timing of peak flows can directly affect aquatic species and habitat as well as the adjacent floodplains and riparian habitat. In cases where the risk of greatly magnified post-fire floods may affect critical habitat for sensitive species, understanding the potential magnitude, frequency, and timing of the post-fire floods can help wildlife managers mitigate potential impacts to the species at risk.

Chen et al. (2013) used pre and post-fire data from the San Dimas Experimental Watersheds to evaluate two empirical and two physically-based hydrologic models (Hydrologic Engineering Center-Hydrologic Modeling System [HEC-HMS] (US Army Corps of Engineers, 2000) and KINematic Runoff and EROSion Model 2 [KINEROS2] (Smith et al., 1995)). They identified a fire-induced shift in runoff mechanism from subsurface or saturation excess overland flow to infiltration excess overland flow. They also concluded that the empirical models were no less accurate in predicting peak discharge rates than the physically-based models, but the physically based models provided insight into the shift in runoff mechanism and therefore had the greater potential for accurate post-fire predictions of peak discharge rates.

Unit hydrographs in various forms have been used to predict peak storm flow rates in catchments with little or no measured data and in hydrologic models, and triangular unit hydrographs are the oldest form (Ramírez, 2000). Triangular unit hydrographs are constructed for a specific rainfall duration that produces a unit of area-specific runoff (e.g., 1 mm), which forms the base of the triangle. The apex of the triangle is the peak discharge rate, and the two other legs are calculated from the lag time between the peak rainfall intensity and the peak discharge rate (lag time to peak), and the difference between the rainfall duration and

the lag time to peak (Dunne and Leopold, 1978). Once constructed the unit hydrographs can be scaled to estimate the hydrograph for a given storm with the same rainfall duration by multiplying each discharge rate by the ratio of the storm area-specific runoff to the unit area-specific runoff. Given the changes in runoff processes resulting from fire, unit hydrographs developed for an unburned catchment would need to be modified to be useful in predicting the shape of the hydrograph in the burned system.

Detecting changes in the hydrologic responses resulting from forest management often requires many years of record before and after the disturbance because of the relatively small magnitude of the changes and the high inter-annual variability in precipitation (Stednick, 1996; Brown et al., 2005). Because of the large post-fire responses, the detection of change often requires a smaller sample. Also, the hydrologic response within the first year or two of a fire can be much greater than later post-fire responses (Robichaud et al., 2013), so the initial responses are usually of greatest concern and statistically comprise a separate population of inference.

Objectives

The goal of this study was to determine the changes in magnitude, frequency, and timing of the catchment responses to snow melt and rainfall following wildfire. We compared the responses of W. Willow Creek in the first two years after the Wallow fire to a 21-year pre-fire record. Specific objectives included: 1) quantify the changes in peak discharge rates caused by the fire; 2) determine if the fire caused changes in the catchment response to rainfall or snow melt; 3) determine if the fire changed the frequency or duration of flood

flows; 4) identify differences in the shape and timing of the pre-fire and post-fire rainfall-driven catchment responses; and 5) relate the measured changes to possible impacts on riparian or aquatic habitat.

Methods

The 2011 Wallow fire burned over several small catchments in eastern Arizona that were used in previous water yield studies (Baker, 1999). W. Willow Creek was instrumented in 1962 and records were maintained through the end of water year (October–September) 1983 (Gottfried et al., 1999). The catchment was re-instrumented in July 2011, a few weeks after it was burned by the Wallow fire.

Site description and pre-fire record

The W. Willow Creek drains an area of 117 ha in the White Mountains of Arizona is part of the Black River drainage. Elevations in the catchment are between 2682 m and 2835 m (Heede, 1985). This catchment served as the control to the treatments in East Willow Creek during a study on post-harvest water yield (Gottfried et al., 1999). It was also used as the treated catchment in a study from 1978 to 1983 to evaluate the effects of the removal of logs on channel bar formation (Heede, 1985). A native-surface road was installed prior to 1962 (Figure 1) and this has been maintained for access by researchers and recreationists. No timber harvest or fires occurred in the catchment during recent history (Dieterich, 1983; Heede, 1985).

Rainfall in the pre-fire period was measured using a weighing bucket rain gage with periodic corrections based on a standard rain gage. Daily rainfall data were available for water years 1963–1981 but only monthly rainfall records were available for water years 1982–1983. Annual precipitation during the pre-fire period averaged 776 mm and ranged from 542 to 1127 mm. About half of this precipitation occurred as snow (Heede, 1987) and most of the remaining precipitation was produced during the North American monsoon from July through September (Heede, 1987; Douglas et al., 1993). The soil was derived from volcanic parent material and its texture was a stony silty clay loam (Gottfried et al., 2003). The pre-fire mixed-conifer forest was mainly composed of quaking aspen (*Populus tremuloides)*, Engelmann spruce (*Picea engelmannii)*, Douglas-fir (*Pseudotsuga menziesii)*, corkbark fir (*Abies lasiocarpa)*, and white fir (*Abies concolor)* (Rich and Thompson, 1974).

A 120° v-notch sharp-crested weir and two upstream stilling basins were installed in 1962. The stage in the weir (h, m) was continuously recorded and converted to discharge rate (Q, $m^3\ s^{-1}$) using the rating equation

$$Q = 2.33h^{2.5} \quad (1)$$

(Grant, 1989).

Annual summaries of the daily runoff and rainfall data were digitized in the 1970–80s. Printouts of the digitized data were retrieved from archives at the USDA Forest Service Forestry Sciences Laboratory in Flagstaff, Arizona. Pages were scanned, converted to spreadsheets, and manually verified. Summaries included daily discharge rates for each water year as well as the three largest instantaneous discharge rates for winter (October through May) and summer (June through September) periods. A large number of rain events occurred

in October, so the runoff events were re-categorized as either summer (June through October) or winter (November through May) (Heede, 1987).

The three largest instantaneous summer discharge rates from each water year were selected as a partial duration series for hydrograph analysis. Some of these peaks occurred in consecutive days and were part of the same storm flow. Several of the early June events were caused by snow melt, and the hydrographs for these events were not analyzed. This resulted in a set of 37 pre-fire summer events, including at least one stormflow from each water year except for 1978 and 1979.

Post-fire measurements

The Wallow fire burned through the study catchment in early June 2011, resulting in about 50% high burn severity, 25% low-moderate burn severity, and 25% unburned (USDA Forest Service, 2011) (Figure 1). The burn severity was manually assessed along two transects in and near the study catchment (Parsons et al., 2010) and this indicated the classifications provided accurate representations of the differences in soil burn severity. Soil water repellency was tested as part of the verification (DeBano, 1981), and strong soil water repellency was found in burned areas with low soil moisture.

In July 2011 rain gages were installed and the weir and stilling ponds were re-furbished and re-instrumented to measure runoff. Four tipping-bucket rain gages were installed in the catchment: one at the outlet and three in the uplands (Figure 1). One of the upland rain gages was used to characterize the rainfall except during the winter months (Nov–May) when the nearby Hannagan Meadows Snow Telemetry site (USDA Natural Resources

Conservation Service, 2013) was used or during a brief period (28 Aug–31 Oct 2012) when the gage was unavailable and the gage at the outlet was used. The maximum 30-min rainfall intensity (I_{30}) was calculated for each rain event and rain gage and the median I_{30} of all available gages was used to characterize individual storms that produced runoff. The stage in the weir was measured with an ultrasonic depth sensor and recorded using a solar-recharged data logger. The stage was converted to discharge rate using Eq. 1. Thirty one rainfall-driven storm flows were measured in 2011–2012 along with the snowmelt runoff in spring 2012 and spring 2013.

The ultrasonic depth sensor used to measure the depth of flow in the weir in the post-fire period does not distinguish between water and snow. Also, the ultrasonic signal can reflect off of heavy precipitation, especially snowfall, which can cause erroneous readings. The post-fire winter data were adjusted to account for this by eliminating apparently erroneous depths that occurred during periods of snowfall and by reducing the measured depth during periods when snow may have accumulated on the surface of the (frozen) stilling pond. The runoff data during the snow accumulation period are therefore less reliable than the data from the melt period or the summer data, and the data during the accumulation period is presented only as a matter of completeness.

Analysis

Seasonal (June to October or November to May) precipitation and runoff were summed by water year and used to compare changes in snowmelt driven and rainfall driven runoff events. Antecedent rainfall indices were calculated for summer days in both records

and these were the sum of the current day's rainfall and the cumulative rainfall from 1 to 30 days prior. The strengths of the relationships between the precipitation characteristics (daily rainfall, seasonal precipitation, antecedent precipitation, and for the post-fire period, 30-min maximum rainfall intensity) and the seasonal, daily or peak discharge rates were evaluated using linear or exponential least-squares regressions. Flow duration curves (Searcy, 1959; Vogel and Fennessey, 1994) were constructed from the pre-fire and post-fire record and for the summer periods for each record.

Baseflow separation for each of the summer storm flows was conducted following methods of Blume et al. (2007) (Figure 2). Briefly, the normalized slope of the hydrograph (k^*, min^{-1}) was calculated at each discharge measurement by dividing the slope at that point by the sum of the average discharge rate at that point plus the mean annual pre-fire discharge rate (0.00549 $m^3 s^{-1}$). The change in k^* with respect to time was calculated at each measurement point and the commencement of baseflow was identified when the change in k^* with respect to time fell below $10^{-7} min^{-2}$ (Blume et al., 2007). This method did not work for two post-fire events with relatively low receding limb slopes (4 and 12 September 2012). For these events the commencement of baseflow was identified as the first measurement point that produced a change in k* with respect to time below $10^{-7} min^{-2}$ after a distinct decrease in discharge rate occurred.

Several hydrograph metrics were calculated for each distinct stormflow (Figure 2), including: peak discharge rate ($m^3 s^{-1}$); total storm runoff (m^3); 24-hr rainfall on the day of the peak (mm); runoff ratio, which was the total storm runoff divided by 24-hr rainfall (mm mm^{-1}); the time to peak (min); the total duration (min); and the mean slope of the rising and receding limbs ($m^3 s^{-2}$). Differences in the hydrograph metrics were tested using t-tests. All

hydrograph metrics were log-transformed prior to statistical analysis because they were approximately log-normally distributed. A significance level of 0.05 was used for all statistical analyses.

Simplified triangular unit hydrographs were constructed following Dunne and Leopold (1978) with the adaptations that the time to peak was the time from the start of storm flow to the time of the peak discharge rate and the storm flow duration was the duration of the unit hydrograph . The mean time to peak, storm duration, and peak flow from each period was used to determine the rising and receding limb slopes. The ordinates of the triangular unit hydrographs were scaled so the storm runoff (the area under the curve) equaled 1 mm.

Indicators of hydrologic alteration (IHA) (Richter et al., 1996) were calculated from the pre-fire and post-fire records to determine if changes in the magnitude, frequency, or timing of 24-hr discharge rates occurred because of the fire. The effects of the fire on the magnitude of runoff were quantified by calculating monthly runoff for April–October. The changes in the magnitude and frequency of the extreme events were quantified by comparing the minimum and maximum 24-hr discharge rates, the minimum and maximum 7-day discharge rates, and the number of days with discharge rates below the 1st quartile or above the 3rd quartile pre-fire rates. The change in timing of the annual extremes was assessed by differences in the date of the minimum and maximum 24-hr discharge rate.

Results

Summary of hydrologic conditions

Annual pre-fire runoff averaged 148 mm and ranged from 8 to 479 mm for the 21 year record. The maximum pre-fire instantaneous (0.466 $m^3 s^{-1}$) and 24-hr discharge rate (20.7 mm d^{-1} or an average of 0.280 $m^3 s^{-1}$) (Figure 3) occurred in October 1972 as a result of a 24-hr period of high intensity thunderstorms that passed over the catchment within two weeks after a Pacific tropical storm (Desert Research Institute, 2013). These thunderstorms produced 100 mm of rainfall in 24 hours and a maximum intensity of 29 mm hr^{-1} (Rich and Thompson, 1974). The return period of this event was estimated as several hundred years (Heede, 1977). In the remaining years of the pre-fire record, 17 of the 20 instantaneous peak flows occurred from rainfall, but 18 of the 20 maximum 24-hr flows were from snow melt (Figure 3). The largest snow melt discharge rate (16.5 mm d^{-1}) occurred on 13 May 1973 (Figure 3). One large runoff event in December 1978 (Figure 3) was caused by rain-on-snow (Aldridge and Hales, 1984).

In summer 2011, 23 rain events produced distinct storm flow events and another 8 events occurred in summer 2012 (Figure 3). Seven of the 23 events in 2011 and 2 of the 8 events in 2012 had peak discharge rates that exceeded the pre-fire maximum discharge rate. The largest of these events produced an instantaneous peak discharge rate of 1.45 $m^3 s^{-1}$ on 2 August 2011, and this was 3.1 times the pre-fire peak discharge rate (Figure 4). All of these events were caused by convective rainstorms, and the 30-min maximum rainfall intensity (I_{30}) was the best predictor of the peak discharge rate (Figure 5). The I_{30} explained about 70% of the variability in the peak discharge rate in both 2011 and 2012, but the mean I_{30} threshold

increased from about 4 mm hr^{-1} to about 7.5 mm hr^{-1} and the slope of the peak discharge response decreased between the two years (Figure 5). The smaller number of storm events and the change in the peak discharge rate relative to rainfall intensity suggests that some hydrologic recovery occurred during the study. All of the post-fire rainfall events had smaller I_{30} values than the 2-yr return period I_{30} at this location (45 mm hr^{-1}) (Bonnin et al., 2004).

The precipitation in the winter of 2011–2012 was 282 mm, and this was less than mean value for the pre-fire record (380 mm). The peak 24-hr snow melt discharge rate for this winter was 2.1 mm d^{-1} and occurred on 27 March 2012 (Figure 3). The winter of 2012-2013 produced close to the pre-fire mean precipitation, totaling 373 mm through 24 April 2013, and this produced a peak 24-hr snow melt discharge rate of 4.6 mm d^{-1} on 22 March 2013 (Figure 3).

Before the fire occurred, approximately 80% of the runoff occurred as a result of snow melt (Gottfried, 1991), and the winter precipitation was a good predictor of the winter runoff ($R^2 = 0.82$) (Figure 6). The two post-fire winter runoff values fell within the confidence intervals for the pre-fire period, suggesting the quantity of winter runoff was not affected by the fire.

The pre-fire summer precipitation did not explain as much variation in the summer runoff ($R^2 = 0.45$) and some of the lack of fit was caused by relatively late snow melt periods (Figure 7). Neither of the post-fire summer runoff points fell within the confidence limits for the linear regression line, and both runoff values were greater than would likely have occurred during the pre-fire period given the relatively low summer precipitation (Figure 7).

The daily precipitation was not an accurate predictor of the daily discharge rate for the summer period (Figure 8), and neither the pre-fire nor post-fire R^2 values exceeded 0.16.

However the daily discharge rate in the post-fire period was between 5 and 60 times greater than the pre-fire value for the same daily precipitation (Figure 8). The antecedent rainfall was evaluated as a predictor for discharge rate to determine if soil moisture or lag time affected the discharge rate. The 20-day antecedent precipitation was the best predictor of daily discharge rate for both the pre-fire and post-fire summer periods (Figure 9).

Flow frequency

Flow duration curves for the pre-fire and post-fire periods show a post-fire increase in the daily discharge rates with probabilities of occurrence between 20 and 97% (Figure 10). The low-probability (<2% exceedance) post-fire daily discharge rates were slightly lower than the pre-fire values. The median daily discharge was 0.037 mm d^{-1} before the fire and this increased to 0.32 mm d^{-1} after the fire.

The summer flow duration curves show a post-fire increase in daily discharge rate across all but the most frequent flow rates (Figure 11). The change in the low-probability discharge rates was slightly less than the discharge rates associated with the higher probabilities. The median pre-fire summer daily discharge rate was 0.029 mm d^{-1}, while the post-fire value increased to 0.19 mm d^{-1}. Assuming the differences between the whole-record and summer flow duration curves in Figures 10 and 11 are valid considering our measurement method, the winter runoff was less affected by the fire than the summer runoff.

Summer storm characteristics

The 24-hr precipitation associated with the pre-fire storms averaged 27 mm d^{-1} and this was greater than the 8.8 mm d^{-1} in the post-fire period (Figure 12). The cause of this difference is not apparent, but the selection of pre-fire storms from the three largest discharge rates probably biased these events toward larger precipitation values. Despite the greater mean daily rainfall in the pre-fire events, there was no difference in the mean storm runoff (Figure 12), which averaged 2360 m^3 in the pre-fire storms and 660 m^3 in the post-fire storms. Similarly there was no difference in the runoff ratios between the two periods (Figure 12).

In contrast, there was a significant difference in the peak discharge rates between the pre-fire and post-fire periods (Figure 12), and the mean peak discharge rate in the post-fire period (0.41 m^3 s^{-1}) was sixteen times greater than the value in the pre-fire period (0.025 m^3 s^{-1}). As there was no difference in the total storm runoff between the two periods, it follows that the greater peak discharge rates in the post-fire period occurred over shorter-duration storms. The pre-fire time to peak (1121 min) and storm duration (3425 min) both decreased significantly (Figure 12), resulting in post-fire values of 26 min and 158 min, respectively. The significant increase in peak flows and decrease in durations mean that the rising and falling limbs of the post-fire storm hydrographs were much steeper the those before the fire (Figure 12). The mean pre-fire rising limb slope was 2.3 x 10^{-6} m^3 s^{-2} and this increased by more than two orders of magnitude to 3.9 x 10^{-4} m^3 s^{-2}. The slope of the receding limb averaged -1.5 x 10^{-7} m^3 s^{-2} before the fire and this changed to -6.6 x 10^{-5} m^3 s^{-2} after the fire. Metrics for each of the analyzed storms are shown in Appendix 2.1 (pre-fire) and 2.2 (post-fire).

We used the mean values of the pre and post-fire hydrograph metrics to construct a triangular unit hydrograph for each period (Figure 13). The steeper slopes of the rising and receding limbs are objective measures of how "flashy" the post-fire flows were relative to the pre-fire condition.

Indicators of hydrologic alteration (IHA)

In addition to the hydrograph metrics relating the change in flashiness of the summer storm flows, several of the IHA suggest the fire substantially altered the hydrologic regime. The post-fire April–June monthly mean runoff values were 63–94% lower than the pre-fire values (Table 1). This indicates the snow melt period in the pre-fire record occurred later than in the post-fire record. The shift in snow melt timing was probably caused by increased energy available for snow melt because of the canopy removal (Owens et al., 2013) and may also be related to earlier snow melt because of climate change effects (Stewart et al., 2005). The post-fire summer months all showed greater average monthly runoff and July–September, the monsoon months, had increases of 170–940% (Table 1).

The next set of indicators, the magnitudes and frequencies of extreme flows, provide at indications of a substantial fire-induced change in catchment response. The post-fire mean 24-hr minimum discharge rate was 98% less than the pre-fire value, but this indicator is not especially meaningful: both periods of record had multiple days of no runoff, and the fire occurred during a drought period, when zero flows are more likely in this catchment. In contrast, however, was the indicator of extended low flows, which increased by 220% in the post-fire period (Table 1). This is another indicator that the low flows increased in the post-

fire period. The mean annual 24-hr maximum discharge rate decreased slightly after the fire. The mean annual 7-day maximum discharge rate decreased by 37% after the fire and this may also reflect on the occurrence of the fire during a dry period (National Oceanic and Atmospheric Administration, 2011). The number of days with daily discharge rates below the pre-fire 1st quartile 24-hr discharge rate (0.00012 m^3 s^{-1}) decreased from 91 days before the fire to just 7 days after the fire (Table 1). While this indicates a significant reduction in the number of days with low runoff, all of the days with flow below the 1st quartile occurred in the first two weeks of post-fire measurements when there was no runoff. Once the first post-fire event occurred, the discharge rate did not fall below this threshold value during the study. The number of days that exceeded the 3rd quartile pre-fire 24-hr discharge rate (0.0028 m^3 s^{-1}) was 91 before the fire and this increased to 109 after the fire (Table 1), indicating a shift toward higher discharge rates.

The average timing of the minimum discharge rate was about two weeks later in the year, but this probably is not a significant change in the ecosystem. In contrast, the annual maximum discharge rate in the first two years after the fire occurred over two months later than the maximum discharge rate in the pre-fire period (Table 1).

Discussion

Several of the results suggest that wildfire may cause shifts in the dominant runoff process or in the dominant runoff source. The measured changes to runoff processes, source of runoff, and the resultant changes in hydrographs will help improve post-fire hydrologic modeling efforts and may help explain other ecosystem impacts.

Change in runoff processes

The peak discharge rates and times to peak suggest that throughflow was the dominant pre-fire runoff mechanism in W. Willow Creek (Kirkby, 1988). In contrast, the shorter time to peak and the larger peak discharge rates indicate surface runoff was the dominant mechanism (Kirkby, 1988). Reductions in infiltration rate caused by the fire's effect on water repellency (Huffman et al., 2001; Stropki et al., 2005; Doerr et al., 2006) and reduced ground cover and resultant increased soil sealing (Larsen et al., 2009) suggest the post-fire overland flow mechanism was infiltration-excess overland flow.

The Wallow fire caused distinct changes in the time to peak, duration, and slopes of the rising and falling limbs of the storm hydrographs. This is reflected in the simplified triangular unit hydrographs developed for the summer storm flows, which reflect the shorter durations and greater peak discharge rates in the storm flows after the fire (Figure 13). Several modern hydrologic models use the unit hydrograph approach to predict the timing of storm flows (e.g., the Hydrologic Modeling System (US Army Corps of Engineers, 2000) and Water Erosion Prediction Project (Ascough et al., 1995)).

The 20-day antecedent rainfall was the best predictor of both the pre-fire and post-fire summer daily discharge rates. This result suggests that the antecedent soil moisture was an important factor in predicting discharge rate before and after the fire and this may be related to the amount of baseflow in both periods. The fact that the 20-day index, and not one of the shorter-duration indices, was the best predictor of the post-fire discharge rate was somewhat unexpected given the apparent conversion from throughflow to infiltration excess overland flow. One likely explanation for this apparent disparity was that a large fraction of the catchment was either unburned (25%) or burned at low or moderate severity (25%). These

areas probably contributed little, if any, overland flow during the storms that were observed (Moody et al., 2008), and the runoff from these areas would have contributed to the baseflow via the throughflow runoff mechanism.

In the more severely burned areas, less water would infiltrate because of the increased effects of the fire on infiltration capacity, but these areas also would have almost no transpiration. This means a larger fraction of the infiltrated water would contribute to baseflow (Figure 11). In this way fire mimics timber harvest and we can compare these results to the earlier experiments near W. Willow Creek. The previous studies measured increases in both snow melt and summer flows, and the increases in summer flows were attributed to reduced evapotranspiration (Rich, 1972; Gottfried, 1991). The change in water yield in these earlier studies was also calculated on a per-unit-impacted-area basis. Using this metric, the post-fire area-specific storm flows would double as most of the storm flow probably originated from the 50% of the catchment that burned at high severity.

Our results are similar to a study that evaluated catchment-scale discharge rates in southeast Australia using 10 years of pre-fire data and 2 years of post-fire data on (Lane et al., 2006). That study also showed a distinct increase in the daily flow duration curves after the fire, especially in the median and more frequent flows, and the increase in summer base flows were attributed to reduced evapotranspiration after the fire.

Impacts to aquatic/ riparian habitat

Unlike the tropical storm-influenced and rain-on-snow events that caused the two largest instantaneous discharge rates in the pre-fire record, the post-fire events were caused by

monsoonal moisture in convective rainstorms. The I_{30} was a fairly good predictor of peak discharge rate for these events (Figure 5) and our results compare well with those of Moody and Martin (2008) who presented similar analysis for post-fire flows in northern New Mexico. Because of the relatively small spatial extent (a few square kilometers) and small volume of water available in convective storms as compared to other precipitation sources (Dingman, 2002), the post-fire flood peaks rapidly attenuate downstream. It follows that the area impacted by these flows would be at the relatively local scale, perhaps smaller than the experimental catchment (Goodrich et al., 1995).

The post-fire changes in the magnitude of the peak and monthly flows as well as the changes in timing of the peak flows could directly impact aquatic and riparian habitats and the biota that depend on these areas. Most of the research on the effects of post-fire flooding and sedimentation has related to fish populations or habitat (e.g., Dunham et al., 2003; Rieman et al., 2012) or macroinvertebrates (e.g., Minshall, 2003; Arkle et al., 2010; Vieira et al., 2011). These impacts are dynamic and temporary in nature, often lasting only a few years after the fire (Gresswell, 1999).

The study stream does not become perennial until a point downstream of the weir, and at that point the potential impacts to fish and other aquatic organisms would increase (Rinne, 2003). At all points along the stream and its riparian area, however, changes in the magnitude, frequency, and timing of flooding would have impacts on the ecosystem (Junk et al., 1989; Poff et al., 1997; Dwire and Kauffman, 2003). General examples include: the timing of inundation that may impact phenology of riparian vegetation (Merritt and Wohl, 2002); travel paths, access to food sources, and refuge for riparian biota (Andersen et al., 2000), and terrestrial or aquatic biota that depend on the stream for nutrition (Junk et al.,

1989). The effects of the changes in flood magnitude, frequency and timing on the ecosystem may be positive or negative, so specific interactions at the local scale would need to be addressed.

Endangered or otherwise sensitive species are of greatest concern because of the potential lack of recovery after disturbance. The Apache-Sitgreaves National Forest recognized 11 threatened or sensitive fish species in their post-fire assessment for the Wallow fire and identified potential post-fire risks to these species which included extirpation, increased sedimentation, and decreased water quality (Meyer, 2011). The populations found in this area are especially at risk because of their relative lack of mobility and the isolation of the subpopulations (Gresswell, 1999). The Apache-Sitgreaves National Forest managers also recognized risks to in-stream habitat including increased peak flows, changes in stream substrate, and transport of woody debris, and infilling of pools by sediment resulting in less deep water habitat. In addition to the 11 fish species of concern, the wildlife assessment for the Wallow fire identified three terrestrial animal species that might be threatened by high flows (Dorum, 2011). Both the fisheries and wildlife reports address the magnitude of post-fire flows, but not the change in timing or the extent of the flood flow across and above the existing floodplains. One of the species, the New Mexico meadow jumping mouse (*Zapus hudsonius luteus*), lives and hibernates in dry areas but forages in riparian areas only during summer months. This species could be directly impacted by the change in timing of peak flows from spring melt to monsoon season.

Conclusions

An experimental catchment used as from 1962–1983 was re-instrumented after the 2011 Wallow fire. Runoff and precipitation data from the 21 year pre-fire record were compared to the results from the first two years after the fire. We measured significant increases in the peak discharge rates and significant decreases in the durations and times to peak during the 31 post-fire summer storm flows. The resulting triangular unit hydrograph quantifies the degree of flashiness of the post-fire runoff responses, and also illustrates a fire-induced shift in runoff mechanism from throughflow to infiltration-excess overland flow. There was no change in the magnitude of snow melt runoff due to the fire, but the timing of the largest daily discharge rates shifted from 8 June to 14 August, signifying the post-fire increase in importance of the monsoon season. Fewer days produced low flows after the fire, and the summer flows increased across the frequency spectrum, signifying an increase in the baseflow that we attributed to a decrease in the evapotranspiration. These results will help address the lack of data on post-fire changes in runoff responses and will thereby support improvements in post-fire hydrologic modeling efforts. We also raise potential ecohydrologic concerns related to changes in the magnitude, frequency, and timing of the peak discharge rates.

Acknowledgments

This work was supported in part by a National Needs Fellowship grant from the US Department of Agriculture, National Institute of Foods and Agriculture, under agreement no. 2008-38420-04761, as well as through the Forest Service: Rocky Mountain Research Station

and Apache-Sitgreaves National Forest. We thank Gerald J. Gottfried and Daniel G. Neary for their foresight to maintain the pre-fire data archives and for field and logistical assistance. Bob Brown led the re-instrumentation of the catchment and he and Keenan Storrar were instrumental in field data collection. We thank Sierra Larson for her help in the field and for the tedious task of converting the scanned pre-fire archives into digital format. Chris Nelson and John Rihs and others from the Apache-Sitgreaves National Forest provided logistical and field support. We are also grateful to the many field assistants: Chris Bacon, Jessie Huntington, Olga Martyusheva, Troy Hensiek, Karen Koestner, Peter Koestner, and especially to Carol and Richard Garcia who volunteered their summer to help with this study.

References

Aldridge, B.N., Hales, T.A., 1984. Floods of November 1978 to March 1979 in Arizona and west-central New Mexico, US Geological Survey Water-Supply Paper 2241. US Geological Survey, Alexandria, Virginia.

Andersen, D.C., Wilson, K.R., Miller, M.S., Falck, M., 2000. Movement patterns of riparian small mammals during predictable floodplain inundation. Journal of Mammalogy 81, 1087–1099.

Anderson, H.W., Hoover, M., Reinhart, K.G., 1976. Forests and water: Effects of forest management on floods, sedimentation, and water supply, General Technical Report PSW-GTR-18. Berkeley, California.

Arkle, R.S., Pilliod, D.S., Strickler, K., 2010. Fire, flow and dynamic equilibrium in stream macroinvertebrate communities. Freshwater Biology 55, 299–314.

Ascough, J.C., Baffaut, C., Nearing, M.A., Flanagan, D.C., 1995. The Water Erosion Prediction Project (WEPP) Model, chapter 13: Watershed model channel hydrology and erosion processes. U.S. Department of Agriculture Agricultural Research Services National Soil Erosion Laboratory, West Lafayette, Indiana.

Badía, D., Martí, C., 2003. Plant ash and heat intensity effects on chemical and physical properties of two contrasting soils. Arid Land Research and Management 17, 23–41.

Baker, M.B., 1999. History of watershed research in the central Arizona highlands. USDA Forest Service, General Technical Report RMRS-GTR-29, Fort Collins, Colorado.

Benavides-Solorio, J.D., MacDonald, L.H., 2001. Post-fire runoff and erosion from simulated rainfall on small plots, Colorado Front Range. Hydrological Processes 15, 2931–2952.

Blume, T., Zehe, E., Bronstert, A., 2007. Rainfall — runoff response, event-based runoff coefficients and hydrograph separation. Hydrological Sciences Journal 52, 843–862.

Bodí, M.B., Doerr, S.H., Cerdà, A., Mataix-Solera, J., 2012. Hydrological effects of a layer of vegetation ash on underlying wettable and water repellent soil. Geoderma 1–10.

Bonnin, G.M., Martin, D., Lin, B., Parzybok, T., Yekta, M., Riley, D., 2004. NOAA atlas 14: Precipitation-frequency atlas of the United States, volume 1, version 5, semiarid Southwest (Arizona, southeast California, Nevada, New Mexico, Utah). Silver Spring, MD.

Brown, A.E., Zhang, L., McMahon, T.A., Western, A.W., Vertessy, R.A., 2005. A review of paired catchment studies for determining changes in water yield resulting from alterations in vegetation. Journal of Hydrology 310, 28–61.

Brown, J.A.H., 1972. Hydrologic effects of a bushfire in a catchment in south-eastern New South Wales. Journal of Hydrology 15, 77–96.

Cerdà, A., Doerr, S.H., 2008. The effect of ash and needle cover on surface runoff and erosion in the immediate post-fire period. Catena 74, 256–263.

Certini, G., 2005. Effects of fire on properties of forest soils: a review. Oecologia 143, 1–10.

Chen, L., Berli, M., Chief, K., 2013. Examining modeling approaches for the rainfall-runoff process in wildfire-affected watersheds: Using San Dimas Experimental Forest. Journal of the American Water Resources Association 16 pp.

DeBano, L.F., 1981. Water repellent soils: a state-of-the-art, General Technical Report PSW-GTR-46. USDA Forest Service, Pacific Southwest Forest and Range Experimental Station, Berkeley, CA.

DeBano, L.F., 2000. Water repellency in soils: A historical overview. Journal of Hydrology 231–232, 4–32.

Desert Research Institute, 2013. ENSO related Pacific tropical storms in American Southwest [WWW Document]. URL http://www.wrcc.dri.edu/enso/tropstorm.nws

Dieterich, J.H., 1983. Fire history of southwestern mixed conifer: A case study. Forest Ecology and Management 6, 13–31.

Dingman, S.L., 2002. Physical hydrology. Waveland Press, Inc., Long Grove, Illinois.

Doerr, S.H., Shakesby, R.A., Blake, W.H., Chafer, C.J., Humphreys, G.S., Wallbrink, P.J., 2006. Effects of differing wildfire severities on soil wettability and implications for hydrological response. Journal of Hydrology 319, 295–311.

Dorum, D., 2011. Wallow fire 2011 large scale event recovery wildlife report. USDA Forest Service Apache-Sitgreaves National Forest, Springerville, Arizona.

Douglas, M.W., Maddox, R.A., Howard, K., Reyes, S., 1993. The Mexican monsoon. Journal of Climate 6, 1665–1677.

Dunham, J.B., Young, M.K., Gresswell, R.E., Rieman, B.E., 2003. Effects of fire on fish populations: landscape perspectives on persistence of native fishes and nonnative fish invasions. Forest Ecology and Management 178, 183–196.

Dunne, T., Leopold, L.B., 1978. Water in Environmental Planning. W.H. Freeman and Company, New York.

Dwire, K.A., Kauffman, J.B., 2003. Fire and riparian ecosystems in landscapes of the western USA. Forest Ecology and Management 178, 61–74.

Ffolliott, P.F., Stropki, C.L., Chen, H., Neary, D.G., 2011. The 2002 Rodeo-Chediski Wildfire's impacts on southwestern ponderosa pine ecosystems, hydrology, and fuels, Research Paper RMRS-RP-85. U.S. Department of Agriculture, Forest Service, Rocky Mountain Research Station, Fort Collins, Colorado.

Gabet, E.J., Sternberg, P., 2008. The effects of vegetative ash on infiltration capacity, sediment transport, and the generation of progressively bulked debris flows. Geomorphology 101, 666–673.

Giovannini, G., Lucchesi, S., 1997. Modifications induced in soil physico-chemical parameters by experimental fires at different intensities. Soil Science 162, 479–486.

Goodrich, D.C., Faurès, J.-M., Woolhiser,D.A., Lane, L.J., Sorooshian,S., 1995. Measurement and analysis of small-scale convective storm rainfall variability, Journal of Hydrology 173, 283–308.

Gottfried, G.J., 1991. Moderate timber harvesting increases water yields from an Arizona mixed conifer watershed. Water Resources Bulletin 27, 537–547.

Gottfried, G.J., DeBano, L.F., Ffolliott, P.F., 1999. Creating a basis for watershed management in high elevation forests, in: Baker Jr., M.B. (Ed.), History of Watershed Research in the Central Arizona Highlands, General Technical Report RMRS-GTR-29. USDA Forest Service, Rocky Mountain Research Station, Fort Collins, Colorado, pp. 35–42.

Gottfried, G.J., Neary, D.G., Ffolliott, P.F., 2003. Snowpack-runoff relationships for forested mid-elevation watersheds and a high-elevation watershed in Arizona, in: Proceedings of the 71st Annual Western Snow Conference. p. 10 pp.

Grant, D.M., 1989. Isco Open Channel Flow Measurement Handbook. Isco, Inc., Lincoln, Nebraska.

Gresswell, R.E., 1999. Fire and aquatic ecosystems in forested biomes of North America. Transactions of the American Fisheries Society 128, 193–221.

Heede, B.H., 1977. Influence of forest density on bedload movement in a small mountain stream, in: White, L.M. (Ed.), Hydrology and Water Resources in Arizona and the Southwest: Proceedings of the 1977 Meetings of the Arizona Section, American Water Resources Association and the Hydrology Section, Arizona Academy of Science.

Arizona Section, American Water Resources Association and the Hydrology Section, Arizona Academy of Science, pp. 103–107.

Heede, B.H., 1985. Channel adjustments to the removal of log steps: an experiment in a mountain stream. Environmental Management 9, 427–432.

Heede, B.H., 1987. Overland flow and sediment delivery five years after timber harvest in a mixed conifer forest, Arizona, U.S.A. Journal of Hydrology 91, 205–216.

Helvey, J.D., 1980. Effects of a north central Washington wildfire on runoff and sediment production. Journal of the American Water Resources Association 16, 627–634.

Hoyt, W.G., Troxell, H.C., 1934. Forests and stream flow. Transactions of the American Society of Civil Engineers 1–111.

Huffman, E.L., MacDonald, L.H., Stednick, J.D., 2001. Strength and persistence of fire-induced hydrophobicity under ponderosa and lodgepole pine, Colorado Front Range. Hydrological Processes 15, 2877–2892.

Johansen, M.P., Hakonson, T.E., Breshears, D.D., 2001. Post-fire runoff and erosion from rainfall simulation: contrasting forests with shrublands and grasslands. Hydrological Processes 15, 2953–2965.

Junk, W.J., Bayley, P.B., Sparks, R.E., 1989. The flood pulse concept in river-floodplain systems. Canadian Special Publication of Fisheries and Aquatic Sciences 106, 110–127.

Keeley, J.E., 2009. Fire intensity, fire severity and burn severity: a brief review and suggested usage. International Journal of Wildland Fire 18, 116–126.

Kirkby, M., 1988. Hillslope runoff processes and models. Journal of Hydrology 100, 315–339.

Lane, P.N.J., Sheridan, G.J., Noske, P.J., 2006. Changes in sediment loads and discharge from small mountain catchments following wildfire in south eastern Australia. Journal of Hydrology 331, 495–510.

Langford, K.J., 1976. Change in yield of water following a bushfire in a forest of eucalyptus regnans. Journal of Hydrology 29, 87–114.

Larsen, I.J., MacDonald, L.H., Brown, E., Rough, D., Welsh, M.J., Pietraszek, J.H., Libohova, Z., Benavides-Solorio, J.D., Schaffrath, K., 2009. Causes of post-fire runoff and erosion; water repellency, cover, or soil sealing? Soil Science Society of America Journal 73, 1393–1407.

Lavabre, J., Torres, D.S., Cernesson, F., 1993. Changes in the hydrological response of a small Mediterranean basin a year after a wildfire. Journal of Hydrology 142, 273–299.

Llovet, J., Josa, R., Vallejo, V.R., 2008. Thermal shock and rain effects on soil surface characteristics: A laboratory approach. Catena 74, 227–234.

Mayor, Á.G., Bautista, S., Llovet, J., Bellot, J., 2007. Post-fire hydrological and erosional responses of a Mediterranean landscape: Seven years of catchment-scale dynamics. Catena 71, 68–75.

Merritt, D.M., Wohl, E.E., 2002. Processes governing hydrochory along rivers: Hydraulics, hydrology, and dispersal phenology. Ecological Applications 12, 1071–1087.

Meyer, K., 2011. Wallow Fire 2011 large scale event recovery fisheries report. USDA Forest Service, Apache-Sitrgreaves National Forest, Springerville, Arizona.

Minshall, G.W., 2003. Responses of stream benthic macroinvertebrates to fire. Forest Ecology and Management 178, 155–161.

Moody, J.A., Ebel, B.A., 2013. Infiltration and runoff generation processes in fire-affected soils. Hydrological Processes.

Moody, J.A., Martin, D.A., 2001a. Initial hydrologic and geomorphic response following a wildfire in the Colorado Front Range. Earth Surface Processes and Landforms 26, 1049–1070.

Moody, J.A., Martin, D.A., 2001b. Post-fire, rainfall intensity-peak discharge relations for three mountainous watersheds in the western USA. Hydrological Processes 15, 2981–2993.

Moody, J.A., Martin, D.A., Haire, S.L., Kinner, D.A., 2008. Linking runoff response to burn severity after a wildfire. Hydrological Processes 22, 2063–2074.

Moody, J.A., Shakesby, R.A., Robichaud, P.R., Cannon, S.H., Martin, D.A., 2013. Current research issues related to post-wildfire runoff and erosion processes. Earth-Science Reviews 122, 10–37.

National Oceanic and Atmospheric Administration, 2011. Extreme weather 2011. [WWW Document]. URL http://www.noaa.gov/extreme2011/wildfire.html

Owens, P.N., Giles, T.R., Petticrew, E.L., Leggat, M.S., Moore, R.D., Eaton, B.C., 2013. Muted responses of streamflow and suspended sediment flux in a wildfire-affected watershed. Geomorphology.

Parsons, A., Robichaud, P.R., Lewis, S.A., Napper, C., Clark, J.T., 2010. Field guide for mapping post-fire soil burn severity, General Technical Report RMRS-GTR-243. US Department of Agriculture, Forest Service, Rocky Mountain Research Station, Fort Collins, Colorado.

Poff, N.L., Allan, J.D., Bain, M.B., Karr, J.R., Prestegaard, K.L., Richter, B.D., Sparks, R.E., Stromberg, J.C., 1997. The natural flow regime a paradigm for river conservation and restoration. BioScience 47, 769–784.

Ramírez, J.A., 2000. Prediction and modeling of flood hydrology and hydraulics, in: Wohl, E.E. (Ed.), Inland Flood Hazards: Human, Riparian and Aquatic Communities. Cambridge University Press, Cambridge.

Rich, L.R., 1962. Erosion and sediment movement following a wildfire in a ponderosa pine forest of central Arizona, Research Note 76. USDA Forest Service, Rocky Mountain Forest and Range Experimental Station, Fort Collins, Colorado.

Rich, L.R., 1972. Managing a ponderosa pine forest to increase water yield. Water Resources Research 8, 422–428.

Rich, L.R., Thompson, J.R., 1974. Watershed management in Arizona's mixed conifer forests: The status of our knowledge, Research Paper RM-130. USDA Forest Service, Rocky Mountain Forest and Range Experiment Station, Fort Collins, Colorado.

Richter, B.D., Baumgartner, J.V., Powell, J., Braun, D.P., 1996. Hydrologic alteration for assessing hydrologic alteration within ecosystems. Conservation Biology 10, 1163–1174.

Rieman, B.E., Gresswell, R.E., Rinne, J., 2012. Fire and fish: A synthesis of observation and experience, Forest Service RMRS-GTR-290. U.S. Department of Agriculture, Forest Service, Rocky Mountain Research Station, Fort Collins, Colorado.

Rinne, J.N., 2003. Flows, fishes, foreigners, and fires: relative impacts on Southwestern native fishes. Hydrology and Water Resources in the Southwest 33, 79–84.

Robichaud, P.R., 2000. Fire effects on infiltration rates after prescribed fire in Northern Rocky Mountain forests, USA. Journal of Hydrology 231–232, 220–229.

Robichaud, P.R., Beyers, J.L., Neary, D.G., 2000. Evaluating the effectiveness of postfire rehabilitation treatments, General Technical Report RMRS–63. USDA Forest Service, Rocky Mountain Research Station, Fort Collins, Colorado.

Robichaud, P.R., Wagenbrenner, J.W., Brown, R.E., 2010. Rill erosion in natural and disturbed forests: 1. Measurements. Water Resources Research 46, W10506.

Robichaud, P.R., Wagenbrenner, J.W., Lewis, S.L., Brown, R.E., Wohlgemuth, P.M., Ashmun, L.E., 2013. Post-fire mulching for runoff and erosion mitigation Part II: Effectiveness in reducing runoff and sediment yields from small catchments. Catena 105, 93–111.

Rowe, P.B., Countryman, C.M., Storey, H.C., 1954. Hydrologic analysis used to determine effects of fire on peak discharges and erosion rates in southern California watersheds. USDA Forest Service, California Forest and Range Experiment Station, Berkeley, California.

Scott, D.F., Van Wyk, D.B., 1990. The effects of wildfire on soil wettability and hydrological behaviour of an afforested catchment. Journal of Hydrology 121, 239–256.

Searcy, J.K., 1959. Flow-duration curves, Manual of Hydrology: Part 2. Low-flow techniques, US Gological Survey water-supply paper 1542-A. Washington, D.C.

Shakesby, R.A., Doerr, S.H., 2006. Wildfire as a hydrological and geomorphological agent. Earth-Science Reviews 74, 269–307.

Smith, R.E., Goodrich, D.C., Quinton, J.N. 1995. Dynamic, distributed simulation of watershed erosion: the KINEROS2 and EUROSEM models. Journal of Soil and Water Conservation, 50, 517–520.

Stednick, J.D., 1996. Monitoring the effects of timber harvest on annual water yield. Journal of Hydrology 176, 79–95.

Stewart, I.T., Cayan, D.R., Dettinger, M.D., 2005. Changes toward Earlier Streamflow Timing across Western North America. Journal of Climate 18, 1136–1155.

Stropki, C.L., Ffolliott, P.F., Debano, L.F., Neary, D.G., 2005. Occurrence and persistence of water repellent soils on the Stermer Ridge watersheds following the Rodeo-Chediski wildfire: A preliminary assessment. Hydrology and Water Resources in Arizona and the Southwest 35, 47–50.

US Army Corps of Engineers, 2000. Hydrologic modeling system: HEC-HMS technical reference manual. US Army Corps of Engineers, Davis, California.

USDA Forest Service, 1995. Burned area emergency rehabilitation handbook. Forest Service Handbook No. 2509.13. USDA Forest Service, Washington, D.C.

USDA Forest Service, 2011. Wallow Fire soil burn severity map. Apache-Sitgreaves National Forest, Springerville, Arizona

USDA Natural Resources Conservation Service, 2013. Hannagan Meadows Snow Telemetry Site [WWW Document]. URL http://www.wcc.nrcs.usda.gov/nwcc/site?sitenum=511&state=az

Veenhuis, J.E., 2002. Effects of wildfire on the hydrology of Capulin and Rito de Los Frijoles Canyons, Bandelier National Monument, New Mexico, US Geological Survey Water Resources Investigations Report 02-4152. Albuquerque, New Mexico.

Vieira, N.K.M., Barnes, T.R., Mitchell, K.A., 2011. Effects of wildfire and postfire floods on stonefly detritivores of the Pajarito Plateau, New Mexico. Western North American Naturalist 71, 257–270.

Vogel, R.M., Fennessey, N.M., 1994. Flow-duration curves. I: New interpretation and confidence intervals. Journal of Water Resources Planning and Management 120, 485–504.

Woods, S.W., Balfour, V.N., 2008. The effect of ash on runoff and erosion after a severe forest wildfire, Montana, USA. International Journal of Wildland Fire 17, 535–548.

Woods, S.W., Balfour, V.N., 2010. The effects of soil texture and ash thickness on the post-fire hydrological response from ash-covered soils. Journal of Hydrology 393, 274–286.

Zavala, L.M., Jordán, A., Gil, J., Bellinfante, N., Pain, C., 2009. Intact ash and charred litter reduces susceptibility to rain splash erosion post-wildfire. Earth Surface Processes and Landforms 34, 1522–1532.

Table 1. Indicators of hydrologic alteration (Richter et al., 1996) for the pre-fire (1963–1983) and post-fire years (July 2011–2012)

Indicator	Pre-fire annual mean	Post-fire annual mean	Deviation
Magnitude of monthly flows (mm d^{-1})			
April	1.6	0.49	-70%
May	1.9	0.12	-94%
June	0.20	0.072	-63%
July	0.042	0.11	170%
August	0.10	1.0	940%
September	0.13	0.42	230%
October	0.19	0.23	26%
Magnitude and frequency of extreme flows			
24-hr minimum discharge rate (mm d^{-1})	0.0024	0.00005	-98%
7-day minimum discharge rate (mm d^{-1})	0.0029	0.0094	220%
24-hr maximum discharge rate (mm d^{-1})	4.6	4.0	-13%
7-day maximum discharge rate (mm d^{-1})	3.8	2.4	-37%
Days below 1st quartile pre-fire discharge rate	91	7 [A]	-84 days
Days above 3rd quartile pre-fire discharge rate	91	109	18 days
Timing of extreme flows			
Date of 24-hr minimum discharge rate	6 August	19 August	13 days
Date of 24-hr maximum discharge rate	8 June	14 August	67 days

[A] The first 14 days of the study had no runoff, resulting in an average of 7 days per year for the two year study.

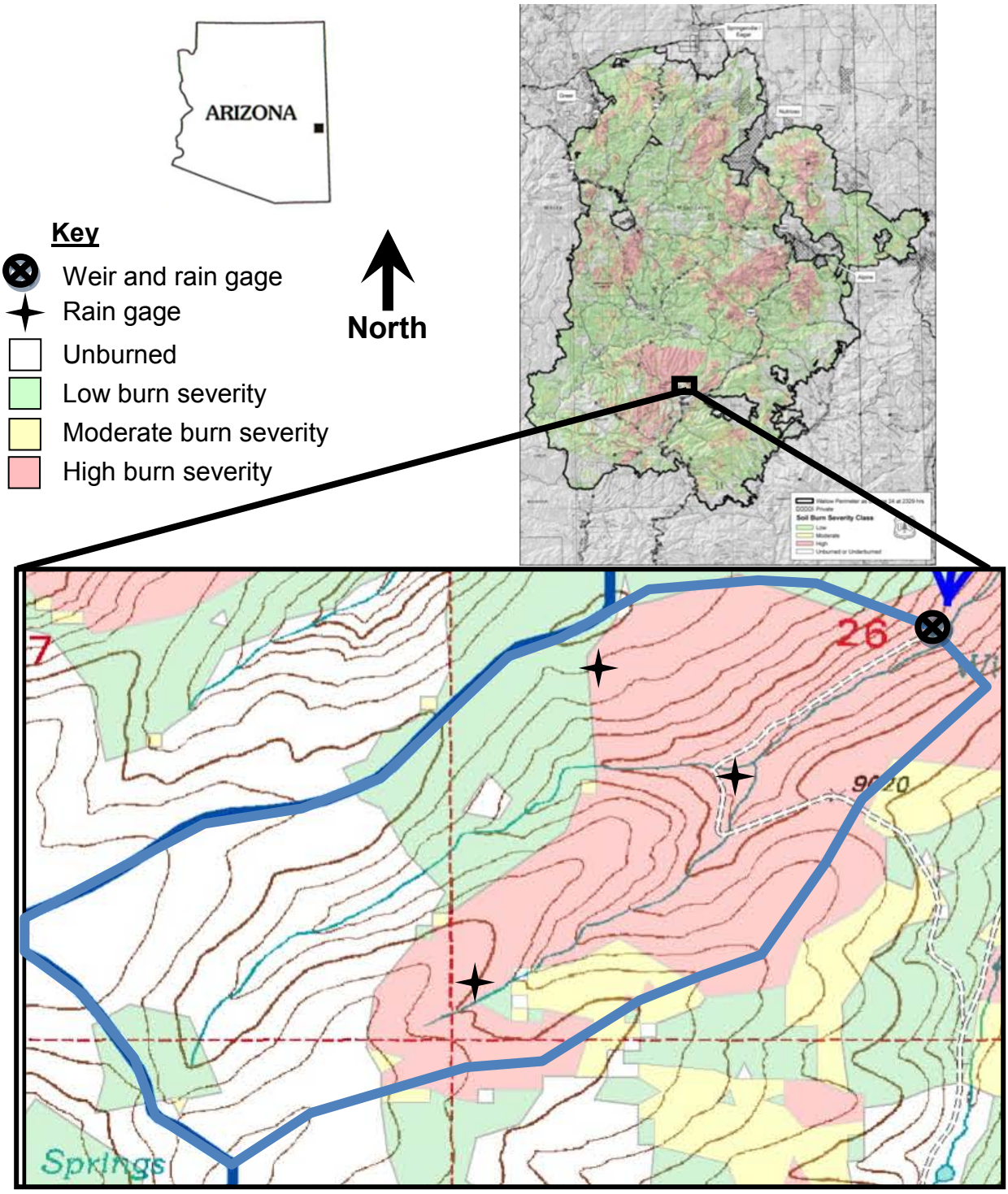

Figure 1. Location of the experimental catchment. Map modified from the Wallow fire soil burn severity map (USDA Forest Service, 2011). The weir is located at 33°39'52" north latitude, 109°18'49" west longitude.

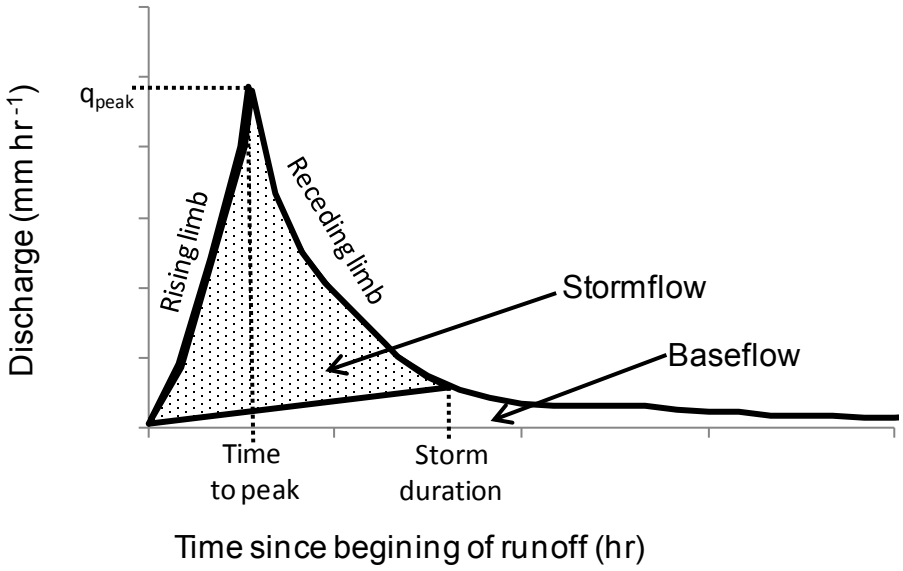

Figure 2. Hydrograph separation terms

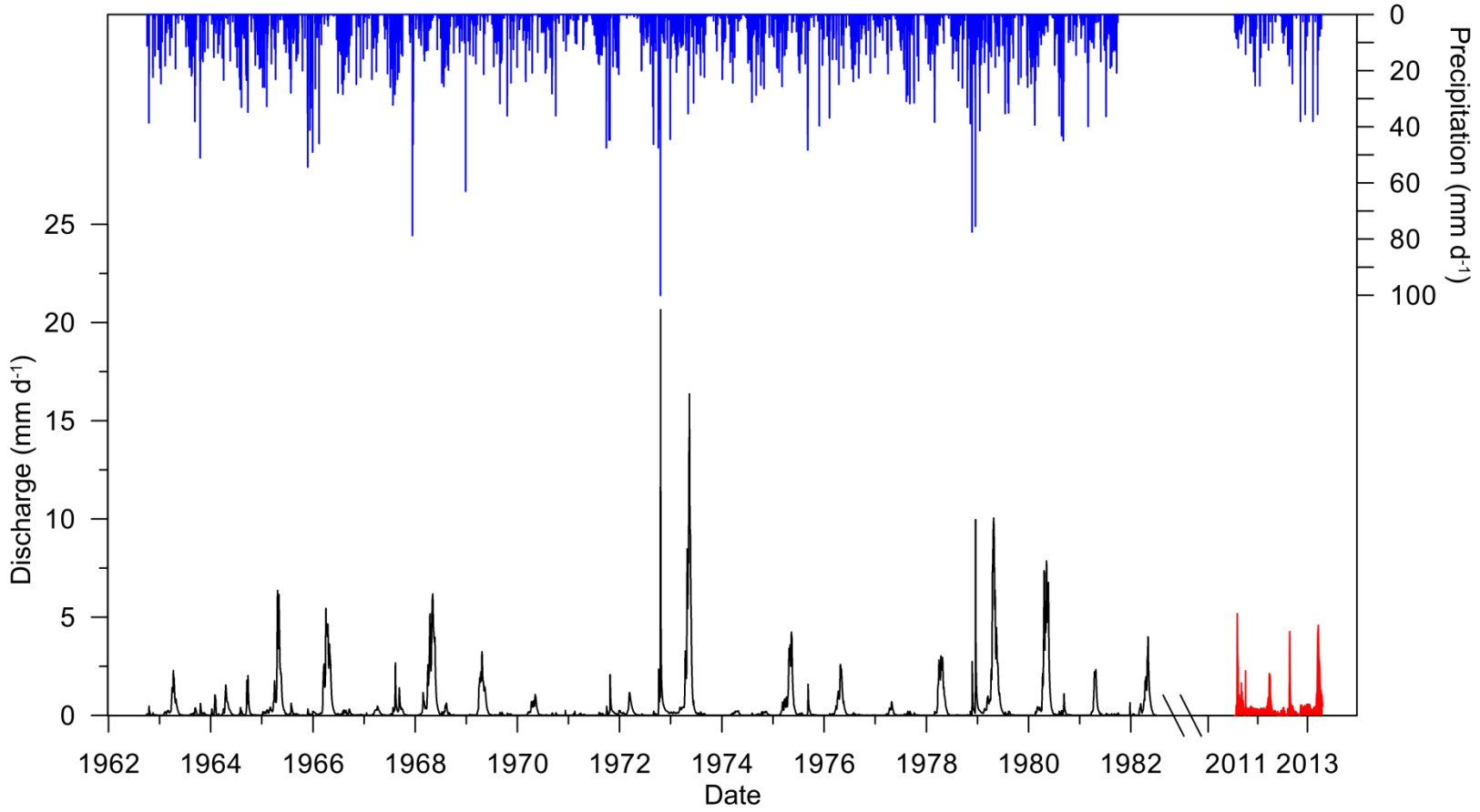

Figure 3. Daily discharge rate and precipitation for W. Willow Creek, pre-fire water years 1963–1983 (black) and the post-fire period 12 July 2011 through 24 April 2013 (red).

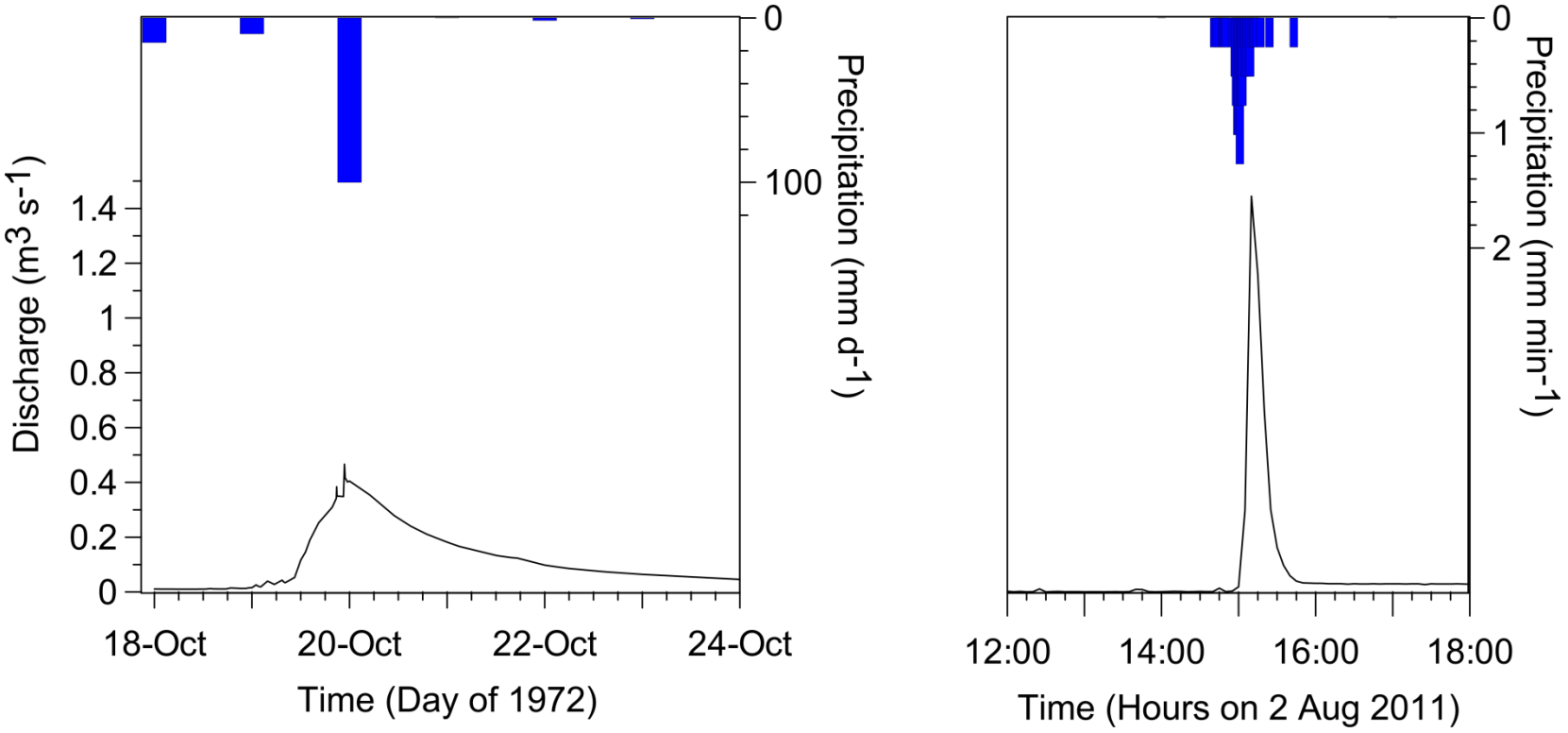

Figure 4. Instantaneous discharge rate versus time for the largest pre-fire (a) and post-fire (b) flows in W. Willow Creek. Note differences in time and precipitation scales.

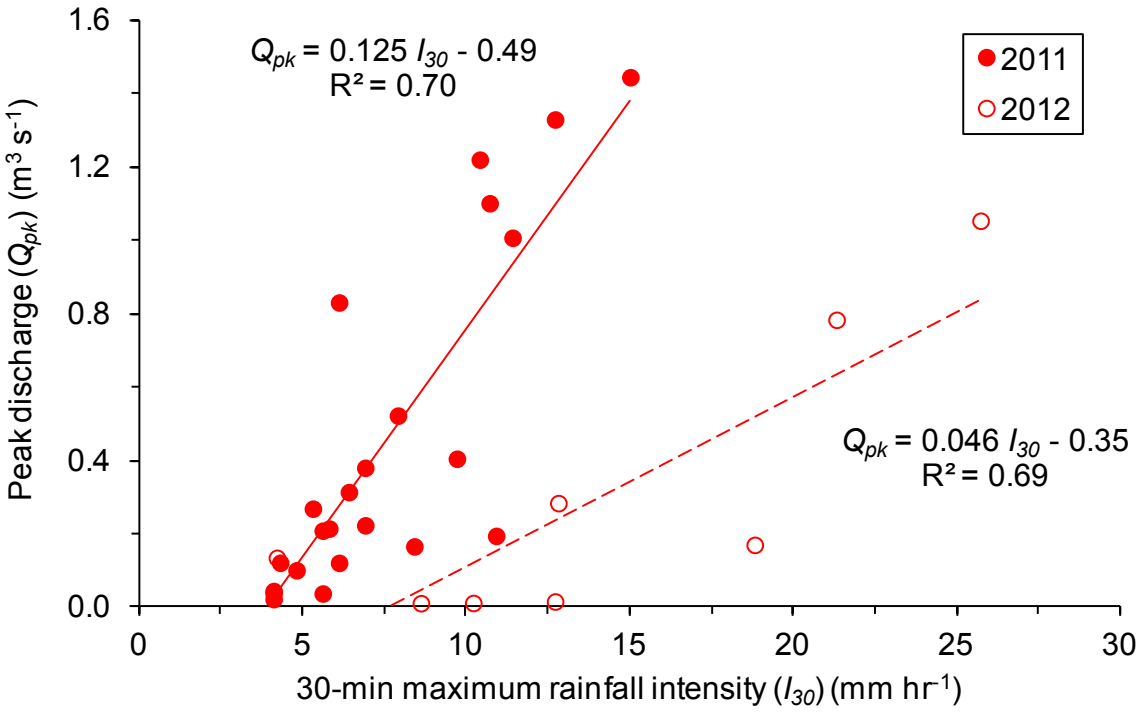

Figure 5. Peak discharge rate (Q_{pk}) versus 30-min maximum rainfall intensity (I_{30}) for post-fire years 2011 and 2012. The peak discharge rate for the 21-yr pre-fire period of record was 0.466 m^3 s^{-1}, and its maximum rainfall intensity (duration unknown) was estimated as 29 mm hr^{-1}. The 2-yr return period I_{30} for this location is 45 mm hr^{-1} (Bonnin et al., 2004).

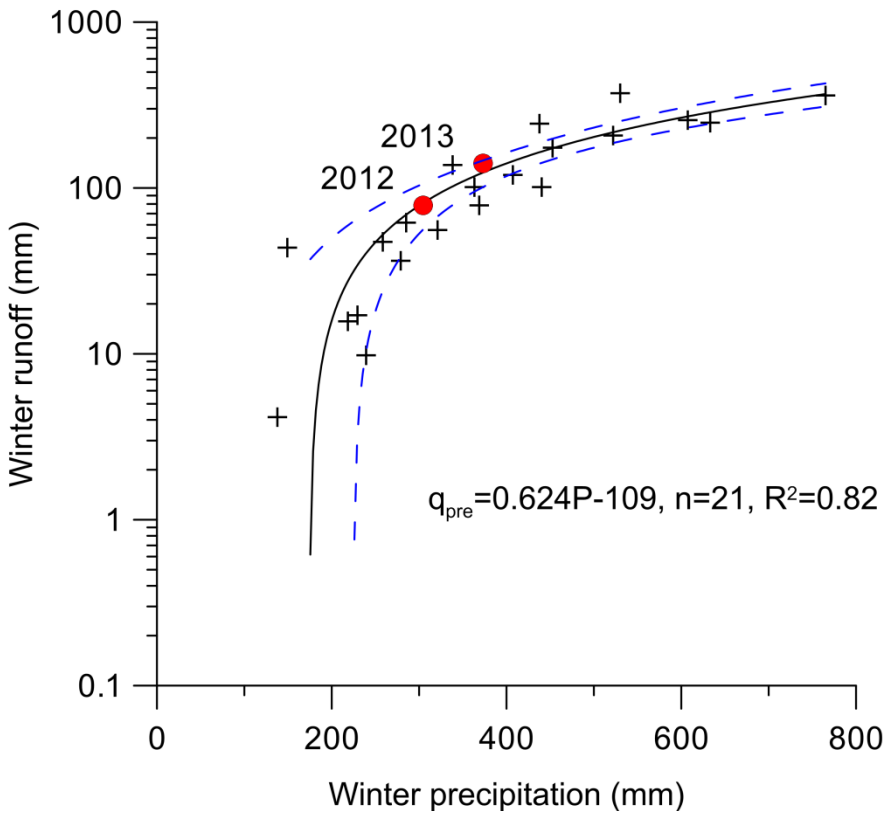

Figure 6. Winter (November–May) runoff (q) versus winter precipitation (P) for water years 1963–1983 (crosses) and 2012–2013 (circles). The period for 2013 is through 24 April, which includes the high flow from snow melt but not all of the days of higher baseflow following the peak melt period. The solid line is the linear regression for pre-fire runoff (q_{pre}) and the dashed lines indicate the 95% confidence interval.

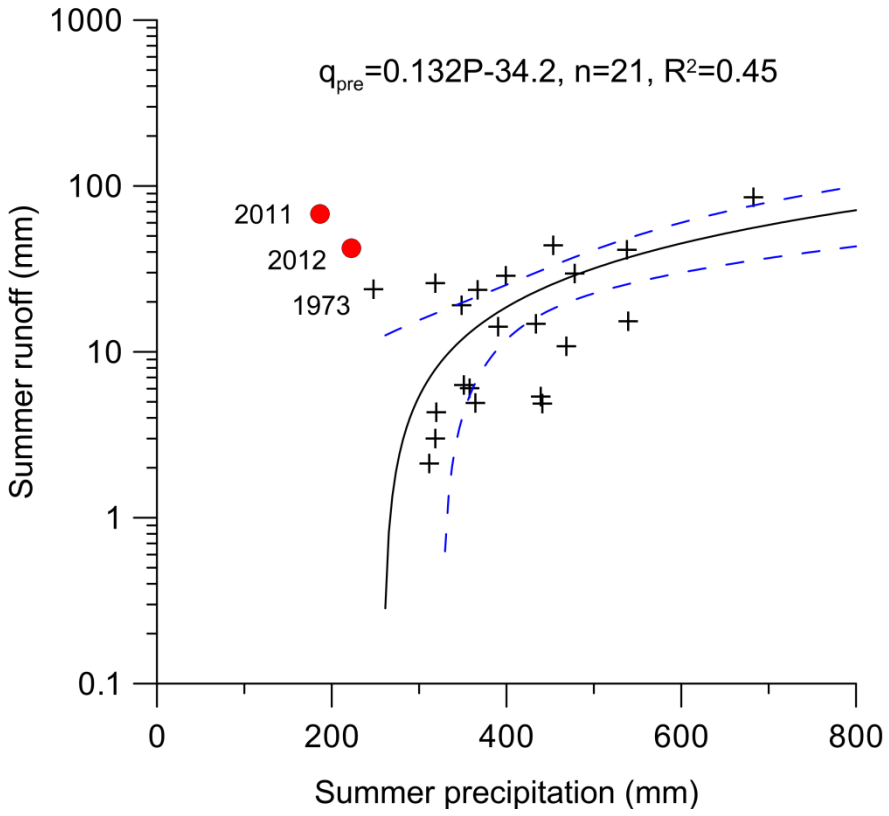

Figure 7. Summer (June–October) runoff (q) versus summer precipitation (P) for pre-fire years 1963–1983 (crosses), and post-fire years 2011–2012 (circles). The 2011 datum starts on 12 July. As there was no runoff on this date and there was no indication of earlier post-fire runoff, the contribution prior to this date was presumed negligible. The high summer runoff associated with low summer precipitation in 1973 resulted from late (June) peak snow melt followed by a dry summer. The solid line shows the linear regression for the pre-fire runoff (q_{pre}) and the dashed lines indicate the 95% confidence interval.

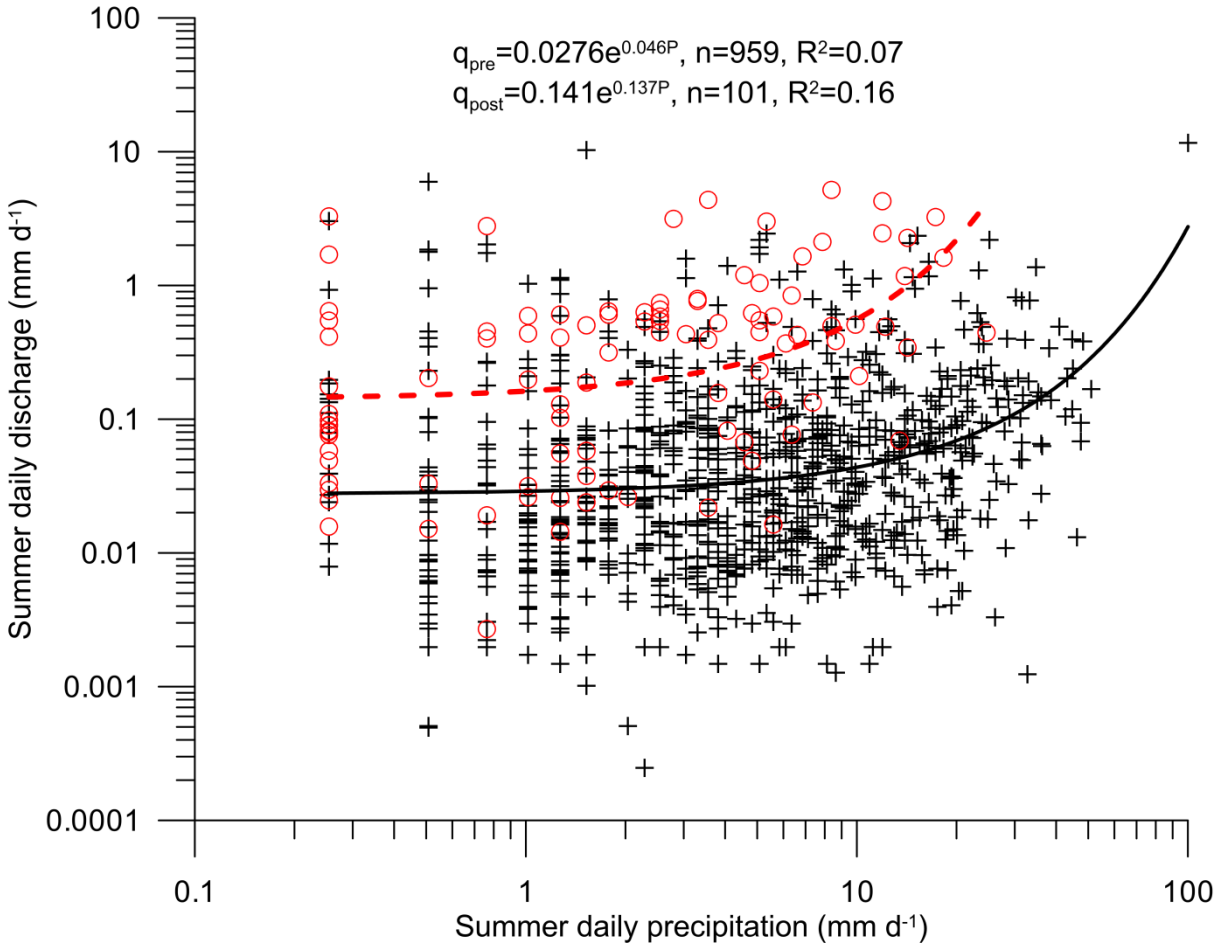

Figure 8. Summer (June–October) daily discharge rate versus summer daily precipitation for pre-fire years 1963–1981 (crosses) and post-fire years 2011–2012 (circles). The curves are exponential regressions for the discharge rate in the pre-fire (q_{pre}) (solid) and post-fire (q_{post}) (dashed) periods.

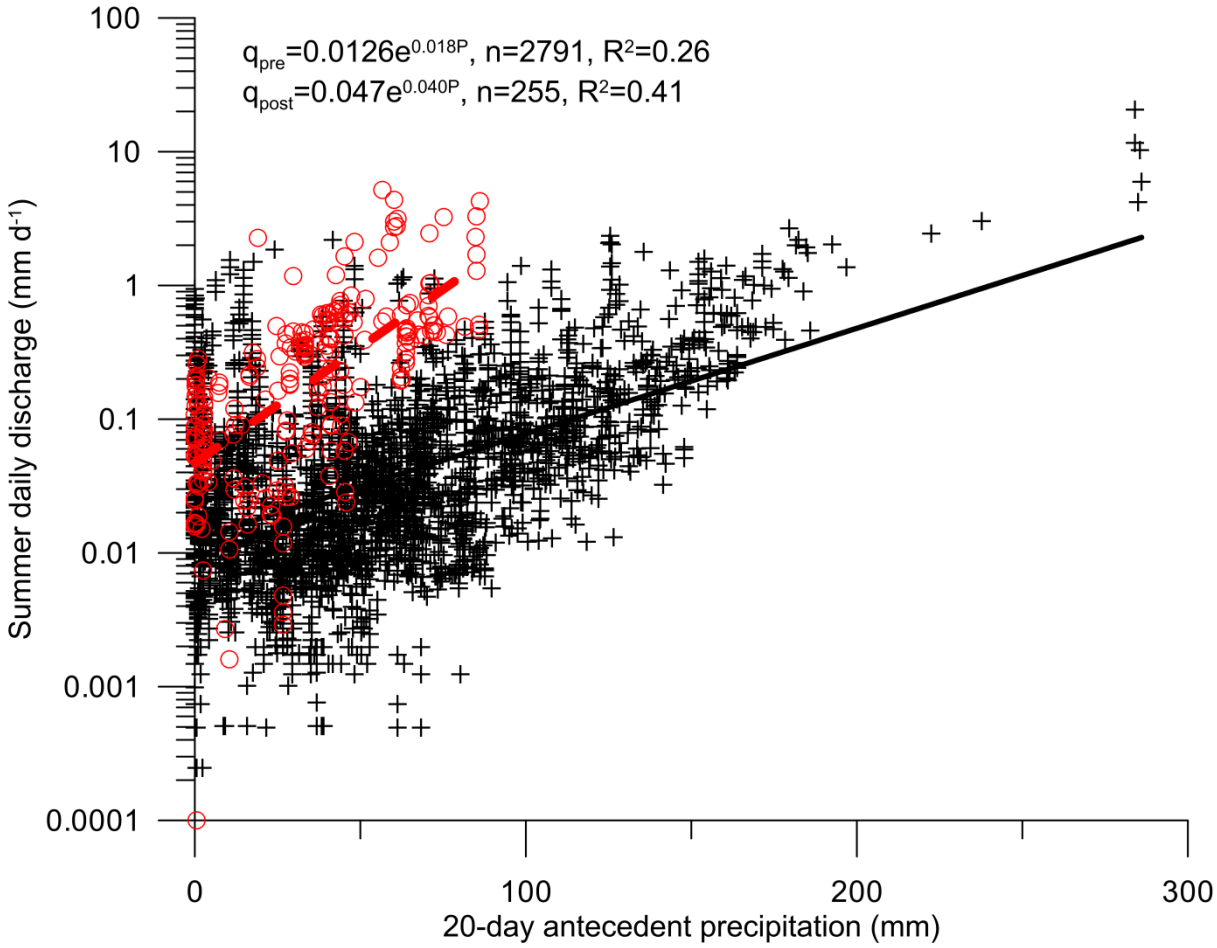

Figure 9. Summer (June–October) daily discharge rate versus 20-day antecedent precipitation (current day plus 19 prior days) for pre-fire years 1963–1981 (crosses) and post-fire years 2011–2012 (circles). The curves are exponential regressions for the discharge rate in the pre-fire (q_{pre}) (solid) and post-fire (q_{post}) (dashed) periods.

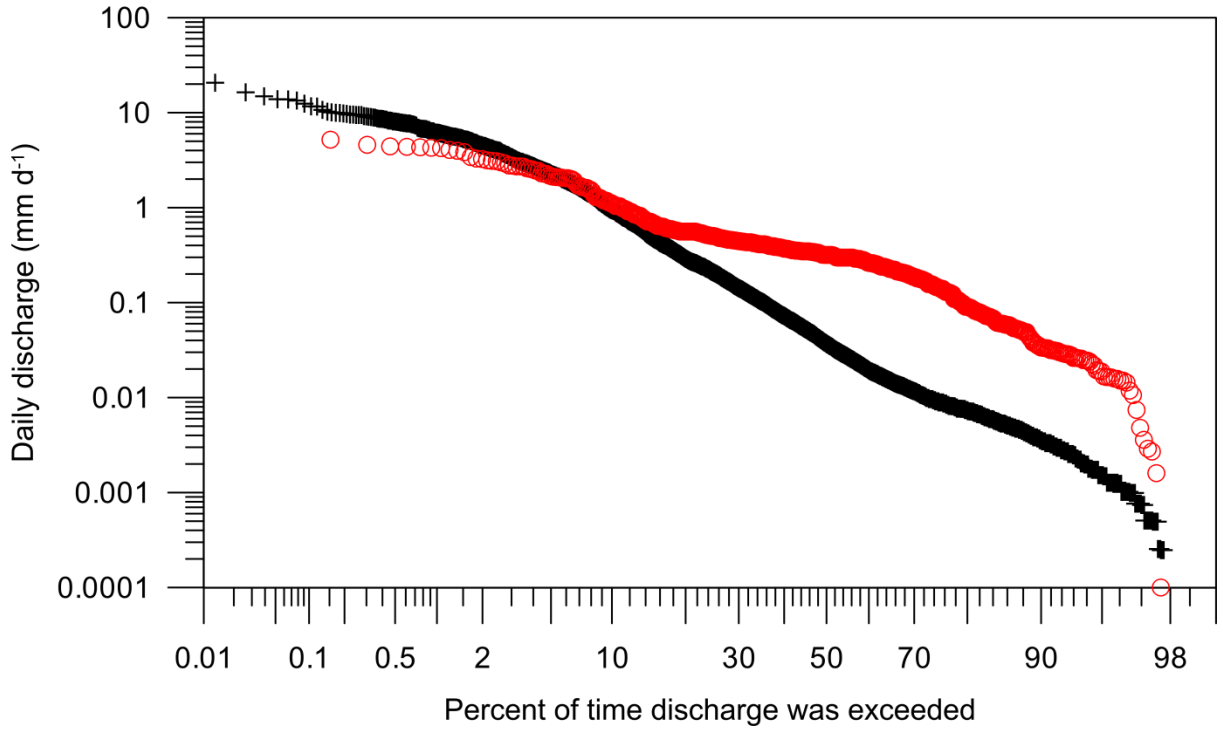

Figure 10. Flow duration curve for W. Willow Creek: daily discharge rate versus exceedance probability for pre-fire water years 1963–1983 (crosses) and post-fire 12 July 2011–24 April 2013 (circles).

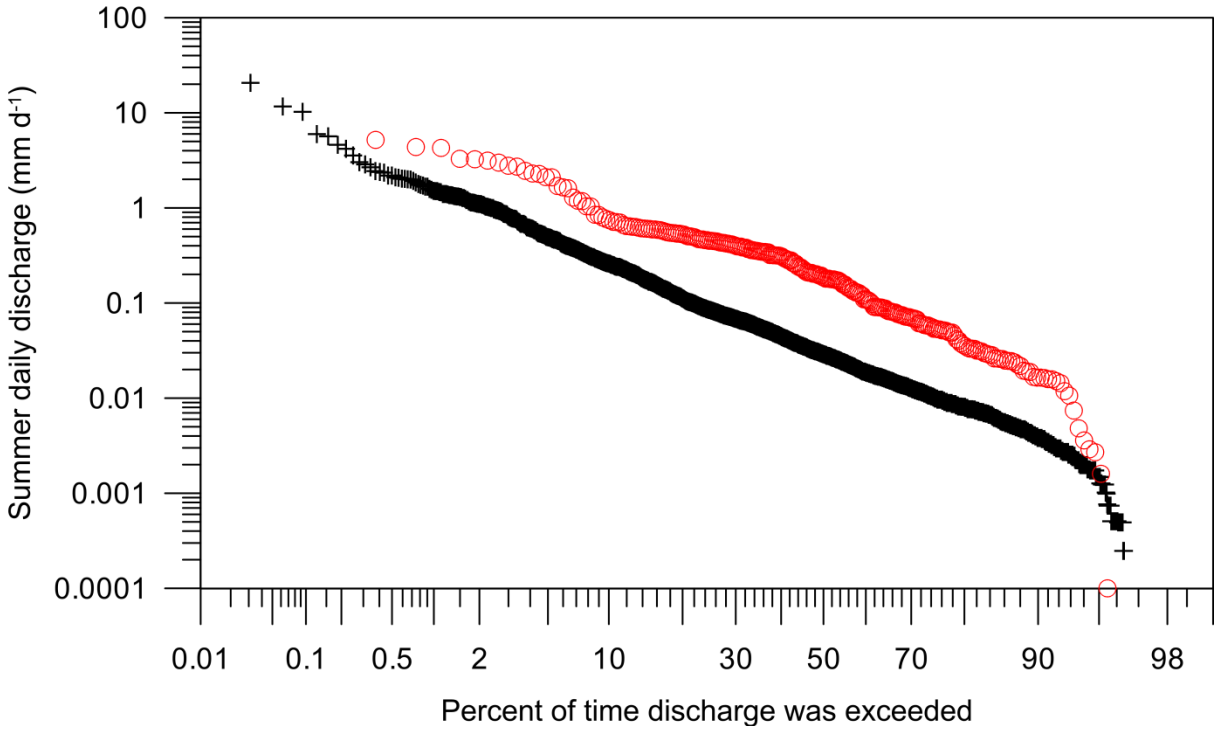

Figure 11. Flow duration curve for summer flows in W. Willow Creek: daily discharge rate versus exceedance probability, pre-fire years 1963–1983 (crosses) and post-fire years 2011–2012 (circles).

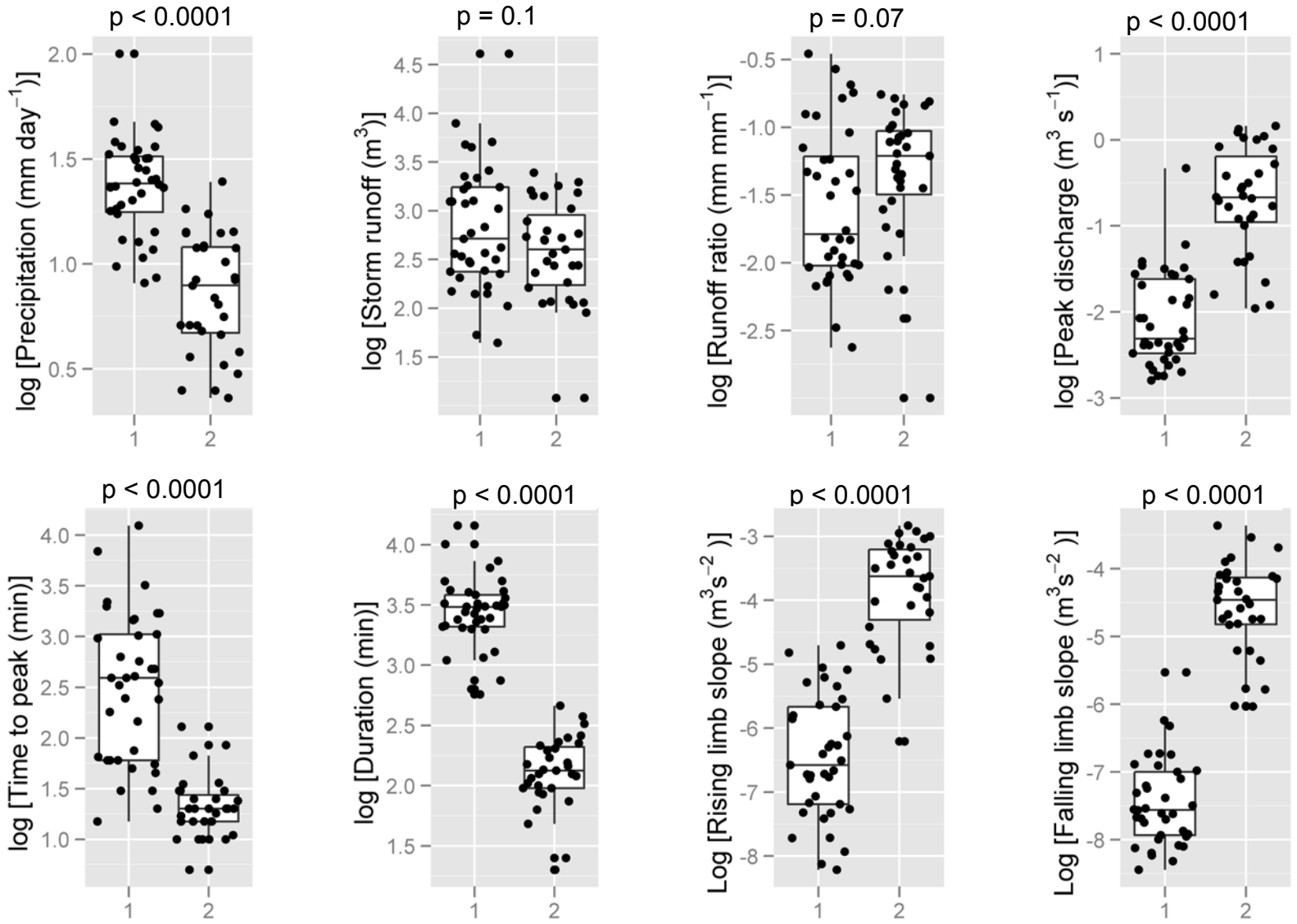

Figure 12. Boxplots for the log-transformed hydrograph metrics. "1" is for pre-fire and "2" is for post-fire.

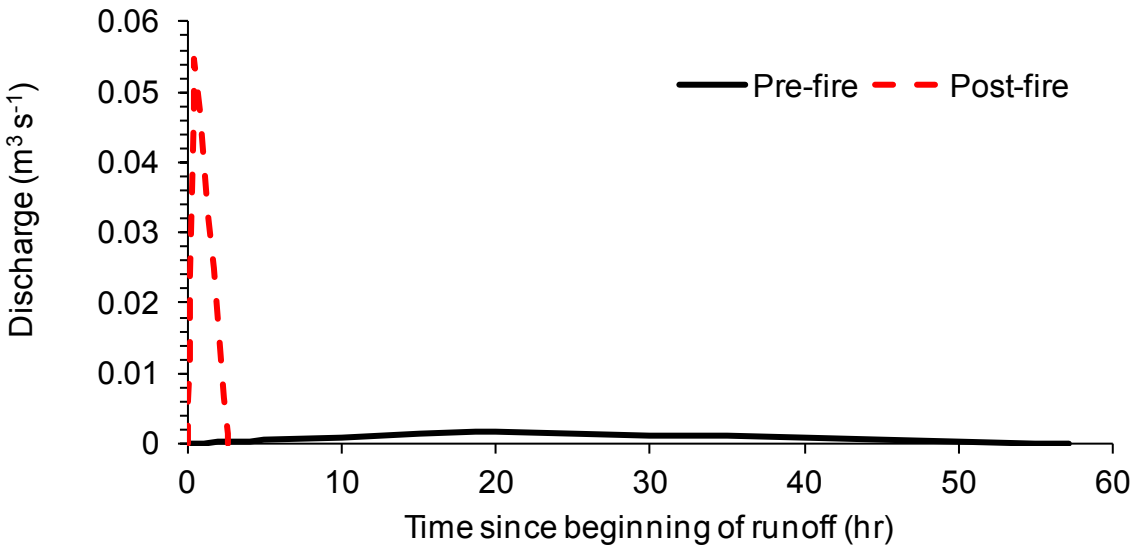

Figure 13. Triangular unit hydrographs showing instantaneous discharge rate versus time since beginning of runoff. Hydrographs were derived from the average peak discharge rate, time to peak, and total duration of analyzed storms. The hydrographs were scaled so that the runoff (area under each curve) was 1 mm.

CHAPTER THREE: POST-FIRE SEDIMENT DELIVERY ACROSS SPATIAL SCALES IN THE INTERIOR WESTERN US

Joseph W. Wagenbrenner[1,2,*] and Peter R. Robichaud[2]

[1] Department of Biological Systems Engineering, Washington State University, Pullman Washington, USA

[2] US Department of Agriculture, Forest Service, Rocky Mountain Research Station, Moscow, Idaho, USA

[*] Correspondence to: Joseph W. Wagenbrenner, US Department of Agriculture, Forest Service, Rocky Mountain Research Station, 1221 South Main St., Moscow, Idaho, 83843, USA, phone: +1 208 883 2353, fax:+1 208 883 2318, email: jwagenbrenner@fs.fed.us

Short title: Post-fire sediment delivery across spatial scales

Sponsors: US Department of Agriculture, National Institute of Food and Agriculture, under Agreement No. 2008-38420-04761; US Department of Agriculture, Forest Service: Rocky Mountain Research Station, Pike-San Isabel National Forest, Apache-Sitgreaves National Forest, and Fishlake National Forest

Abstract

Post-fire sediment yields can be up to three orders of magnitude greater than sediment yields in unburned forests. Much of the research on post-fire erosion rates has been at small scales (100 m^2 or less), and post-fire sediment delivery rates across spatial scales have not yet been quantified. We developed relationships for post-fire sediment delivery rates for spatial scales up to 117 ha using sediment yield data from six published studies and two recently established study sites. Sediment yields and sediment delivery ratios were related to site factors including rainfall metrics, area, length, and ground cover. Unit-area sediment yields significantly decreased with increasing area in five of the six sites. The annual sediment delivery ratios ranged from 0.0089 to 1.02 and these were more closely related to the ratio of the plot lengths than the ratio of plot areas. The developed relationships will help quantify post-fire sediment delivery rates across spatial scales and develop process-based scaling relationships.

Keywords: erosion, hillslope, catchment, sedimentation, rainfall intensity

Introduction

Hillslope erosion rates after forest fires can increase dramatically (DeBano et al., 1998; Moody and Martin, 2009; Shakesby and Doerr, 2006; Swanson, 1981) because of temporary changes to hydrologic properties (Ebel et al., 2012; Larsen et al., 2009; Martin and Moody, 2001; Robichaud, 2000). There is evidence that these erosion rates depend on the severity of the wildfire (Benavides-Solorio and MacDonald, 2001, 2005; Moody et al., 2008b; Robichaud, 2000), the magnitude or intensity of the rainfall that occurs after the fire (Lanini

et al., 2009; Moody and Martin, 2001b, 2009; Robichaud et al., 2008b), and the geomorphic setting of the burned area (Moody et al., 2008a; Robichaud et al., 2013a).

Much of the research into the hydrologic and geomorphic effects of wildfires has occurred at spatial extents of 100 m^2 or less. A few observational studies have recorded elevated sediment yields at larger (e.g., > 1 km^2) scales (Brown, 1972; Helvey, 1980; Lane et al., 2006; Malmon et al., 2007; Meyer et al., 1992; Moody and Martin, 2001a; Noske et al., 2010; Reneau et al., 2007; Rowe et al., 1954; Troendle and Bevenger, 1996). However there are relatively few studies relating the post-fire sediment response across spatial scales (Ferreira et al., 2008; Mayor et al., 2011).

Sediment delivery across scales has been a focus in the hydrologic and geomorphic literature for the past several decades (Walling, 1983). It is clear that there is no simple ratio applicable across locations, spatial scales, or land cover type (e.g., forest, range, or grassland) or condition, and that the sediment delivery rate relative to the hillslope erosion rate is a complex, dynamic, approximate concept (Parsons et al., 2006b; de Vente and Poesen, 2005; de Vente et al., 2007; Walling, 1983). Still, there is much practical value in determining an approximate proportion of the delivery of eroded sediment to points downstream (Lu et al., 2005; Parsons et al., 2006a).

Given the impacts of forest fires on storm flows and erosion rates, the sediment delivery issue is of great concern to those trying to manage downstream resources. In the US and increasingly in other countries, post-fire assessments attempt to predict the risk of sedimentation, among other issues, in streams and reservoirs below burned areas. Often the best information available to these managers is an erosion rate measured at a relatively small spatial scale, and there is little guidance on the error associated with extrapolating these small-

scale erosion rates to basin scale sediment yields. Physically-based erosion models may help address the difference in sediment delivery across spatial scales but models should be validated at each scale of inference, and few data are available on post-fire sediment delivery rates at the larger spatial scales.

Controls on post-fire sediment yields at the hillslope scale have been fairly well described, and include amount of ground cover (Benavides-Solorio and MacDonald, 2001, 2005; Cerdà and Doerr, 2005; Doerr et al., 2006; Larsen et al., 2009; Prosser and Williams, 1998; Robichaud, 2000; Vega and Diaz-Fierros, 1987; Wagenbrenner et al., 2006); the degree of heating of the soil, usually inferred after the fire by assessing soil burn severity (Keeley, 2009); the observed post-fire rainfall amount or intensity (Desilets et al., 2007; Kunze and Stednick, 2006; Moody and Martin, 2001b, 2009; Robichaud et al., 2008b; Spigel and Robichaud, 2007; Vega and Diaz-Fierros, 1987; Wondzell and King, 2003); hillslope shape (planar, convex, or concave) (Benavides-Solorio and MacDonald, 2005); and time since burning (Benavides-Solorio and MacDonald, 2005; Larsen et al., 2009; Morris and Moses, 1987; Pierson et al., 2009; Robichaud et al., 2008b, 2013a, 2013c; Wagenbrenner et al., 2006).

Some progress has been made in establishing scaling relationships in burned areas. Channel network patterns were characterized and related across three spatial scales (1 to 1000 m^2, 0.1 to 100 ha, and 1 to 1000 km^2) in a study three years after the Buffalo Creek fire in Colorado (Moody and Kinner, 2006). The authors concluded that the scaling ratios in the largest size class (1 to 1000 km^2) applied to the middle size class (0.1 to 100 ha), but the rill networks in the smallest size class (1 to 1000 m^2) produced a less-dense channel network than predicted by scaling from the two larger classes (Moody and Kinner, 2006).

The goal of the current study was to use field-measured sediment yields to determine how post-fire sediment delivery rates vary across spatial scales. The specific objectives were to: 1) develop an empirical relationship between sediment yields, spatial extent, site characteristics, and rainfall properties; 2) determine if this relationship holds across multiple locations with diverse climate and topography; and 3) calculate the post-fire sediment delivery ratio across spatial scales and relate this to physical properties.

Methods

Site description

Study sites were installed after wildfires in six forests in Colorado, Washington, Utah, Montana, and Arizona (Figure 1). Detailed site descriptions and methods are presented in previous studies for four of the sites: Bobcat (Wagenbrenner et al., 2006); Hayman (Robichaud et al., 2008b, 2013a, 2013c); North 25 (Robichaud et al., 2006, 2008b) and Valley (Robichaud et al., 2008a, 2008b). The methods at the Twitchell site in Utah and the Wallow site in Arizona (Figure 1) followed the methods used in the earlier studies and these are briefly summarized below along with the earlier sites' descriptions (Table 1).

The Twitchell site was located within the 180 km^2 Twitchell Canyon fire of July 2010 on the Fishlake National Forest in Utah. This was the only site that was not a mixed-conifer forest before the fire, and its vegetation was composted of pinyon pine, juniper, and gambel oak (Table 1). The current study used data from 5 untreated catchments (0.22 to 1.6 ha) that were part of a larger study on post-fire channel treatments (Storrar, 2013). Hillslope plots were installed in the headwaters of four of these untreated catchments. An additional five hillslope plots were installed upstream of treatments in paired treated catchments. The nine

plots were 3 m wide by 9 to 63 m along the slope, and had gradients between 25% and 67% (Table 2). Rain gages were installed in or adjacent to each catchment and the nearest gage was used to characterize rainfall for each plot.

The Wallow site was located in the 117 ha West Fork of Willow Creek catchment, which burned in June 2011 during the 2200 km^2 Wallow fire on the Apache-Sitgreaves National Forest in Arizona (Figure 1). A concrete weir was installed in W. Willow Creek in 1962 as part of an earlier study (Heede, 1985). In July 2011 the weir was re-instrumented and the stilling ponds were emptied and surveyed. Four slope-length plots were installed near the weir, and these were between 130 and 322 m long (Table 2). Twelve 12-m long untreated plots were installed as part of a study on the effectiveness of post-fire seeding, and these were bounded by trenches to exclude flow from above the plots. The width of each plot was 3 m. Slope gradients ranged from 30 to 36% for the hillslope plots (Table 2). Four rain gages were installed throughout the catchment. The nearest gage was used to characterize rainfall for the hillslope plots and the median of the four rain gage values was used to characterize the rainfall for the catchment. Additional site details are described in Chapter 2.

Four area classes were defined by breaks in plot or catchment contributing area so that similar areas fell into the same area class. Breaks between area classes were: 80 m^2, 0.1 ha, and 10 ha (Table 2). The smallest two classes (area < 80 m^2 and 80 m^2 < area < 1000 m^2) were non-convergent and each site included at least one of these area classes (Table 2). The two larger classes (0.1 ha < area < 10 ha and area >10 ha) were convergent hillslopes or catchments and each site also included at least one of these larger classes (Table 2). Well-defined channels were present in the catchments in the two largest classes, except for the plots in the 0.1 ha – 10 ha class at the Bobcat site. The Wallow catchment was unique in that it was

only partly (~50%) burned at high severity, with an additional 20% of the area burned at low or moderate severity (USDA Forest Service, 2011), and it historically had runoff through most of the year (Heede, 1985). Each of the other plots and catchments in each site was burned at high severity (Parsons et al., 2010) and had only ephemeral runoff.

Sediment yields in the smallest plots were measured using silt fences (Robichaud and Brown, 2002). The sediment yields in the catchments were measured using weirs made of wood and geotextile (Twitchell) (Storrar, 2013), galvanized sheet metal (North 25, Valley, and Hayman) (Robichaud, 2005) or concrete (Wallow). The accumulated sediment in the silt fences was weighed on site and subsampled for gravimetric soil moisture content. Sediment volume in the weirs was calculated from repeat surveys and sampled for bulk density. Dry sediment mass was calculated from the field-measured weights or volumes, and the soil moisture content or bulk density. Sediment yields were the dry sediment mass divided by the planimetric contributing area at the weir or silt fence.

Multiple tipping bucket rain gages were located at all sites except North 25, which had just one. Storm events were separated by a 6-hr period with no rainfall and summarized by the event total rainfall (mm), maximum 10-min, 30-min, and 60-min rainfall intensities (I_{10}, I_{30}, and I_{60}, respectively) (mm hr^{-1}). Sediment yields at all scales were measured on an event basis as much as feasible, but in several cases the sediment yields spanned multiple rainfall events. For these events the sum of the rainfall and the maximum rainfall intensity that occurred between site visits was associated with each sediment yield value. Ground cover was measured in late summer or early fall using point-intercept classification methods on transects or quadrats within each study catchment or plot. The ground cover in the Wallow catchment was measured in areas of high burn severity.

Analysis

The sediment delivery ratio was calculated for sites with plots nested within catchments (North 25, Twitchell, and Wallow) (Table 2), and was the catchment sediment yield divided by the plot sediment yield. Similarly, the area ratio and length ratio were the ratios of the catchment value to those of the plot.

Repeated-measures linear mixed effects models were used to assess differences in non-zero sediment yields and sediment delivery ratios among sites, area classes, and controlling site characteristics (SAS Institute, 2008). The "subject" of the repeated measures analysis was the individual plot or catchment, and the serial correlation among measurements was modeled using a spatial power function on the number of days between the start of the fire and the sediment-producing event (Littell et al., 2006). The sediment yields and sediment delivery ratios were log-transformed prior to statistical analysis to improve the normality of the statistical models' residuals, while the contributing areas and area ratios were log-transformed to improve the graphical presentation and increase the precision of the model's estimates. Forward selection was used to decide whether to include significant predictor variables in the statistical models. The post-fire year was a categorical variable and continuous variables included: I_{10}, I_{30}, and I_{60}; event rainfall; ground cover; slope; relief; and planimetric plot or channel length. None of the predictor variables were controlled. If multiple rainfall characteristics were significant, only the most significant was included in the model. Models were run for all sites combined and by site to distinguish specific site responses. Relationships between sediment yields and individual predictor variables were developed using the model coefficients and the average values for the other predictor variables. The significance level was 0.05 for all analyses.

Only the events that occurred in the first two post-fire years were used for analysis of the sediment yield data for two reasons: few data were available for later post-fire years; and there is some indication that post-fire sediment yields decline considerably after the second post-fire year (Robichaud et al., 2013c). The North 25 second post-fire year data were not included in above analysis because there was no sediment produced at the larger scale.

The contributing area classes were used to assess the effects of contributing area and rainfall intensity on sediment yields using repeated-measures models with the same structure as described above. This model related event sediment yields to I_{10} by area class.

Results

Factors affecting event sediment yields

Statistical modeling showed the event sediment yields within the first two post-fire years were affected by the time since burning (post-fire year), the plot contributing area, the amount of ground cover, and the rainfall intensity (Table 3). The differences among post-fire years were described by the different intercepts in the linear models as the slopes for the continuous predictor variables (log(area), ground cover, and I_{10}) did not significantly vary across post-fire years. The intercepts for the fire year and the first post-fire year did not differ from each other or from zero (Table 3), but the intercept for the second post-fire year (-0.43) was significantly lower. The lower intercept reflects lower sediment yields in the second post-fire year as the sites began to recover (Figure 2).

The modeled slope terms (Table 3) showed the event unit-area sediment yields decreased significantly with increasing area (Figure 2) and ground cover (Figure 3) and increased significantly with increasing event I_{10} (Figure 4). These coefficients were used to

develop an exponential relationship between event sediment yield, *SY* (Mg ha^{-1}), contributing area (m^2), and the other significant variables for each post-fire year:

$$SY = k_i Area^{-0.25} \quad (1)$$

where k_i was the combined coefficient that accounted for the ground cover, I_{10}, and model intercept. The k_i was

$$k_i = 10^{-0.015C_n + 0.045I_i + b_n} \quad (2)$$

where I_i was the I_{10} of the i^{th} event (mm hr^{-1}); C_n was the ground cover (%) for the n^{th} year; and b_n was the intercept for the n^{th} year (Table 3). The k_i values across all sites and events were 5.62 for the year of the fire, 4.57 for the first post-fire year, and 1.35 for the second post-fire year (Figure 2).

Site differences in factors affecting sediment yields

Some of the modeled slope terms differed across sites (Table 3). The slope for log(area) for the Bobcat site was more negative (-0.74) than the log(area) slope for all sites (-0.25), indicating the sediment delivery rates decreased more steeply across the range of contributing areas at this site as compared to all sites combined, and this may have been due to the lack of channelization in the larger plots at this site (Table 3). In contrast, the log(area) slope for the Hayman site (0.076) was greater than the slope for the combined sites (-0.25) (Table 3). More importantly, this term was not significantly different than zero, which indicates the unit-area sediment yields did not vary within the range of contributing areas at the Hayman site. The log(area) slope terms for the other three sites where confidence limits were estimable were no different than the slope for the combined model (Table 3).

The ground cover slope was larger at the Twitchell site (0.0074) and more negative at the Wallow site (-0.031) as compared to the combined-sites value (-0.015) (Table 3). The Twitchell site had very high sediment yields in some of the plots with high ground cover, especially in the second post-fire year when high intensity rain events (I_{10} up to 61 mm hr^{-1}) produced large sediment yields (up to 63 Mg ha^{-1}) (Figures 3 and 4). The ground cover increased in the first post-fire year at the Wallow site (average 55%), which led to relatively low sediment yields (Figure 3) and the corresponding steep negative slope for ground cover at this site (-0.031) (Table 3). The Valley site also had a relatively steep negative slope (-0.045) for ground cover but this value was not significantly different than the value for all sites combined.

Five of the six sites had modeled slopes for the I_{10} term that were between 0.036 and 0.054, and the value (-0.0043) for the sixth site (North 25) was not significantly different than the value for the combined-sites (0.045) (Table 3). The negative I_{10} slope term with a wide confidence interval at North 25 was related to two relatively large sediment yields (averaging 16–20 Mg ha^{-1} in affected plots) from two relatively low intensity rain events (I_{10} values of 11–13 mm hr^{-1}) in the first post-fire year (Robichaud et al., 2006). The model intercepts differed across sites as well as among post-fire years (Table 3), and we attribute these differences to the different modeled slope terms for log(area), ground cover, and I_{10} at the different sites.

Contributing area and rainfall intensity as controls on sediment yields

The contributing area and the I_{10} were the most significant predictor variables in the statistical models described above. When the sediment yield data were separated by the

contributing area classes, there were positive relationships between sediment yield and I_{10} across all area classes, and the slopes were significantly greater than zero for all but the largest area class (>10 ha) (Figure 5). The largest area class had the lowest sediment yields, and the sediment yield-I_{10} slope for this class (0.016) was lower than the slope for the two middle classes (0.046–0.053) although it was not significantly different than the slope for the smallest area class (0.035) because of the small number of observations in the largest area class.

Post-fire sediment delivery ratios

The event-based sediment delivery ratios in the sites with nested plots (North 25, Twitchell, and Wallow) ranged from to 0.0016 to 4.0 for the 126 events with data at multiple scales (Figure 6). The sediment delivery ratio declined as both the length ratio and the area ratio between plots increased, but the length ratio was a more significant factor (F = 53) than the log-transformed area ratio (F = 42). This means that as the length ratio and therefore the distance downstream increased, the amount of sediment delivered decreased. The equation for the relationship between post-fire sediment delivery ratio (SDR) and length ratio (LR) was

$$\log(SDR) = -0.62 - 0.0078LR\,. \qquad (3)$$

The annual sediment delivery ratios (Figure 7) had a smaller range (0.0089 to 1.02) than the event based ratios (Figure 6). The modeled line between the annual sediment delivery ratio and length ratio was similar to that of the event-based sediment delivery ratio except that the slope was steeper in the annual model (Figure 7).

Discussion

Spatial scales and processes

The contributing area, time since burning, and rainfall intensity are three scalar controls on post-fire sediment yields. The area above a point in the hillslope or catchment controlled the sediment delivery at that point under given rainfall and post-fire conditions, as described by (Eq. 1). The downstream reduction in sediment delivery also was affected by the length of the plot—which was correlated to the area of the plots because of the small range in plot widths in the sites with plots nested within catchments—with significantly less sediment delivery as the catchment length increased relative to the plot length (Figure 6). Assuming constant variability in infiltration, roughness properties, and microrelief, the flow path length indirectly controls the likelihood of the runoff infiltrating, encountering increased resistance to flow, or being held in detention storage, and thereby controls the connectivity of runoff (Bracken and Croke, 2007; Mayor et al., 2008) and the resultant ability of the runoff to transport sediment.

The spatial scales addressed in the current study (20 m^2 – 117 ha) comprise several major processes of fluvial sediment transport. Rainsplash is a dominant process at scales on the order of a meter (Planchon and Mouche, 2010), but the soil detached during rainsplash is an important sediment source for sediment delivery at larger spatial scales, including sheetwash (Fox and Bryan, 1999; Morgan, 1978; Young and Wiersma, 1973), and rilling (Asadi et al., 2007; McGuire et al., 2013). Rainsplash also increases sealing on bare soil (Bradford et al., 1987; Bryan, 2000; Larsen et al., 2009), thereby increasing runoff and providing a positive erosion feedback because of the deeper flow if no protective crust forms. Sheetwash dominates sediment transport on non-convergent slopes (Montgomery and

Dietrich, 1994) but it produces less erosion than rainsplash at finer scales or rilling at larger scales (Bryan, 2000).

Rills were observed in some of the smallest hillslope plots and in many of the larger hillslope plots and catchments. Rilling is the dominant hillslope erosion mechanism in burned areas (Larsen et al., 2009; Moody and Kinner, 2006; Moody and Martin, 2001a; Pietraszek, 2006; Robichaud et al., 2010) and the apparent increase in sediment delivery with increasing area at the hillslope scale has been attributed to rill erosion (Parsons et al., 2006a). Hillslope surface roughness partly controls the resultant rill pattern (Favis-Mortlock et al., 2000), and smoother slopes that are commonly found in recently burned areas would tend to have parallel rather than dendritic drainage patterns (McGuire et al., 2013) and therefore shorter flow paths, steeper gradients, increased energy for erosion and sediment transport, and increased sediment delivery potential.

Small gullies were also observed at some of the sites. Gullies can be a significant source of sediment in burned areas (Istanbulluoglu et al., 2002) as well as an efficient pathway for post-fire sediment transport (Blake et al., 2009). De Vente and Poesen (2005) suggest a critical-area threshold for gully formation in unburned areas of 3 ha, whereas reports from burned areas suggest this threshold might be on the order of 0.1 to 0.2 ha (Moody and Kinner, 2006). Gully assessments in burned areas indicate the degree of burn severity and rainfall intensity are important factors for reactivation of gullies (Hyde et al., 2007) and that rilling may lead to debris flows and leave deep gullies in burned areas (Gabet and Bookter, 2008).

Channel erosion and sediment transport and deposition are the dominant sediment delivery processes at larger spatial scales (De Vente and Poesen, 2005). At the largest scales

in our study, we observed channel processes including incision and bank erosion, deposition in point bars and associated with woody debris jams, and energy dissipation associated with roughness elements including boulders, tree roots, and channel steps. Rapid, large-scale channel incision via flood or debris flows commonly cited in the post-fire literature (Benda et al., 2003; Cannon and Reneau, 2000; Cannon et al., 2001a, 2001b; Gabet and Bookter, 2008; Legleiter et al., 2003; Meyer and Wells, 1997; Santi et al., 2008; Shakesby and Doerr, 2006) did not occur uniformly at any of the six study sites, but there were several instances of local channel scour.

Effect of time on post-fire sediment delivery

Our event-based sediment delivery ratios spanned at least two orders of magnitude at the Twitchell and Wallow sites (Figure 6). The annual sediment delivery ratios were less variable, indicating the importance of the selected time scale in the accounting for the sediment delivery rates (Keller et al., 1997; Moody and Martin, 2001a). This result also demonstrates the variability in post-fire delivery ratios and their dependence on site conditions including vegetation, flow path length, rainfall intensity, and factors not explicitly measured here such as runoff rate and duration, channel confinement and geologic parent material. A few other studies have addressed the potential time scale of post-fire sediment delivery, and these have estimated that sediment delivered to main stem channels may remain there for years (Kunze and Stednick, 2006; Reneau et al., 2007), decades (Heede et al., 1988; Mayor et al., 2007), or longer (Meyer et al., 1992; Moody and Martin, 2001a).

The time since burning (post-fire year), which has been shown to be a control on sediment yields in earlier studies (Cerdà and Doerr, 2005; Helvey, 1980; Mayor et al., 2007;

Morris and Moses, 1987; Pierson et al., 2008; Robichaud et al., 2008b, 2013a, 2013c; Wagenbrenner et al., 2006), is an indirect measure of vegetative and hydrologic recovery. Ground cover increases at different rates across different ecosystems, and this can be seen by the relatively broad range of cover values over the two post-fire years (Figure 3). Increases in vegetation and litter cover in later post-fire years (e.g., Figure 3) directly reduce rain drop impact on the soil surface, and thereby lead to lower rates of splash erosion (Planchon and Mouche, 2010). Reduced rain drop impact also results in higher infiltration and lower overland flow rates (Cerdà and Doerr, 2005; Johansen et al., 2001; Pierson et al., 2009). Ground cover also increase surface roughness and so may increase the flow path length (McGuire et al., 2013) and reduce runoff velocity and sediment transport capacity (Robichaud et al., 2010, 2013b). The sediment supply on hillslopes may become source limited as sediment-producing events occur (Smith and Dragovich, 2008), and this may lead to lower sediment yields with the occurrence of subsequent erosional events.

Effect of rainfall intensity on sediment delivery

The third scalar control on sediment delivery, rainfall intensity, indirectly measures the amount of energy conveyed by rainfall to the soil surface, and thereby controls rain splash erosion rates (Dunkerley, 2008; Young and Wiersma, 1973). Rainfall intensity also affects the amount of surface runoff that is generated via infiltration excess overland flow and the amount of rill erosion on hillslopes (Berger et al., 2010) as well as peak discharge rates (Moody and Martin, 2001b) and suspended sediment loads (Kunze and Stednick, 2006) in burned areas. The sediment-producing events were almost all very local, high-intensity, convective storms. In our analysis of the sediment yield-I_{10} relationship across area classes

(Figure 5) the largest area class had the lowest slope. The lower slope suggests the rainfall intensity was less of a control on sediment yields at the largest (>10 ha) scale, and this may be related to the relatively small spatial extent of the convective storms relative to the burned catchments.

Other considerations

The spatial extent of the rain storm relative to the burned area of interest influences the connectivity of post-fire runoff and sediment delivery. The severity and size of burned patches affect the amount of runoff and sediment generated (Benavides-Solorio and MacDonald, 2001, 2005; DeBano et al., 1998; Moody et al., 2008b; Robichaud et al., 2010; Turner et al., 1994), and the severity, size, and spatial arrangement of burned patches control the downstream transport of runoff and sediment (Bracken and Croke, 2007; Mayor et al., 2011). The spatial extent of rain storms interacts with the patch size and connectivity of burned areas to control the amount of runoff and sediment delivery. Surface runoff generated by intense rainstorms that are smaller than the burned patch (or catchment) may infiltrate soil downstream of the storm or patch, resulting in low sediment delivery rates. Conversely, surface runoff generated by intense rainstorms that are larger than the burned patch (or catchment) will be less likely to infiltrate downstream and will therefore increase sediment delivery.

The Hayman site appears unique among these six sites in that the sediment yields did not decline with increasing contributing area (Table 3) and that little reduction in sediment yield occurred over the first two post-fire years. The underlying geology varied among the six sites (Table 1) but the Pike's Peak Batholith at the Hayman site weathers to grüs (Moody

and Kinner, 2006). This gravelly soil has relatively high infiltration rates in unburned conditions (Graham, 2003) but has low vegetative recovery rates (Robichaud et al., 2013a) and can produce high runoff rates and become very mobile in post-fire conditions (Moody and Martin, 2001a; Robichaud et al., 2013c). The highly mobile soil may have contributed to greater rill erosion rates in the catchments at this site compared to the other sites and thus the lack of a relationship between contributing area and sediment yields (Robichaud et al., 2013c; de Vente et al., 2007).

The Hayman results demonstrate that the post-fire sediment delivery rates across scales will depend on specific site factors such as soil properties or parent material and other hydrologic characteristics as they do in unburned catchments (Lu et al., 2005; de Vente and Poesen, 2005; Walling, 1983). Other limitations on the use of the sediment delivery ratio, especially the lack of specific description of the erosion, transport, and deposition processes, have been well described (Parsons et al., 2006b; Walling, 1983). However, despite the lack of accounting for processes in the sediment delivery ratio, this approach can be used to estimate the downstream post-fire sediment delivery rates from values measured in small monitoring plots or predicted by hillslope erosion models.

Future research should address physical processes so that we can better understand and physically model downstream post-fire sediment delivery. There are several immediate research needs including: the identification of sediment sources, possibly using tracer methods (Blake et al., 2009; Smith et al., 2013); defining the key physical controls on sediment delivery in burned catchments; establishing explicit rainfall-runoff responses for burned areas (Moody and Martin, 2001b; Moody et al., 2008b, 2013); addressing the

connectivity in runoff given the patchiness of burned areas; and the changes of these processes and controls during the post-fire recovery period.

Conclusions

Six sites with plot and catchment measurements were used to develop and test statistical relationships between post-fire sediment yields, rainfall metrics, and site characteristics. The contributing areas ranged from 20 m^2 to 117 ha. The sediment yields significantly decreased with increasing contributing area at all but one site. The sediment yields also were positively related to rainfall intensity and negatively related to ground cover, as has been shown in previous studies. The sediment delivery ratios in the sites with nested plots decreased significantly as the difference in size between the plot and catchment increased and the ratio of lengths more significantly affected the delivery ratio than the ratio of areas. An equation relating sediment yield to controlling site factors and rainfall intensity and a second equation relating sediment delivery ratio to length ratio were developed from the measured data. These results will help constrain estimates of catchment-scale post-fire sediment delivery rates developed from hillslope measurements or models.

Acknowledgments

This work was supported in part by a National Needs Fellowship grant from the US Department of Agriculture, National Institute of Foods and Agriculture, under agreement no. 2008-38420-04761. Additional funding was provided by the US Department of Agriculture Forest Service: Rocky Mountain Research Station; Pike-San Isabel National Forest; Apache-Sitgreaves National Forest; and Fishlake National Forest. We thank the employees from the

above Forest Service offices as well as the Arapahoe-Roosevelt, Bitterroot, and Okanagan-Wenatchee National Forests for their assistance in data collection and processing. We appreciate early discussions with Lee MacDonald, Isaac Larsen, and Peter Nelson that helped focus this study.

References

Arkell RE, Richards F. 1986. Short duration rainfall relations for the western United States. In Proceedings of the Conference on Climate and Water Management-A Critical Era and Conference on the Human Consequences of 1985's Climate ,. American Meteorological Society: Boston; 136–141.

Asadi H, Ghadiri H, Rose CW, Rouhipour H. 2007. Interrill soil erosion processes and their interaction on low slopes. Earth Surface Processes and Landforms **32** : 711–724. DOI: 10.1002/esp.1426

Benavides-Solorio JD, MacDonald LH. 2001. Post-fire runoff and erosion from simulated rainfall on small plots, Colorado Front Range. Hydrological Processes **15** : 2931–2952. DOI: 10.1002/hyp.383

Benavides-Solorio JD, MacDonald LH. 2005. Measurement and prediction of post-fire erosion at the hillslope scale, Colorado Front Range. International Journal of Wildland Fire **14**: 457–474. DOI: 10.1071/WF05042

Benda LE, Miller D, Bigelow P, Andras K. 2003. Effects of post-wildfire erosion on channel environments, Boise River, Idaho. Forest Ecology and Management **178** : 105–119.

Berger C, Schulze M, Rieke-Zapp D, Schlunegger F. 2010. Rill development and soil erosion: a laboratory study of slope and rainfall intensity. Earth Surface Processes and Landforms **35**: 1456–1467. DOI: 10.1002/esp.1989

Blake WH, Wallbrink PJ, Wilkinson SN, Humphreys GS, Doerr SH, Shakesby RA, Tomkins KM. 2009. Deriving hillslope sediment budgets in wildfire-affected forests using fallout radionuclide tracers. Geomorphology **104** : 105–116.

Bonnin GM, Martin D, Lin B, Parzybok T, Yekta M, Riley D. 2004. NOAA atlas 14: Precipitation-frequency atlas of the United States, volume 1, version 5, semiarid Southwest (Arizona, southeast California, Nevada, New Mexico, Utah) . Silver Spring, MD

Bracken LJ, Croke J. 2007. The concept of hydrological connectivity and its contribution to understanding runoff-dominated geomorphic systems. Hydrological Processes **21** : 1749–1763. DOI: 10.1002/hyp.6313

Bradford JM, Ferris JE, Remley PA. 1987. Interrill soil erosion processes: I. Effect of surface sealing. Soil Science Society of America Journal **51** : 1566–1571.

Brown JAH. 1972. Hydrologic effects of a bushfire in a catchment in south-eastern New South Wales. Journal of Hydrology **15** : 77–96.

Bryan RB. 2000. Soil erodibility and processes of water erosion on hillslope. Geomorphology **32** : 385–415.

Cannon SH, Bigio ER, Mine E. 2001a. A process for fire-related debris flow initiation, Cerro Grande fire, New Mexico. Hydrological Processes **15** : 3011–3023. DOI: 10.1002/hyp.388

Cannon SH, Kirkham RM, Parise M. 2001b. Wildfire-related debris-flow initiation processes, Storm King Mountain, Colorado. Geomorphology **39** : 171–188.

Cannon SH, Reneau SL. 2000. Conditions for generation of fire-related debris flows, Capulin Canyon, New Mexico. Earth Surface Processes and Landforms **25** : 1103–1121.

Cerdà A, Doerr SH. 2005. The influence of vegetation recovery on soil hydrology and erodibility following fire: an eleven-year investigation. International Journal of Wildland Fire **14** : 1–24.

DeBano LF, Neary DG, Ffolliott PF. 1998. Fire's Effects on Ecosystems . Wiley: New York

Desilets SLE, Nijssen B, Ekwurzel B, Ferré TPA. 2007. Post-wildfire changes in suspended sediment rating curves: Sabino Canyon, Arizona. Hydrological Processes **21** : 1413–1423. DOI: 10.1002/hyp.6352

Doerr SH, Shakesby RA, Blake WH, Chafer CJ, Humphreys GS, Wallbrink PJ. 2006. Effects of differing wildfire severities on soil wettability and implications for hydrological response. Journal of Hydrology **319** : 295–311.

Dunkerley D. 2008. Rain event properties in nature and in rainfall simulation experiments: A comparative review with recommendations for increasingly systematic study and reporting. Hydrological Processes **22** : 4415–4435. DOI: 10.1002/hyp.7045

Ebel BA, Moody JA, Martin DA. 2012. Hydrologic conditions controlling runoff generation immediately after wildfire. Water Resources Research **48** : 1–13. DOI: 10.1029/2011WR011470

Favis-Mortlock DT, Boardman J, Parsons AJ, Lascelles B. 2000. Emergence and erosion: A model for rill initiation and development. Hydrological Processes **14** : 2173–2205.

Ferreira AJD, Coelho C de OA, Ritsema CJ, Boulet A-K, Keizer JJ. 2008. Soil and water degradation processes in burned areas: Lessons learned from a nested approach. Catena **74**: 273–285. DOI: 10.1016/j.catena.2008.05.007

Fox DM, Bryan RB. 1999. The relationship of soil loss by interrill erosion to slope gradient. Catena **38** : 211–222.

Gabet EJ, Bookter A. 2008. A morphometric analysis of gullies scoured by post-fire progressively bulked debris flows in southwest Montana, USA. Geomorphology **96** : 298–309.

Graham RT (ed). 2003. Hayman fire case study. General Technical Report RMRS-GTR-114 . USDA Forest Service, Rocky Mountain Research Station: Fort Collins, Colorado

Heede BH. 1985. Channel adjustments to the removal of log steps: an experiment in a mountain stream. Environmental Management **9** : 427–432.

Heede BH, Harvey MD, Laird JR. 1988. Sediment delivery linkages in a chaparral watershed following a wildfire. Environmental Management **12** : 349–358. DOI: 10.1007/BF01867524

Helvey JD. 1980. Effects of a north central Washington wildfire on runoff and sediment production. Journal of the American Water Resources Association **16** : 627–634. DOI: 10.1111/j.1752-1688.1980.tb02441.x

Hyde K, Woods SW, Donahue J. 2007. Predicting gully rejuvenation after wildfire using remotely sensed burn severity data. Geomorphology **86** : 496–511. DOI: 10.1016/j.geomorph.2006.10.012

Istanbulluoglu E, Tarboton DG, Pack RT, Luce C. 2002. A probabilistic approach for channel initiation. Water Resources Research **38** : 1325. DOI: 10.1029/2001wr000782

Johansen MP, Hakonson TE, Breshears DD. 2001. Post-fire runoff and erosion from rainfall simulation: contrasting forests with shrublands and grasslands. Hydrological Processes **15**: 2953–2965. DOI: 10.1002/hyp.384

Keeley JE. 2009. Fire intensity, fire severity and burn severity: a brief review and suggested usage. International Journal of Wildland Fire **18** : 116–126. DOI: 10.1071/WF07049

Keller EA, Valentine DW, Gibbs DR. 1997. Hydrological response of small watersheds following the southern California Painted Cave fire of June 1990. Hydrological Processes **11**: 401–414.

Kunze MD, Stednick JD. 2006. Streamflow and suspended sediment yield following the 2000 Bobcat fire, Colorado. Hydrological Processes **20** : 1661–1681. DOI: 10.1002/hyp.5954

Lane PNJ, Sheridan GJ, Noske PJ. 2006. Changes in sediment loads and discharge from small mountain catchments following wildfire in south eastern Australia. Journal of Hydrology **331**: 495–510.

Lanini JS, Clark EA, Lettenmaier DP. 2009. Effects of fire-precipitation timing and regime on post-fire sediment delivery in Pacific Northwest forests. Geophysical Research Letters **36**: L01402. DOI: 10.1029/2008gl034588

Larsen IJ, MacDonald LH, Brown E, Rough D, Welsh MJ, Pietraszek JH, Libohova Z, Benavides-Solorio JD, Schaffrath K. 2009. Causes of post-fire runoff and erosion; water repellency, cover, or soil sealing? Soil Science Society of America Journal **73** : 1393–1407. DOI: 10.2136/sssaj2007.0432

Legleiter CJ, Lawrence RL, Fonstad MA, Marcus WA, Aspinall R. 2003. Fluvial response a decade after wildfire in the northern Yellowstone ecosystem: a spatially explicit analysis. Geomorphology **54** : 119–136.

Littell RC, Milliken G, Stroup W, Wolfinger R, Schabenberger O. 2006. SAS for Mixed Models, 2nd ed. SAS Institute, Inc.: Cary, North Carolina

Lu H, Moran CJ, Sivapalan M. 2005. A theoretical exploration of catchment-scale sediment delivery. Water Resources Research **41** : W09415. DOI: 10.1029/2005WR004018

Malmon D V., Reneau SL, Katzman D, Lavine A, Lyman J. 2007. Suspended sediment transport in an ephemeral stream following wildfire. Journal of Geophysical Research **112**: F02006. DOI: 10.1029/2005jf000459

Martin DA, Moody JA. 2001. Comparison of soil infiltration rates in burned and unburned mountainous watersheds. Hydrological Processes **15** : 2893–2903. DOI: 10.1002/hyp.380

Mayor ÁG, Bautista S, Bellot J. 2011. Scale-dependent variation in runoff and sediment yield in a semiarid Mediterranean catchment. Journal of Hydrology **397** : 128–135. DOI: 10.1016/j.jhydrol.2010.11.039

Mayor ÁG, Bautista S, Llovet J, Bellot J. 2007. Post-fire hydrological and erosional responses of a Mediterranean landscape: Seven years of catchment-scale dynamics. Catena **71** : 68–75.

Mayor ÁG, Bautista S, Small EE, Dixon M, Bellot J. 2008. Measurement of the connectivity of runoff source areas as determined by vegetation pattern and topography: A tool for assessing potential water and soil losses in drylands. Water Resources Research **44** : W10423. DOI: 10.1029/2007WR006367

McGuire LA, Pelletier JD, Gómez JA, Nearing MA. 2013. Controls on the spacing and geometry of rill networks on hillslopes: Rain splash detachment, initial hillslope roughness, and the competition between fluvial and colluvial transport. Journal of Geophysical Research: Earth Surface DOI: 10.1002/jgrf.20028

Meyer GA, Wells SG. 1997. Fire-related sedimentation events on alluvial fans, Yellowstone National Park, U.S.A. Journal of Sedimentary Research **67** : 776–791. DOI: 10.1306/d426863a-2b26-11d7-8648000102c1865d

Meyer GA, Wells SG, Balling Jr. RC, Jull AJT. 1992. Response of alluvial systems to fire and climate change in Yellowstone National Park. Nature **357** : 147–150.

Miller JF, Frederick RH, Tracey RJ. 1973. NOAA atlas 2: Precipitation-frequency atlas of the western United States . Silver Spring, Maryland

Montgomery DR, Dietrich WE. 1994. Landscape dissection and drainage area-slope thresholds. In Process Models and Theoretical Geomorphology , Kirkby MJ (ed). John Wiley & Sons, Ltd.: Chichester; 221–246.

Moody JA, Kinner DA. 2006. Spatial structures of stream and hillslope drainage networks following gully erosion after wildfire. Earth Surface Processes and Landforms **31** : 319–337. DOI: 10.1002/esp.1246

Moody JA, Martin DA. 2001a. Initial hydrologic and geomorphic response following a wildfire in the Colorado Front Range. Earth Surface Processes and Landforms **26** : 1049–1070. DOI: 10.1002/esp.253

Moody JA, Martin DA. 2001b. Post-fire, rainfall intensity-peak discharge relations for three mountainous watersheds in the western USA. Hydrological Processes **15** : 2981–2993. DOI: 10.1002/hyp.386

Moody JA, Martin DA. 2009. Synthesis of sediment yields after wildland fire in different rainfall regimes in the western United States. International Journal of Wildland Fire **18** : 96–115. DOI: 10.1071/WF07162

Moody JA, Martin DA, Cannon SH. 2008a. Post-wildfire erosion response in two geologic terrains in the western USA. Geomorphology **95** : 103–118.

Moody JA, Martin DA, Haire SL, Kinner DA. 2008b. Linking runoff response to burn severity after a wildfire. Hydrological Processes **22** : 2063–2074. DOI: 10.1002/hyp.6806

Moody JA, Shakesby RA, Robichaud PR, Cannon SH, Martin DA. 2013. Current research issues related to post-wildfire runoff and erosion processes

Morgan RPC. 1978. Field studies of rainsplash erosion. Earth Surface Processes **3** : 295–299.

Morris SE, Moses TA. 1987. Forest fire and the natural soil erosion regime in the Colorado Front Range. Annals of the Association of American Geographers **77** : 245–254.

Noske PJ, Lane PNJ, Sheridan GJ. 2010. Stream exports of coarse matter and phosphorus following wildfire in NE Victoria, Australia. Hydrological Processes **24** : 1514–1529. DOI: 10.1002/hyp.7616

Parsons A, Robichaud PR, Lewis SA, Napper C, Clark JT. 2010. Field guide for mapping post-fire soil burn severity, General Technical Report RMRS-GTR-243. US Department of Agriculture, Forest Service, Rocky Mountain Research Station: Fort Collins, Colorado

Parsons AJ, Brazier RE, Wainwright J, Powell DM. 2006a. Scale relationships in hillslope runoff and erosion. Earth Surface Processes and Landforms **31** : 1384–1393. DOI: 10.1002/esp.1345

Parsons AJ, Wainwright J, Brazier RE, Powell DM. 2006b. Is sediment delivery a fallacy? Earth Surface Processes and Landforms **1328** : 1297–1308. DOI: 10.1002/esp.1395

Pierson FB, Moffet CA, Williams CJ, Hardegree SP, Clark PE. 2009. Prescribed-fire effects on rill and interrill runoff. Earth Surface Processes and Landforms **34** : 193–203. DOI: 10.1002/esp.1703

Pierson FB, Robichaud PR, Moffet CA, Spaeth KE, Hardegree SP, Clark PE, Williams CJ. 2008. Fire effects on rangeland hydrology and erosion in a steep sagebrush-dominated landscape. Hydrological Processes **22** : 2916–2929.

Pietraszek JH. 2006. Controls on post-fire erosion at the hillslope scale, 124 pp., Colorado State University: Fort Collins, Colorado

Planchon O, Mouche E. 2010. A Physical Model for the Action of Raindrop Erosion on Soil Microtopography. Soil Science Society of America Journal **74** : 1092. DOI: 10.2136/sssaj2009.0063

Prosser IP, Williams L. 1998. The effect of wildfire on runoff and erosion in native Eucalyptus forest. Hydrological Processes **12** : 251–265.

Reneau SL, Katzman D, Kuyumjian GA, Lavine A, Malmon D V. 2007. Sediment delivery after a wildfire. Geology **35** : 151–154. DOI: 10.1130/g23288a.1

Robichaud PR. 2000. Fire effects on infiltration rates after prescribed fire in Northern Rocky Mountain forests, USA. Journal of Hydrology **231–232** : 220–229.

Robichaud PR. 2005. Measurement of post-fire hillslope erosion to evaluate and model rehabilitation treatment effectiveness and recovery. International Journal of Wildland Fire **14**: 475–485. DOI: 10.1071/WF05031

Robichaud PR, Brown RE. 2002. Silt fences: an economical technique for measuring hillslope soil erosion, General Technical Report RM-GTR-94 . USDA Forest Service, Rocky Mountain Research Station: Ft. Collins, Colorado

Robichaud PR, Lewis SA, Wagenbrenner JW, Ashmun LE, Brown RE. 2013a. Post-fire mulching for runoff and erosion mitigation Part I: Effectiveness at reducing hillslope erosion rates. Catena **105** : 75–92. DOI: 10.1016/j.catena.2012.11.015

Robichaud PR, Lillybridge TR, Wagenbrenner JW. 2006. Effects of postfire seeding and fertilizing on hillslope erosion in north-central Washington, USA. Catena **67** : 56–67. DOI: 10.1016/j.catena.2006.03.001

Robichaud PR, Pierson FB, Brown RE, Wagenbrenner JW. 2008a. Measuring effectiveness of three postfire hillslope erosion barrier treatments, western Montana, USA. Hydrological Processes **22** : 159–170. DOI: 10.1002/Hyp.6558

Robichaud PR, Jordan P, Lewis SL, Ashmun LE, Covert SA, Brown RE. 2013b. Evaluating the effectiveness of wood shreds and agricultural straw mulches as a treatment to reduce post-fire hillslope erosion in southern British Columbia, Canada. Geomorphology. DOI: 10.1016/j.geomorph.2013.04.024

Robichaud PR, Wagenbrenner JW, Brown RE. 2010. Rill erosion in natural and disturbed forests: 1. Measurements. Water Resources Research **46** : W10506. DOI: 10.1029/2009wr008314

Robichaud PR, Wagenbrenner JW, Brown RE, Wohlgemuth PM, Beyers JL. 2008b. Evaluating the effectiveness of contour-felled log erosion barriers as a post-fire runoff and erosion mitigation treatment in the western United States. International Journal of Wildland Fire **17** : 255–273. DOI: 10.1071/Wf07032

Robichaud PR, Wagenbrenner JW, Scholes SL, Brown RE, Wohlgemuth PM, Ashmun LE. 2013c. Post-fire mulching for runoff and erosion mitigation Part II: Effectiveness in reducing runoff and sediment yields from small catchments. Catena **105** : 93–111. DOI: 10.1016/j.catena.2012.11.016

Rowe PB, Countryman CM, Storey HC. 1954. Hydrologic analysis used to determine effects of fire on peak discharges and erosion rates in southern California watersheds . USDA Forest Service, California Forest and Range Experiment Station: Berkeley, California

Santi PM, DeWolfe VG, Higgins JD, Cannon SH, Gartner JE. 2008. Sources of debris flow material in burned areas. Geomorphology **96** : 310–321.

SAS Institute. 2008. SAS version 9.2. SAS Institute, Inc.: Cary, North Carolina

Shakesby RA, Doerr SH. 2006. Wildfire as a hydrological and geomorphological agent. Earth-Science Reviews **74** : 269–307.

Smith HG, Blake WH, Owens PN. 2013. Discriminating fine sediment sources and the application of sediment tracers in burned catchments: a review. Hydrological Processes **27**: 943–958. DOI: 10.1002/hyp.9537

Smith HG, Dragovich D. 2008. Post-fire hillslope erosion response in a sub-alpine environment, south-eastern Australia. Catena **73** : 274–285. DOI: 10.1016/j.catena.2007.11.003

Spigel KM, Robichaud PR. 2007. First-year post-fire erosion rates in Bitterroot National Forest, Montana. Hydrological Processes **21** : 998–1005. DOI: 10.1002/Hyp.6295

Storrar KA. 2013. Effectiveness of straw bale check dams at reducing post-fire sediment erosion from ephemeral channel catchments, University of Montana

Swanson FJ. 1981. Fire and geomorphic processes. 401–420 pp.

Troendle CA, Bevenger GS. 1996. Effect of fire on streamflow and sediment transport in Shoshone National Forest, Wyoming. In The ecological implications of fire in greater Yellowstone , Greenlee JM (ed). International Association of Wildland Fire: Fairfield, Washington; 43–52.

Turner MG, Hargrove WW, Gardner RH, Romme WH. 1994. Effects of fire on landscape heterogeneity in Yellowstone National Park, Wyoming. Journal of Vegetation Science **5**: 731–742.

USDA Forest Service. 2011. Wallow Fire soil burn severity map. Apache-Sitgreaves National Forest, Springerville, Arizona

Vega JA, Diaz-Fierros F. 1987. Wildfire effects on soil erosion. Ecologia Mediterranea **13**: 119–125.

De Vente J, Poesen J. 2005. Predicting soil erosion and sediment yield at the basin scale: Scale issues and semi-quantitative models. Earth-Science Reviews **71** : 95–125. DOI: 10.1016/j.earscirev.2005.02.002

De Vente J, Poesen J, Arabkhedri M, Verstraeten G. 2007. The sediment delivery problem revisited. Progress in Physical Geography **31** : 155–178. DOI: 10.1177/0309133307076485

Wagenbrenner JW. 2013. Post-fire stream channel processes: Runoff, sediment delivery, and mitigation, Doctoral dissertation, Washington State University: Pullman, Washington

Wagenbrenner JW, MacDonald LH, Rough D. 2006. Effectiveness of three post-fire rehabilitation treatments in the Colorado Front Range. Hydrological Processes **20** : 2989–3006. DOI: 10.1002/Hyp.6146

Walling DE. 1983. The sediment delivery problem. Journal of Hydrology **65** : 209–237.

Wondzell SM, King JG. 2003. Postfire erosional processes in the Pacific Northwest and Rocky Mountain regions. Forest Ecology and Management **178** : 75–87.

Young RA, Wiersma JL. 1973. The role of rainfall impact in soil detachment and transport. Water Resources Research **9** : 1629–1636.

Table 1. Fire year, post-fire years used in the study, latitude, longitude, elevation, soil texture, geologic parent material, dominant pre-fire vegetation, 2-yr return interval 10-min maximum rainfall intensity (I_{10}), and number of plot-events for each site

Site	Fire year	Post-fire years*	Latitude (°)	Longitude (°)	Elev. (m)	Soil texture	Parent material	Pre-fire vegetation ±	2-yr I_{10} (mm hr^{-1})	*n*
Bobcat[1]	2000	0–2	40.45	-105.35	2300	gravelly sandy loam	schist, gneiss	Mixed: ponderosa pine	52 [7]	89
Hayman[2,3,4]	2002	0–2	39.18	-105.36	2400	gravelly sandy loam	granitic	Mixed: ponderosa pine	56 [7,8]	83
North 25[2,5]	1998	1+	47.99	-120.34	1600	ashy sandy loam	volcanic	Mixed: grand fir	32 [7]	17
Twitchell	2010	1–2	38.53	-112.40	2200	gravelly loam	volcanic tuff and rhyolite	Pinyon pine, juniper, gamble oak	48 [9]	119
Valley[2,7]	2000	1–2	45.91	-114.03	1700	gravelly sandy loam	granitic colluvium	Mixed: Douglas-fir	31 [7]	29
Wallow	2011	0–1	33.66	-109.31	2600	sandy loam	basalt	Mixed: Douglas-fir	81 [9]	58

* Post-fire year 0 is the fire year
+ Data from second post-fire year were not analyzed because no sediment was produced in the catchment.
± "Mixed" indicates mixed conifer forest. In these cases the dominant tree type is indicated.
[1] (Wagenbrenner et al., 2006)
[2] (Robichaud et al., 2008b)
[3] (Robichaud et al., 2013a)
[4] (Robichaud et al., 2013c)
[5] (Robichaud et al., 2006)
[6] (Robichaud et al., 2008a)
[7] (Miller et al., 1973)
[8] (Arkell and Richards, 1986)
[9] (Bonnin et al., 2004)

Table 2. Total number of plots per site (*N*), the number of plots or catchments in each area class (*n*), and minimum and maximum slope (*S*) and length (*L*) for each area class

	Total	Class 1: 20–80 m^2 (non-convergent)			Class 2: 80–1000 m^2 (non-convergent)			Class 3: 0.1 ha–10 ha (convergent, channelized)			Class 4: > 10 ha (convergent, channelized)		
Site	N	*n*	*S* (%)	*L* (m)	*n*	*S* (%)	*L* (m)	*n*	*S* (%)	*L* (m)	*n*	*S* (%)	*L* (m)
Bobcat	12	0			3	28–37	22–48	9[±]	24–60	60–212	0		
Hayman	10	8	19–44	7–14	0			2	31–33	429–452	0		
North 25	9	8[*]	28–54	8–9	0			0			1	50	537
Twitchell	14	5[*]	39–67	9–19	4[*]	25–62	37–64	5	38–57	115–188	0		
Valley	5	0			4	52–61	17–18	1	46	285			
Wallow	15	10[*]	30–36	11–13	4[*]	30–36	129–321	0			1	6.8	1297

[*] Number of plots includes nested plots used in sediment delivery ratio calculations: Two Class 1 plots at North 25; two Class 1 and two Class 2 plots at Twitchell; and six Class 1 and four Class 2 plots at Wallow

[±] None of the Bobcat plots had defined channels.

Table 3. Number of plot-events (*n*), the linear model intercepts for each year, and the linear model slope terms for the log(area), I_{10}, and ground cover; 95% confidence limits are shown in parenthesis.

	Fire year		1st post-fire year		2nd post-fire year		Linear model slope terms		
Site	*n*	Intercept	*n*	Intercept	*n*	Intercept	Log(area)	Ground cover	I_{10}
All	87	0.21 (-0.046, 0.46)	23 8	0.11 (-0.065, 0.29)	166	-0.43 (-0.76, -0.09)	-0.25 (-0.32, -0.18)	-0.015 (-0.019, -0.011)	0.045 (0.039, 0.050)
Bobcat	13	2.2 (1.6, 2.8)	53	2.1 (1.7, 2.5)	36	1.4 (0.24, 2.6)	-0.74 (-1.1, -0.39)	-0.027 (-0.037, -0.017)	0.046 (0.033, 0.060)
Hayman	8	-0.98 (-1.5, -0.44)	27	-1.20 (-1.5, -0.88)	47	-1.5 (-2.3, -0.76)	0.076 (-0.047, 0.20)	0.00045 (-0.011, 0.012)	0.036 (0.026, 0.047)
North 25	0	--[1]	17	1.2 (0.11, 2.3)	18	ne[2]	-0.35 (ne[2])	0.018 (-0.030, 0.065)	-0.0043 (-0.10, 0.094)
Twitchell	0	--[1]	65	-0.49 (-0.91, -0.077)	54	-1.1 (-2.2, -0.043)	-0.24 (-0.39,-0.085)	0.0074 (-0.0077, 0.022)	0.036 (0.024, 0.049)
Valley	0	--[1]	18	-0.46 (-1.2, 0.32)	11	-0.20 (-1.4, 0.99)	-0.36 (-0.64,-0.090)	-0.045 (-0.089,-0.0017)	0.054 (0.034, 0.074)
Wallow	66	0.51 (0.11, 0.92)	58	0.88 (0.22, 1.5)	0	--[1]	-0.20 (-0.29, -0.12)	-0.031 (-0.043, -0.020)	0.049 (0.035, 0.062)

[1] No data
[2] Not estimable

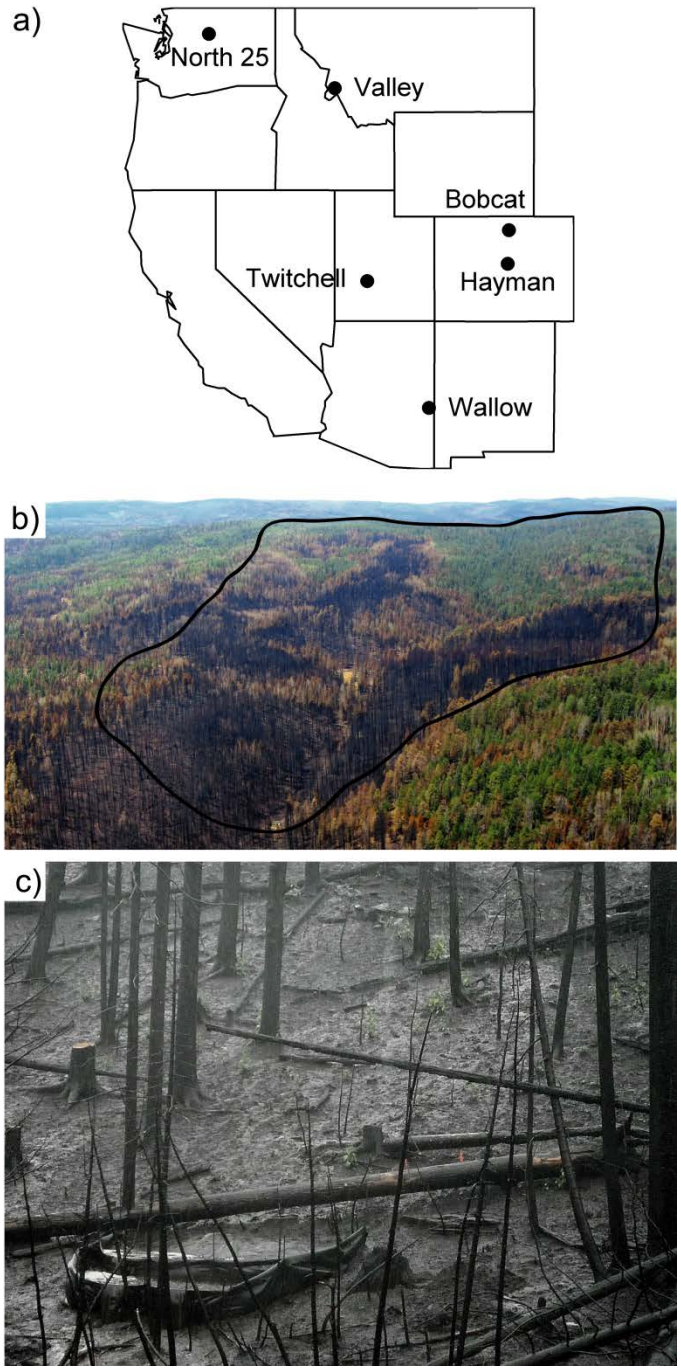

Figure 1.a) Locations of the six study sites in the western US. b) Oblique view looking up the W. Willow Creek drainage at the Wallow site on 30 June 2011; outline shows approximate catchment boundary. c) Hillslope plot and silt fence at the Wallow site during a runoff event 10 Aug 2011. Photos are available in color online.

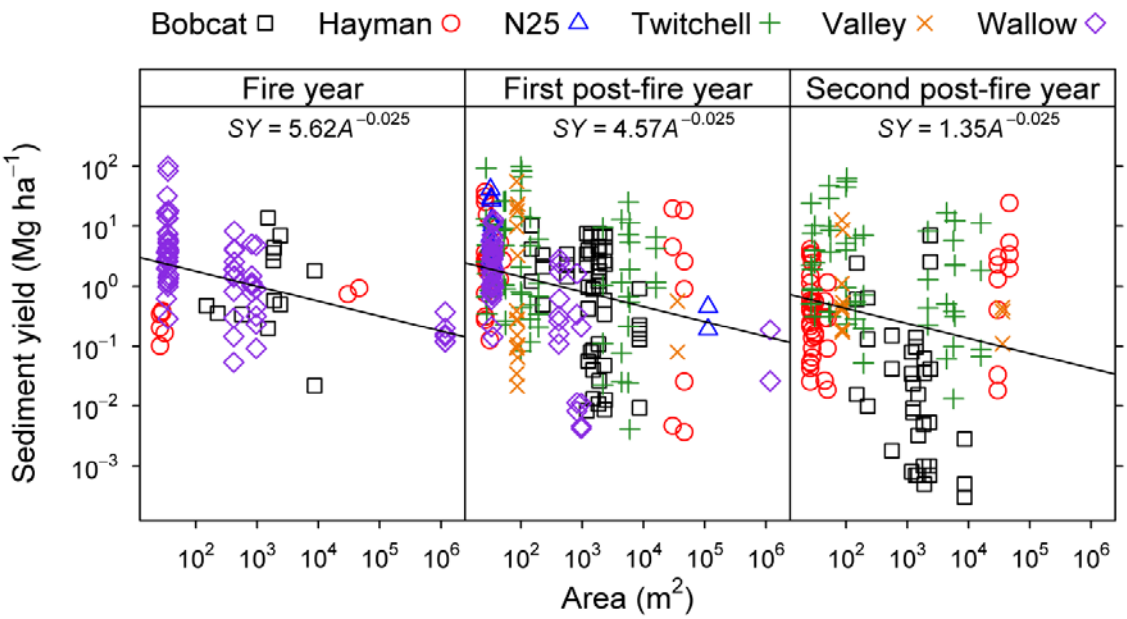

Figure 2. Sediment yield (*SY*) versus contributing area (*A*) by post-fire year. Lines and equations were derived from model coefficients (Table 3; Eq. 1 and Eq. 2) and average values for ground cover and I_{10} by year. Figure is available in color online.

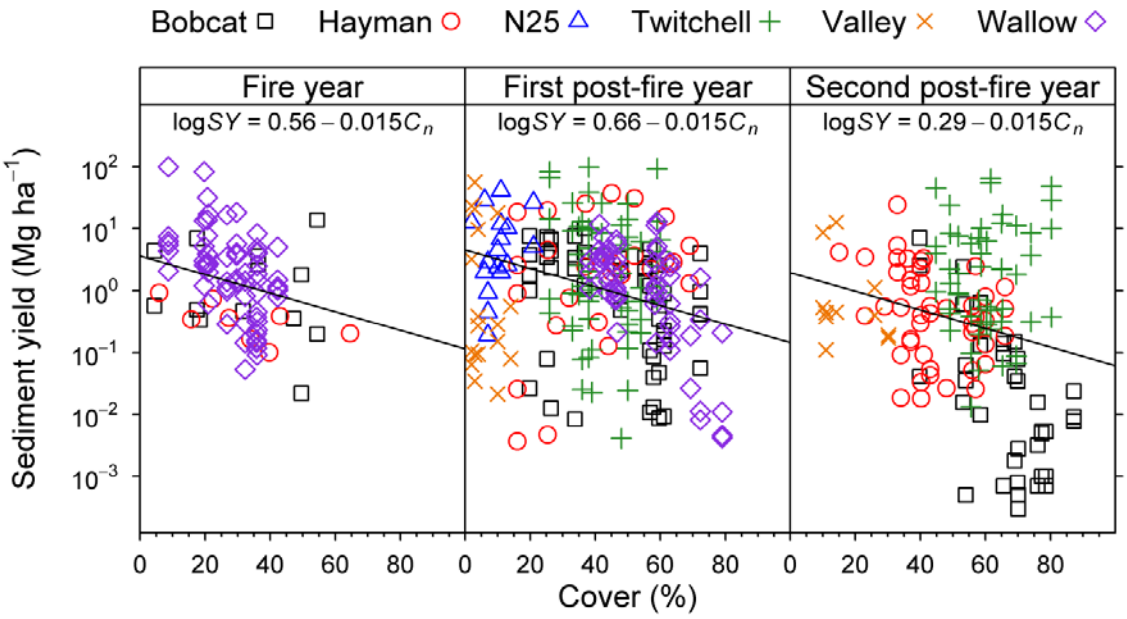

Figure 3. Event sediment yield (SY) versus ground cover (C_n) by post-fire year. Lines and equations were derived from model coefficients (Table 3) and average values for log(area) and I_{10} by year. Figure is available in color online.

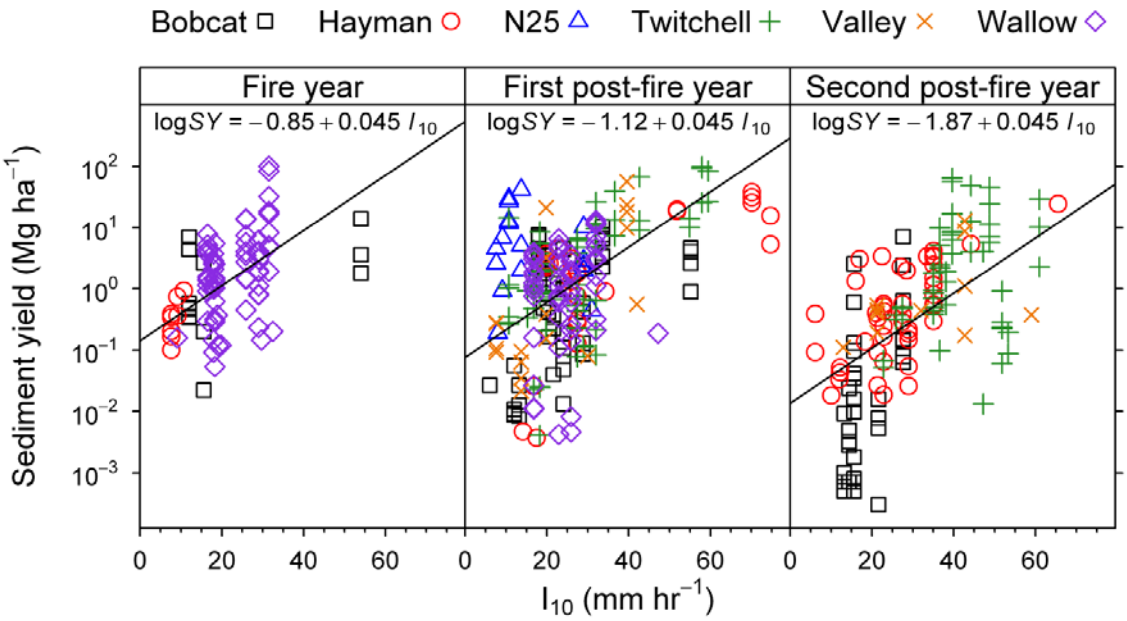

Figure 4. Event sediment yield (*SY*) versus I_{10}. Lines and equations were derived from model coefficients (Table 3) and average values for log(area) and ground cover by year. Figure is available in color online.

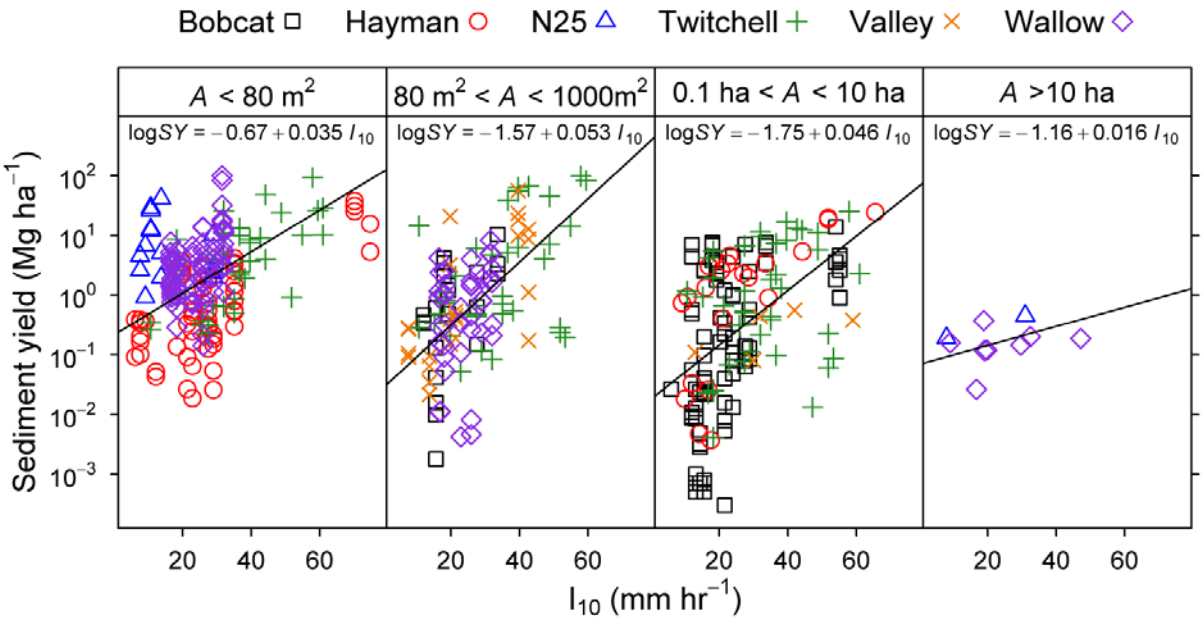

Figure 5. Event sediment yield (*SY*) versus I_{10} by area class for six sites. Lines and equations were derived from model coefficients and average ground cover values for each area class. Figure is available in color online.

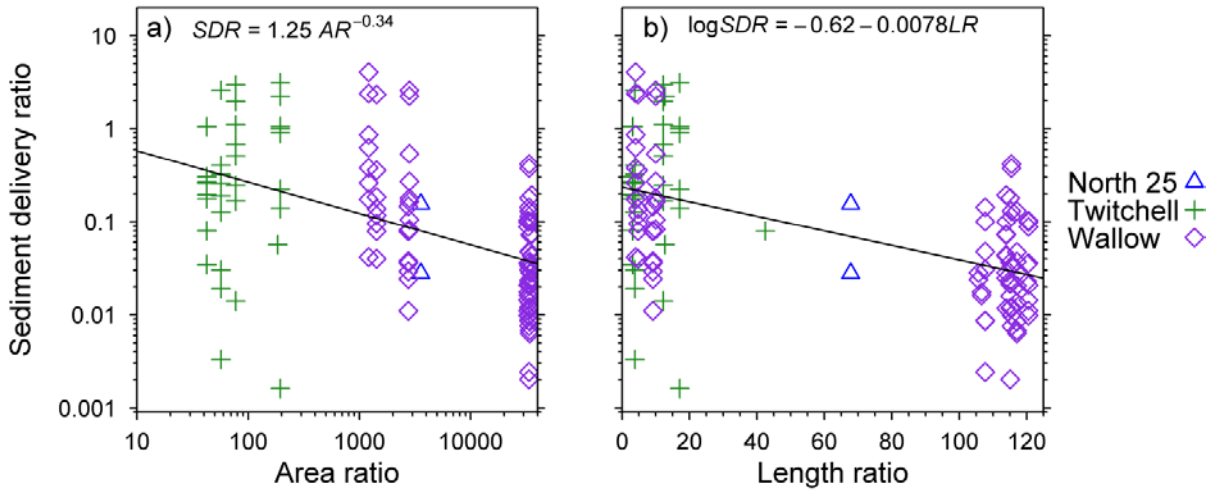

Figure 6. Sediment delivery ratio (*SDR*) versus a) area ratio (*AR*) and b) length ratio (*LR*) for the three sites with nested plots (North 25, Twitchell, and Wallow). All ratios are the catchment value divided by the plot value. Lines and equations were derived from model coefficients. Total number of plot-events is 125 (North 25: 2; Twitchell: 35; Wallow: 88). Figure is available in color online.

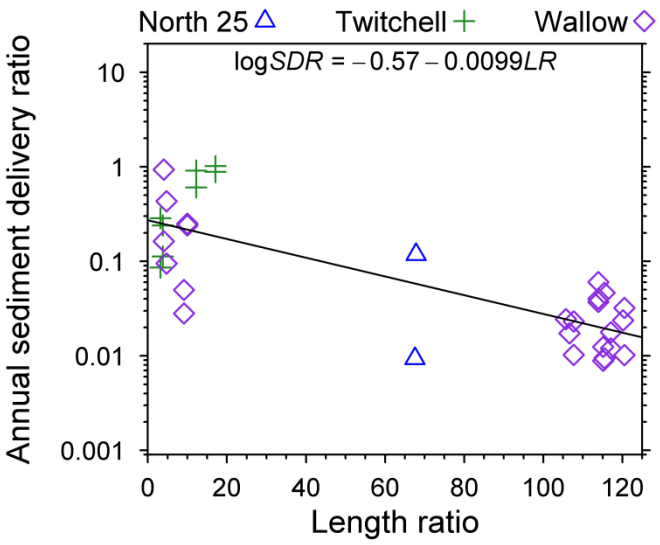

Figure 7. Annual sediment delivery ratio (*SDR*) versus length ratio (*LR*) for the three sites with nested plots (North 25, Twitchell, and Wallow). Both ratios are the catchment value divided by the plot value. Line and equation were derived from model coefficients. Total number of plot-years is 34 (North 25: 2; Twitchell: 8; Wallow: 24). Figure is available in color online.

CHAPTER FOUR: SEDIMENT YIELDS AND CHANNEL MORPHOLOGY IN A MODELED BURNED EPHEMERAL STREAM TREATED WITH CHECK DAMS

Joseph W. Wagenbrenner[1], S.M.ASCE

Peter R. Robichaud[2], M.ASCE

Peter Goodwin[3], F.ASCE

Abstract

Post-fire channel treatments are used to reduce sediment yields and channel incision, but few studies have tested their effectiveness. Five post-fire runoff events with varying sediment concentrations were simulated in a steep laboratory flume. The events were repeated after installation of straw bale check dams to test whether the dams affected post-fire sediment yields and channel morphology. We also compared seven sediment transport equations to determine which best predicted the measured sediment fluxes. Two events with higher sediment inflows resulted in aggradation in the untreated channel, while the three events with lower sediment inflows resulted in channel incision. The check dams stored 18% and 47% of the delivered sediment in the two comparable control events, but sediment delivery from subsequent treated events did not differ from the controls. A sediment transport

[1] Ph.D. candidate, Department of Biological Systems Engineering, Washington State University, Pullman, WA 99164, USA. and Engineer, US Department of Agriculture, Forest Service, Rocky Mountain Research Station, Moscow, ID 83843 USA, jwagenbrenner@fs.fed.us

[2] Research Engineer, US Department of Agriculture, Forest Service, Rocky Mountain Research Station, Moscow, ID 83843 USA, probichaud@fs.fed.us

[3] Professor and Director, Center for Ecohydraulics Research, College of Engineering, University of Idaho, Boise, ID 83702 USA, pgoodwin@uidaho.edu

equation designed to accommodate sediment that is not supply-limited best predicted the measured results. These results and field observations were used to develop a classification system addressing hydraulic and functional conditions of check dams in field installations.

Subject headings: channel stabilization, fire, flumes, models, morphology, sediment transport, stream channels

Introduction

Wildfires can change several parts of the hydrologic cycle, including interception, evapotranspiration, infiltration, and runoff mechanisms (DeBano et al. 1998; Shakesby and Doerr 2006). These changes often result in substantial increases in runoff volumes, peak flow rates, hillslope and channel erosion rates, and downstream sedimentation. Upland post-fire erosion processes have been fairly well described and there is some understanding of the effects of fire on hillslope erosion (Cerdà and Robichaud 2009; Shakesby and Doerr 2006). Mitigation treatments are often applied to hillslopes, roads, or channels to reduce the effects of the increased runoff and/or erosion (Robichaud et al. 2000). A better understanding of the efficacy of these treatments will help land managers make more informed decisions about protecting soil, stream, and downstream resources.

Check dams are the most common post-fire channel treatments, and generally are constructed of straw bales, rocks, or felled trees in ephemeral streams (Napper 2006). Treatment guidelines for burned areas suggest spacing the check dams so that the spill from one dam falls into the pond area of the downstream dam, and objectives include trapping sediment and reducing channel incision (Napper 2006). Check dams also have been used

extensively in unburned systems to reduce sedimentation (Abedini et al. 2012; Boix-Fayos et al. 2008; Collins and Johnston 1995; Heede and Mufich 1973), controlling incision (Castillo et al. 2007), and restoring gullies (Heede and Mufich 1973; Nyssen et al. 2004), and improving riparian conditions (Bombino et al. 2008; Debano and Schmidt 1990).

One recent post-fire study found that check dams constructed of logs or intertwined branches in channels with 6 to 9% slope captured 1.6 m^3 of relatively coarse sediment per structure (Fox 2011). During the 18-month assessment, however, the dams were not subject to large flows and did not fill to capacity (Fox 2011). Earlier evaluations of the effectiveness of straw bale check dams as a post-fire channel treatment in California used surveys of dams after they had experienced multiple rain storms (Collins and Johnston 1995; Miles et al. 1989). In one study the dams stored an average of 1.1 m^3 of sediment, and about 13% of the dams failed in the first year due to flow under or between bales or because of undercutting caused by channel scour during spillway overflow (Miles et al. 1989). The same study also evaluated 14 larger log or rock check dams and found that these dams stored between 1.5 and 95 m^3 (mean 30 m^3) of sediment, and that none of the log or rock dams failed in the first wet season (Miles et al. 1989). The second study measured an average sediment storage of 0.3–0.7 m^3 per dam and a 60% failure rate (Collins and Johnston 1995). They concluded that the risk of damage to the riparian corridor caused during installation or by the failure of the dams outweighed the benefits provided by the dams.

Wildfires are expected to increase in parts of the western US over the next several decades as the climate changes (Chmura et al. 2011; Littell et al. 2009; Westerling et al. 2006). This will lead to increases in post-fire runoff and greater sediment transport rates in streams (Goode et al. 2012) where the rates have been relatively low since fire suppression

became widespread in the early 1900s. A few studies (Barry et al. 2004; Cohen et al. 2010; Smart 1984) have addressed the applicability of sediment transport equations in steep terrain in general, and some predictions of channel extension or shape change have been evaluated in post-fire conditions (Canfield et al. 2005; Istanbulluoglu et al. 2004). Improving our sediment transport prediction capability for steep ephemeral streams will help prepare for and mitigate the effects of increased post-fire flows and sediment transport.

Our goal was to evaluate the effectiveness of straw bale check dams for reducing sediment delivery and changes in channel morphology in simulated post-fire conditions. We modeled an ephemeral stream channel and post-fire storm flows in a laboratory flume to address the following objectives: 1) determine if straw bale check dams affect post-fire channel degradation; 2) determine if straw bale check dams reduce sediment delivery in post-fire runoff events; 3) assess the ability of common sediment transport equations to predict the modeled conditions; and 4) apply the modeled results to field conditions.

Methods

A model of a burned ephemeral stream channel was installed in a laboratory flume and used to compare sediment delivery rates and channel morphology between an untreated channel (control) and a similar channel treated with straw bale check dams (treated). The laboratory flume is located in the Center for Ecohydraulics Research at the University of Idaho, Boise (Budwig and Goodwin 2011). Five simulated post-fire events were designed for the flume based on field measurements made in another study (Robichaud et al. 2013). These five events were run in the control model, the channel bed was removed and remade with the addition of three straw bale check dams, and the five events were re-run. Sediment samples,

bed topography, and other measurements were made for each of the 10 events. Flow and sediment data measured during the 10 events were used to assess the performance of seven sediment transport equations. Observations of straw-bale check dams in a field installation near the prototype site as well as in the 5 treated events in the flume experiment were used to develop a classification system. Brief description of the model and measurements follow; additional details are in Appendix 2.

Field (prototype) conditions

Five runoff events that occurred in the first two years after the Hayman fire in a small (4.6 ha) burned catchment (Robichaud et al. 2013) were selected to span the observed sediment and runoff conditions (Table 1). Peak and total runoff rates and sediment yields were measured using typical field instruments (Robichaud et al. 2013). The particle size distribution from a sediment sample from each of the field events was determined following ASTM standard D422-63 (ASTM 2007) (Table 1). The flow velocity, width, and depth at a cross-section with a channel gradient of 17% (Fig. 1) were estimated using Manning's equation, a roughness (n) value of 0.040 (Sturm 2010: p.133 "Mountain streams, no vegetetation in channel…Bottom: gravels, cobbles, and few boulders: 0.030–0.050), the cross-section dimensions, and the peak flow rates measured at the outlet of the catchment. The event bed-load sediment concentration was the sediment trapped in the weir pond divided by the total runoff and this assumed 100% trap efficiency. The time scale used to characterize each event was defined as the runoff divided by the peak flow rate and the average sediment flux used to establish the upstream boundary conditions was the sediment yield divided by the duration. These assumed constant flow rate and sediment concentrations, and are reasonable

estimates of the sediment concentrations and discharge rates in the flashy, sediment-laden post-fire flows that were typical at this field site (Robichaud et al. 2013).

The flume was modeled using the above conditions, but a range of prototype roughness values (0.040 to 0.065) were considered. The lowest roughness value represented the conditions for the earliest events (Fig. 1a) but lead to flow conditions close to critical. As the channel incised woody debris, particularly from exposed tree roots, increased the roughness (Fig. 1b). As supercritical flows are unusual in natural channels except in local conditions (Jarrett 1984), the roughness value of 0.065 was used to simulate the prototype conditions and develop the model scaling. The additional roughness created by tree roots and woody debris in the prototype conditions was not simulated in the laboratory resulting in a lower roughness, higher Froude number, and higher sediment transport rates which simulated the most severe condition in the field and will provide conservative prediction of how the check dams will behave in the field. The difference in the flow characteristics between the prototype and flume provide a conservative assessment of the performance of the check dams despite the limitations on scaling the hydraulic conditions back to the prototype (Peakall et al. 1996).

Flume model

The test section was 0.40 m wide by 11.4 m long. All longitudinal locations are relative to the entrance of the test section (0 m). The left wall was glass and the right wall was plywood covered in smooth vinyl sheeting. The slope was 8.5% for all events and the sediment concentrations simulated are given in Table 1. The flow rates, durations, and sediment grain sizes for each flume event were modeled using Froude criterion scaling

condition with an n of 0.04. The scaled durations (< 12 min) were increased (14–20 min) to allow for all samples and measurement to be taken during each event.

Sediment from a post-fire runoff event was screened and used in the bed material and added to the supply water. The bed material was a blend of the screened sediment and 10 mm crushed gravel. Bed material was packed on top of a layer of cobbles to a depth of 0.5 m and then shaped with a triangular screed with 10% side-slopes. A 29.5% ramp was installed downstream of the test section to return the flow to the metal floor of the flume but the flow conditions upstream were insensitive to this transition due to the steep slopes.

Supply water was re-circulated from a settling pond and gravity fed from an elevated storage tank. A needle valve and an electromagnetic flow meter (McCrometer, Inc., Hemet, CA) controlled the discharge. The sediment concentration of the 19 °C re-circulated supply water was not controlled but did not exceed 1.2 g L^{-1}.

Screened sediment was conveyed to a vibrating, plastic-covered distributor that deposited the sediment in the supply water at the entrance of the test section. The sediment feed rates were calibrated to within 0.1 kg s^{-1} of the design feed rates (0.5 to 2.4 kg s^{-1}) prior to each event and later adjusted for moisture content to obtain the inflowing dry sediment flux rates (Table 2). The particle size distributions were measured in three samples of the inflowing sediment (ASTM 2007) and the d_{50} ranged from 0.95 to 1.33 mm. The sediment feed lagged the start of flow by 2–2.1 min and was stopped 0.5 min before the supply water control valve was closed. Water continued to flow into the test section at low rates for several minutes after the valve was closed (Table 2).

Model-sized bales were compacted and hand-tied from loose straw and used to construct three check dams in the treated channel. The dams were two bales (0.40 m) wide,

two bales (0.18 m) high, and one bale (14 cm) deep and staked in place with the upstream edges at 3.95 m, 6.97 m, and 9.94 m. The dams were spaced to accommodate the backwater lengths that we estimated from perturbation analysis (Samuels 1989). Cobbles (10 cm) were used to fill gaps around bales and to armor the spillway below each dam, replicating standard field practice for installing straw bale check dams (Napper 2006). The bed aggraded during the last four treated events and for these events the slope was measured just upstream of the third check dam.

Measurements

The bed material surface was sampled for particle size analysis (ASTM 2007) at three locations in the control series and above and below each dam in the treated series before and after each event. Most of the samples were split before particle size analysis was conducted, and in these cases the mean of the distribution characteristic of interest (e.g., d_{50}, d_{90}, or % finer than 0.25 mm) was used in analysis. The mean d_{50} values were log-transformed and compared across locations using analysis of variance (SAS Institute 2008). Flow depth was measured in the lower third of the test section using a scale five times during each event. The depth was measured at the crest of the check dams as well as just downstream in the treated events. Flow velocity was estimated using the float method and a correction factor of 0.9 (Robins and Crawford 1954) since the high sediment transport rates precluded the use of other methods.

Sediment flux rates and yields were calculated using three independent methods: a built-in slot sampler; a mass balance using changes in volumes derived from surface elevations and inflowing sediment feed rates; and grab samples. Bed-load sediment was

continuously sampled through a slot in the floor of the flume 5 cm downstream from the ramp and weighed using a sediment weighing system (Schoenfelder 2010). The slot sampler bed-load sediment flux rates were converted to dry sediment flux rates by multiplying by the ratio $\gamma_s/(\gamma_s-\gamma)$ where γ_s and γ were the specific weights (N m^{-3}) of sediment and water, respectively.

The bed surface elevation was measured before and after each event using a laser scanner (Keyence Corporation, Osaka, Japan). The locations and elevations of the dams were manually entered in the data set. The scans were filtered to remove data with values more than three standard deviations above the mean elevation (C. Hocut, University of Idaho, unpublished program), and the volume change between events was calculated using Surfer (Golden Software 2003). The scans can not extend to the walls of the flume so the volume changes were multiplied by the ratio of the flume width to the scan width (1.25). Volumes were converted to mass using the measured bulk density for the control and treated channels (1530 kg m^{-3} and 1750 kg m^{-3}, respectively). Delivered sediment yields were the loss of mass in the bed (gains were negative values) plus the dry mass of inflowing sediment. Delivered sediment flux rates were the sediment yield divided by the duration of the inflowing sediment.

Five timed bed-load grab samples were taken during each event on the ramp downstream of the test section using a 76 mm Helley-Smith sampler fitted with a 0.25 mm mesh sample bag. A total-load grab sample was taken with a sample bottle immediately after each bed-load sample. Particle size analysis (ASTM 2007) indicated the mesh biased the bed-load grab samples toward coarser particles, so the bed-load samples were adjusted using the sub-0.25 mm fraction from the total-load samples (11 to 43%) when calculating fluxes. The delivered sediment flux rates were the adjusted bed-load grab sample dry mass divided by the sample duration and multiplied by the ratio of the width of the test section to the width of the

bed-load sampler (5.26). The grab sample sediment yields were the flux rates integrated over the duration of the inflowing sediment feed. Further details of supplemental measurements are given by Wagenbrenner (2013).

Sediment transport predictors

Seven sediment transport models were evaluated using the conditions measured in the flume and these were selected for suitability based on Yang (2003) and their applicability to steep ephemeral streams (Wagenbrenner 2013). The Schoklitsch (1943), Meyer-Peter and Müller (1948), Engelund and Hansen (1972) and Ackers and White (1973) equations were derived from Yang (2003) and three other equations were obtained from original sources (Bagnold 1980; Cohen et al. 2010; Smart 1984). The flow depths on top of the check dams were used for the treated events. The predicted sediment transport rates were converted to dry sediment transport capacities (kg s^{-1}). The discrepancy ratio (modeled sediment transport capacity / observed delivered sediment flux) was calculated for each equation and event (Yang 2003).

Results

Flow conditions

The flow appeared rough and turbulent and covered the full width of the test section in each event except for a narrow strip between 3.1 and 7.4 m during the first control event. Flow depths averaged 3.5 cm in the first control event and did not vary substantially from this value during the five control events (Table 3). The velocity in the first control event was 1.0

m s^{-1}, and this was the lowest velocity of the controls. The maximum velocity was 1.3 m s^{-1}, which occurred in the second and fourth control events (Table 3).

The straw bale check dams were not keyed into the channel before the first treated event, and this resulted in flow and scour underneath each dam. The dams were keyed into the remaining channel to a depth of about 5 cm prior to the subsequent events. The depths measured on the check dams (0.027–0.033 m) were similar to those measured in the control events (Table 3). The depths measured just below the check dams (0.048–0.173 m) were much greater, and the difference was likely due to observed scour from flow over the dams during the events.

The flows were heavily sediment laden, and the sediment concentrations in all the samples exceeded 42 g L^{-1}. The sediment concentrations in the control events generally followed the concentrations resulting from the inflowing sediment (Table 2), with the notable exceptions that the concentration in the first event (143 g L^{-1}) was 3.1 times greater than the concentration due to the inflowing sediment alone (46 g L^{-1}) and the concentrations in the second (164 g L^{-1}) and fourth (118 g L^{-1}) events were lower than the concentrations from the inflowing sediment (Tables 2 and 3). The high sediment concentration in the first event was due to channel scour while the lower concentrations in the second and fourth events were due to sediment deposition that occurred in parts of the channel that had been scoured by earlier events.

Except for the fourth event, the treated events had lower mean sediment concentrations than the controls, and we attribute this to the reduced channel gradients and flow velocities caused by the check dams (Table 3). The sediment concentrations in the second and third treated events were much lower than the concentrations in the corresponding

control events because of the high proportion of sediment deposited upstream of the check dams during these events. The mean sediment concentration in the fourth treated event (163 g L^{-1}) was greater than in the corresponding control event (118 g L^{-1}) which was lower because of in-channel storage, but still less than the sediment concentration from the inflowing sediment (186 g L^{-1}) (Table 2).

Channel morphology

The changes in channel shape during the control events were largely controlled by the inflowing sediment fluxes. The lower inflowing sediment fluxes in events one, three, and five resulted in channel incision whereas the higher fluxes in events two and four caused aggradation. The greatest scour occurred during the first event (Fig. 2), as this event had the lowest inflowing sediment flux and so more energy for bed erosion. The aggradation during events two and four suggests that the inflowing sediment exceeded the transport capacity during these events. Most of the changes in the channel occurred in the upper two-thirds of the test section (Fig. 2) because the wall at the end of the test section held the lower section of the bed in place.

The amount of channel incision during the first treated event was essentially the same as that of the first control event (Fig. 2), but the check dams stored sediment after they were keyed into the channel (Fig. 2). This clearly demonstrates the importance of how the structures are installed and failure to key the structures into the channels means they are likely to be ineffective. The storage volume upstream of the check dams averaged 0.11 m^3 per dam and all of the storage occurred in the channel sections affected by the dams' backwaters. Most of the deposition and resultant sediment storage occurred during the second and third

events, as there was little change in the channel surface between the third and fifth events (Fig. 2). The high sediment loads quickly filled the storage capacity above the dams.

Despite the amount of erosion in the upper part of the test section, the mean bed material d_{50} did not change significantly ($p > 0.35$) with distance downstream (Fig. 3). There was some fining of the bed material through each series, and this was more pronounced in the controls (Fig. 3). The d_{50} of the sediment deposited above the dams did not differ substantially from the bed sediment below the dams (Fig. 3). No trends in d_{50} were identified in the five bed-load or total-load samples in any control or treated event.

The low flows at the end of each event caused some re-organization of the bed sediments and may have affected the surface material grain size distributions. These low flows also tended to cause minor deposition in the scoured areas just below the check dams, resulting in less measured local scour than what was observed during the events.

Sediment yields

Using the mass balance method for all but the fourth and fifth treated events, the delivered sediment yields in the control events were between 960 kg and 1870 kg per event, producing sediment flux rates between 1.3 and 1.9 kg s^{-1} (Table 3). The net deposition in the treated series resulted in lower sediment yields than the controls, and these ranged from 760 to 1530 kg. Delivered sediment flux rates were also lower in the treated events (1.0–1.8 kg s^{-1}) than in the controls (1.3–1.9 kg s^{-1}) (Table 3).

Within the controls, the events with the lower inflowing sediment fluxes (one, three, and five) produced net incision in the channel (Fig. 2), resulting in sediment yields greater than the amount of inflowing sediment (Tables 2 and 3). Conversely, the events with the

higher inflowing sediment fluxes (two and four) produced aggradation in the channel (Fig. 2) and lower delivered sediment yields (Table 3) than the amount of dry inflowing sediment (Table 2). The fourth control event produced the greatest delivered sediment flux (1.9 kg s^{-1}), but this was still less than the inflowing sediment flux (2.2 kg s^{-1}), and this difference was attributed to the measured in-channels storage (Fig. 2).

The sediment yield from the first treated event, where the dams were undermined, was essentially the same as that of the first control event (Table 3). After the dams were keyed into the channel, the sediment yields for the second and third events were substantially lower (18% and 47%, respectively) than the corresponding control events, as the dams stored sediment in the channel (Fig. 2). The combined delivered sediment yield and flux for the fourth and fifth treated events were similar to the values for the fourth and fifth control events combined (Table 3). The delivered sediment flux calculated from the grab samples for the fourth treated event (1.5 kg s^{-1}) was similar to that of the fifth event (1.6 kg s^{-1}), although this method produced lower fluxes than the average from the mass balance method (1.8 kg s^{-1}) (Table 3). This suggests that the storage space upstream of the dams was completely filled with sediment by the end of the fourth event, which was the third event after keying in the check dams.

The slot-sampler sediment yields were on average only 25% of the sediment yields calculated by the mass balance or grab sample methods, so the slot sampler data were only used to assess within-event trends in delivered sediment fluxes. The slot sampler analysis showed fairly constant sediment fluxes in all events except for the fourth event in the control and treated series (Fig. 4). These fourth events had distinct increases in the delivered sediment fluxes at about 11 min into each event (Fig. 4). Aggradation occurred in both of

these events and the increases in delivered sediment fluxes at around 11 min probably occurred when the storage capacity in the channel or upstream of the dams had been filled. The greater sediment fluxes after 11 min represent the steady-state conditions for these two events.

Evaluation of sediment transport predictors

The equations predicted transport capacities ($Q_{s,m}$) ranged from 0.003 to 13.3 kg s^{-1} for the ten events whereas the measured sediment fluxes ($Q_{s,o}$) ranged from 1.0 to 1.9 kg s^{-1}. All of the equations predicted lower transport capacities for the treated events (Table 4) because of the lower gradients at the check dams. The mean discrepancy ratio for each model was greater for the control events (0.2 to 5.2) than for the treated events (0.03 to 1.3), indicating a greater tendency to under-predict the sediment fluxes for the treated events (Table 4). Across all events the mean discrepancy ratios ranged from 0.2 to 3.1, and the ratios for the equations by Bagnold (1980) (0.7) and Cohen et al. (2010) (0.4) were closest to 1 (Table 4).

Discussion

Check dam classification

Our observations at the prototype field site and in the treated events provide a basis to propose a classification scheme for field assessment of check dams in ephemeral streams. The classification describes six hydraulic and eight functional conditions (Fig. 5). The six hydraulic classes relate the three flow characteristics at the spillway, the depth of flow relative to the check dams, and the roughness attributed to the check dams. The three spill conditions describe the spacing of the check dams relative to the backwater length (L_b) (Fig. 5) (Samuels

1989). The *Isolated* class describes check dams that are spaced farther apart than the backwater effect of the downstream check dam, and this would result in the largest roughness but would also result in the spill falling directly on the channel bed and increased scour (Lenzi and Comiti 2003; Mason and Arumugam 1985; Napper 2006), and possibly lead to undercutting. The spill in both the *Connected* and *Influenced* classes would fall into a backwater (Fig. 5). In the *Connected* class the backwater would not extend past the next dam upstream, and so the lower dam would not act as a downstream control for flow over the upper dam. The *Connected* class represents the best spacing among dams as the flows over the dams would be independent of downstream conditions and the backwater would absorb some of the energy of the spill. In the *Influenced* class the check dam spacing is less than the backwater length and the free-overflow condition at the dam is compromised. In this case the backwater effect would extend above the location of the next dam upstream, and therefore would increase the depth of flow over the upper dam (Fig. 5). The *Submerged* classes would occur when the flow depth drowns out the upstream dam, and the slope of the channel and thereby the flow regime ((sub)critical or supercritical) would determine the *Submerged* sub-class (Fig. 5). In each sub-class of the *Submerged* class the check dams would function as large roughness elements (e.g., boulders) rather than discrete check dams. The check dams in the *Submerged*-(sub)critical and supercritical classes would no longer act as downstream controls on the flow. Finally, the *Transitional* hydraulic class might occur in steep channels with check dams spaced much greater than the backwater length (Fig. 5). In this case the flow regime would transition from supercritical to (sub)critical with a hydraulic jump when the flow approached the backwater. The transition from critical to supercritical would occur in the spill of the dam.

The eight functional classes describe the states of sediment storage and expansion of the sediment deposition upstream (Fig. 5). *Infilling* is deposition upstream of a check dam and would occur in the initial flow events after the dams were installed, as in our second treated event. The *Expanding* class would occur as sediment was deposited upstream of the dam's crest elevation and created by the backwater effect of the dam. This occurred during the fourth treated event in the current study. In the *Storing* class, sediment would be stored but little additional sediment would be retained (e.g., the fourth treated event in the flume). An estimate of the volume per unit width stored by each check dam in the *Storing* class would be $h^2 / 2S$, where h is the check dam height and S is the channel slope, and this estimate is conservative because it assumes a level surface of the stored sediment. The *Aggrading* class would occur if the check dam-affected channel slope was low, thereby greatly reducing the sediment transport capacity (Fig. 5). Scouring in the spillway would likely occur in all classes except the *Aggrading* and *Bypassing* classes, and the *Scouring* class is shown in Fig. 5 in combination with the *Expanding* class. *Cutting* would occur if the scour resulted in headcut migration and would result in unstable dams. *Bypassing* is indicative of faulty installation or poor site conditions and could occur from flow beneath the dams (e.g., the first treated event in the flume) or around the dams. Both of these conditions could lead to general channel degradation. The *Regressing* class would occur as the straw decomposed (Fig. 5) or the straw or other construction material was moved by flows over time, and resulting in re-mobilization of the stored sediment. Check dams made from rocks or logs might extend the time to reach the *Regressing* stage (Collins and Johnston 1995; Miles et al. 1989).

Sediment yields

The effect of the events on the control channel alternated between aggradation and degradation depending on the sediment loads. In contrast, once the check dams were keyed into the channel, the dams stored sediment and there was no subsequent channel incision. The check dams locally reduced the channel slope, and thereby provided a control on the transport capacity and erosive energy of the stream flow. Despite our observations of local scour downstream of the dams during the events, the straw bale check dams mitigated channel incision in the flume.

Using the length scale of the fourth event and assuming the prototype channel had a slope of 8.5% and a rectangular cross-section, the calculated storage volume per dam would be 5.5 m^3 in the field site. This means it would take at least 14 check dams to store the 77 m^3 of sediment produced by this single event in the 4.6 ha prototype catchment. But the storage per dam would be considerably less in steeper channels typical of the prototype site. Also, the check dams would fall into the *Storing* class after this one event, so no further reduction in sediment yield would occur in the steep channels.

Sediment transport modeling

The channel beds in the model and in the prototype field conditions were composed of sand and fine gravel, and the availability of sediment during initial post-fire flows, whether from hillslope or channel sources, appeared to be unlimited. The Cohen et al. (2010) equation was developed for flashy flows in ephemeral streams with unarmored beds, and this allows for linear scaling of sediment transport to excess shear stress (Cohen et al. 2010; Dietrich et

al. 1989; Emmett and Wolman 2001). This equation performed relatively well in this study (Table 4).

As part of the modeling approach, the Bagnold (1980) equation was calibrated using conditions from the first control event. While this approach best re-produced the observed sediment fluxes (mean discrepancy ratio of 0.7) (Table 4), it has limited applicability in catchments without field data for calibration. When we substituted the calibration values used in the original study (Bagnold 1980) the mean discrepancy ratio decreased to 0.5, indicating some sensitivity to the calibration conditions.

While the flume was modeled on conditions that represent typical post-fire storm flows after the Hayman fire, this data set is lacking the variability in measured conditions necessary to conclusively test a modeling approach. Thus there is a need to assess these and other sediment transport equations under post-fire conditions using a larger set of field data to improve our ability to predict sediment transport and delivery from burned areas.

Conclusions

Five post-fire runoff events with varying sediment concentrations were simulated in a laboratory flume to assess the impact of straw bale check dams on post-fire sediment yields and stream channel morphology. The events with higher inflowing sediment concentrations caused aggradation in the test section, while the events with the lower inflowing sediment concentrations resulted in channel incision.

The straw bale check dams, when keyed into the channel, stored 18% and 47% (340 kg and 630 kg, respectively) of the sediment that was delivered in the first two comparable control events, or a total of about 320 kg per check dam in the flume. There was no reduction

in sediment yield in subsequent events, and some scour was observed from the flow over the check dams during the events.

Sediment transport predictive equations are well known to give widely disparate results. These difficulties are magnified in steep headwater streams, especially in post-fire conditions where flows are flashy, may be unsteady and non-uniform, and have high sediment loads. On the basis of these experiments, Bagnold's (1980) equation gave the best results but required calibration. Of the six commonly used equations that do not need calibration, Cohen et al.'s (2010) excess shear stress equation performed best. The predicted sediment transport capacities for the treated events were lower overall, but these were not necessarily more accurate.

Transient check dams constructed of straw bales can result in several channel responses. Fig. 5 describes a simple classification system for the hydraulic and functional conditions of check dams in ephemeral streams, and this can be used to assess check dams in both burned and unburned stream systems. The flume experiments fell into the *Connected* hydraulic class and we observed several functional classes throughout the five events, including *Infilling*, *Expanding*, *Storing*, and *Bypassing*. This classification system, devised from experimental results, will be useful for evaluating the hydraulic and functional conditions of check dams in field installations.

Acknowledgements

This work was supported in part by a National Needs Fellowship grant from the US Department of Agriculture, National Institute of Foods and Agriculture, under agreement no. 2008-38420-04761, and by the USDA Forest Service, Rocky Mountain Research Station

(RMRS). Some laboratory equipment was purchased via the National Science Foundation Idaho EPSCoR Program (award number EPS-0814387). We thank Ralph Budwig and the staff at the University of Idaho's Center for Ecohydraulics Research laboratory as well as the employees of the RMRS Forest Sciences Laboratory in Moscow, Idaho for assistance in running the experiments. We recognize the logistical assistance provided by Jan Boll, Fred Pierson, Denver Water, and the Payette and Pike-San Isabel National Forests.

References

Abedini, M., Said, M. A. M., and Ahmad, F. (2012). "Effectiveness of check dam to control soil erosion in a tropical catchment (The Ulu Kinta Basin)." *Catena*, 97, 63–70.

ASTM. (2007). "Test method for particle size analysis of soils, standard D422-63." American Society of Testing and Materials International, West Conshohocken, Pennsylvania.

Bagnold, R. A. (1980). "An empirical correlation of bedload transport rates in flumes and natural rivers." *Proceedings of the Royal Society of London A: Mathematical, Physical and Engineering Sciences*, 372, 453–473.

Barry, J. J., Buffington, J. M., and King, J. G. (2004). "A general power equation for predicting bed load transport rates in gravel bed rivers." *Water Resources Research*, 40(10), W10401.

Boix-Fayos, C., De Vente, J., Martíınez-Mena, M., Barberá, Gonzalo G., and Castillo, V. M. (2008). "The impact of land use change and check-dams on catchment sediment yield." *Hydrological Processes*, 22, 4922–4935.

Bombino, G., Gurnell, A. M., Tamburino, V., Zema, D. A., and Zimbone, S. M. (2008). "Sediment size variation in torrents with check dams: Effects on riparian vegetation." *Ecological Engineering*, 32(2), 166–177.

Budwig, R. S., and Goodwin, P. (2011). "The Center for Ecohydraulics Research Mountain Stream Lab – a facility for collaborative research and education." *Proceedings of the 17th International Conference on Engineering Education*, International Network for Engineering Education and Research, Potomac, Maryland, 9.

Canfield, H. E., Wilson, C. J., Lane, L. J., Crowell, K. J., and Thomas, W. A. (2005). "Modeling scour and deposition in ephemeral channels after wildfire." *Catena*, 61(2–3), 273–291.

Castillo, V. M., Mosch, W. M., García, C. C., Barberá, G. G., Cano, J. A. N., and López-Bermúdez, F. (2007). "Effectiveness and geomorphological impacts of check dams for soil erosion control in a semiarid Mediterranean catchment: El Cárcavo (Murcia, Spain)." *Catena*, 70(3), 416–427.

Cerdà, A., and Robichaud, P. R. (2009). *Fire Effects on Soils and Restoration Strategies*. Science Publishers, Enfield, New Hampshire, 605.

Chmura, D. J., Anderson, P. D., Howe, G. T., Harrington, C. A., Halofsky, J. E., Peterson, D. L., Shaw, D. C., and Brad St.Clair, J. (2011). "Forest responses to climate change in the

northwestern United States: Ecophysiological foundations for adaptive management." *Forest Ecology and Management*, 261(7), 1121–1142.

Cohen, H., Laronne, J. B., and Reid, I. (2010). "Simplicity and complexity of bed load response during flash floods in a gravel bed ephemeral river: A 10 year field study." *Water Resources Research*, 46(11), 1–14.

Collins, L. M., and Johnston, C. E. (1995). "Effectiveness of straw bale dams for erosion control in the Oakland Hills following the fire of 1991." *Brushfires in California Wildlands: Ecology and Resource Management*, J. E. Keeley and T. Scott, eds., International Association of Wildland Fire, Missoula, MT, 171–183.

DeBano, L. F., Neary, Daniel G., and Ffolliott, P. F. (1998). *Fire's Effects on Ecosystems*. Wiley, New York, 333.

Debano, L. F., and Schmidt, L. J. (1990). "Potential for enhancing riparian habitats in the southwestern United States with watershed practices." *Forest Ecology and Management*, 33, 385–403.

Dietrich, W. E., Kirchner, J. W., Ikeda, H., and Iseya, F. (1989). "Sediment supply and the development of the coarse surface layer in gravel-bedded rivers." *Nature*, 340(6230), 215–217.

Emmett, W. W., and Wolman, M. G. (2001). "Effective discharge and gravel-bed rivers." *Earth Surface Processes and Landforms*, 26(13), 1369–1380.

Fox, D. M. (2011). "Evaluation of the efficiency of some sediment trapping methods after a Mediterranean forest fire." *Journal of Environmental Management*, 92(2), 258–265.

Golden Software. (2003). "Surfer version 8.03." Golden Software, Inc., Golden, Colorado.

Goode, J. R., Luce, C. H., and Buffington, J. M. (2012). "Enhanced sediment delivery in a changing climate in semi-arid mountain basins: Implications for water resource management and aquatic habitat in the northern Rocky Mountains." *Geomorphology*, 139–140, 1–15.

Heede, B. H., and Mufich, J. G. (1973). "Functional relationships and a computer program for structural gully control." *Journal of Environmental Mnagement*, 1, 321–344.

Istanbulluoglu, E., Tarboton, D. G., Pack, R. T., and Luce, C. H. (2004). "Modeling of the interactions between forest vegetation, disturbances, and sediment yields." *Journal of Geophysical Research*, 109, F01009.

Jarrett, R. D. (1984). "Hydraulics of high-gradient streams." *Journal of Hydraulic Engineering*, 110(11), 1519–1539.

Lenzi, M. A., and Comiti, F. (2003). "Local scouring and morphological adjustments in steep channels with check-dam sequences." *Geomorphology*, 55(1–4), 97–109.

Littell, J. S., McKenzie, D., Peterson, D. L., and Westerling, A. L. (2009). "Climate and wildfire area burned in western U.S." *Ecological Applications*, 19(4), 1003–1021.

Mason, P. J., and Arumugam, K. (1985). "Free jet scour below dams and flip buckets." *Journal of Hydraulic Engineering*, 111(2), 220–235.

Miles, S. R., Haskins, D. M., and Ranken, D. Q. (1989). "Emergency burn rehabilitation: cost, risk, and effectiveness." *Proceedings of the Symposium on Fire and Watershed Management, General Technical Report PSW–109*, N. H. Berg, ed., US Department of Agriculture, Forest Service, Pacific Southwest Forest and Range Experiment Station, Berkeley, California, 97–102.

Napper, C. (2006). *Burned area emergency response treatments catalog*. *Watershed, Soil, Air Management 0625 1801-SDTDC*, US Department of Agriculture, Forest Service, National Technology & Development Program, Washington, D.C., 214.

Nyssen, J., Veyret-Picot, M., Poesen, J., Moeyersons, J., Haile, M., Deckers, J., and Govers, G. (2004). "The effectiveness of loose rock check dams for gully control in Tigray, northern Ethiopia." *Soil Use and Management*, 20(1), 55–64.

Peakall, J., Ashworth, P., and Best, J. (1996). "Physical modelling in fluvial geomorphology: Principles, applications and unresolved issues." *The Scientific Nature of Geomorphology: Proceedings of the 27th Symposium in Geomorphology held 27–29 September 1996*, B. L. Rhoads and C. E. Thorn, eds., 221–253.

Robichaud, P. R., Beyers, J. L., and Neary, D G. (2000). *Evaluating the effectiveness of postfire rehabilitation treatments, General Technical Report RMRS–63*. *General Technical Report RMRS–63*, USDA Forest Service, Rocky Mountain Research Station, Fort Collins, Colorado, 85.

Robichaud, P. R., Wagenbrenner, J. W., Lewis, S. L., Brown, R. E., Wohlgemuth, P. M., and Ashmun, L. E. (2013). "Post-fire mulching for runoff and erosion mitigation Part II: Effectiveness in reducing runoff and sediment yields from small catchments." *Catena*, 105, 93–111.

Robins, C. R., and Crawford, R. W. (1954). "A short accurate method for estimating the volume of stream flow." *Journal of Wildlife Management*, 18(3), 366–369.

Samuels, P. G. (1989). "Backwater lengths in rivers." *Proceedings of the Institution of Civil Engineers*, 87, 571–582.

SAS Institute. (2008). "SAS version 9.2." *SAS Institute, Inc.*, Cary, North Carolina.

Schoenfelder, J. (2010). "Design and implementation of a sediment weighing and transport system for a large scale tilting sediment flume." M.S. thesis, University of Idaho, Boise, Idaho.

Shakesby, R. A., and Doerr, S. H. (2006). "Wildfire as a hydrological and geomorphological agent." *Earth-Science Reviews*, 74(3–4), 269–307.

Smart, G. M. (1984). "Sediment transport formula for steep channels." *Journal of Hydraulic Engineering*, 110(3), 267–276.

Sturm, T. W. (2010). *Open Channel Hydraulics*. McGraw-Hill, Boston, 546.

Wagenbrenner, J. W. (2013). "Post-fire stream channel processes: Changes in runoff rates, sediment delivery across spatial scales, and mitigation effectiveness." Doctoral dissertation, Washington State University, Pullman, Washington.

Westerling, A. L., Hidalgo, H. G., Cayan, D. R., and Swetnam, T. W. (2006). "Warming and earlier spring increases western U.S. forest wildfire activity." *Science*, 313, 1–9.

Yang, C. T. (2003). *Sediment transport: Theory and practice*. Krieger Publishing Co., Malabar, Florida, 396.

Notation

Symbol	Meaning
C_s	Sediment concentration (g L^{-1})
d_{50}	Median particle size (mm or m)
d_{90}	90th percentile particle size (mm or m)
D	Flow depth (m or cm)
h	Check dam height (m)
L_b	Backwater length (m)
n	Manning's roughness coefficient ($m^{-1/3}$ s)
n_0	Channel Manning's roughness coefficient ($m^{-1/3}$ s)
n_{cr}	Critical Manning's roughness coefficient ($m^{-1/3}$ s)
N_L	Length ratio (L(prototype)/L(model))
Q	Discharge (L s^{-1})
Q_{pk}	Peak discharge (L s^{-1})
Q_s	Sediment flux (kg s^{-1})
$Q_{s,m}$	Modeled sediment transport capacity (kg s^{-1})
$Q_{s,o}$	Observed sediment flux (kg s^{-1})
$Q_{s,in}$	Inflowing sediment flux (kg s^{-1})
$Q_{s,out}$	Delivered sediment flux (kg s^{-1})
S	Slope (% or m m^{-1})
S_0	Initial slope (% or m m^{-1})
S_f	Final slope (% or m m^{-1})
S_{cr}	Critical slope (% or m m^{-1})
V	Velocity (m s^{-1})
w	Width (m or cm)
x	Check dam spacing (m)
Y	Sediment yield (Mg or kg)
γ	Specific weight of water (9795 N m^{-3})
γ_s	Specific weight of sediment (25997 N m^{-3})
ΔM	Change in mass (kg)
τ_c	Critical shear stress (N m^{-2})

Table 1. Field (prototype) runoff and sediment conditions

	Measured conditions [a]			Estimated conditions				
	Q_{pk} (L s^{-1})	Y (Mg)	d_{50} (mm)	V (m s^{-1})	D (cm)	w (cm)	C_s (g L^{-1})	Time (min)
1	67	1.2	1.2	1.02	13	100	44	6.7
2	64	12.0	--[b]	1.00	13	98	193	16.1
3	100	6.9	1.3	1.13	16	116	136	8.5
4	260	50.1	2.2	1.42	22	165	202	15.9
5	330	11.0	2.5	1.51	24	180	109	5.1

Note: event dates were 1 Oct 02 (1), 30 Aug 03 (2), 27 Sep 04 (3), 19 Aug 04 (4), and 28 Jul 04 (5). Q_{pk} is peak discharge; Y is sediment yield; d_{50} is sediment d_{50}; V is velocity; D is flow depth; w is flow width; C_s is sediment concentration; and Time is the time scale. V, D, and w were estimated using n = 0.065.

[a] Q_{pk} and Y data are from Robichaud et al. (2013)

[b] Sample not available

Table 2. Flume design for the 5 control and treated events

	Q (L s^{-1})	Q_s (kg s^{-1})	C_s (g L^{-1})	d_{50} (mm)	Durations (min) at Q	Durations (min) Tot.
1	10.85	0.5	46	0.58	14.8	26.1
2	10.91	2.0	183	--[a]	19.7	30.5
3	11.10	1.4	126	0.54	16.0	22.0
4	11.80	2.2	186	0.64	15.5	25.0
5	11.99	1.2	100	0.67	17.5	25.5

Note: Q is discharge; Q_s is inflowing sediment flux; C_s is inflowing sediment concentration; d_{50} is for the scaled sediment; and Durations are the times at design flow rate ("at Q") and the total flow duration ("Tot.")

[a] Prototype sediment sample not available; sediment was scaled using prototype sediment size from event 1.

Table 3. Control (C) and treated (T) event outputs

	S (%)	V (m s^{-1})	D (cm)	Q_s (kg s^{-1})	C_s (g L^{-1})	ΔM (kg)	Y (kg)
C1	8.5	1.0	3.5	1.3	143	610	960
C2	8.5	1.3	3.5	1.8	164	−190	1870
C3	8.5	1.1	3.1	1.8	110	330	1430
C4	8.5	1.3	3.6	1.9	118	−240	1500
C5	8.5	1.1	3.0	1.7	101	420	1520
T1	8.5	0.9	ND	1.3	112	640	990
T2	2.1	0.8	3.3	1.5	70	−530	1530
T3	1.4	0.8	3.0	1.0	77	−340	760
T4	1.0	1.2	2.7	ND	163	ND	ND
T5	2.6	1.0	3.2	1.8[a]	79	130[a]	2970[a]

Note: S is slope; Q_s and C_s are delivered sediment flux and concentration, respectively; ΔM is lost bed mass (− is gained); V, D and Y are as in Table 1; and ND is no data.

[a] Q_s is average over T4 and T5; ΔM and Y are relative to T3.

Table 4. Mean transport capacities and discrepancy ratios

	Control		Treated		Combined	
	$Q_{s,m}$	$Q_{s,m}/Q_{s,o}$	$Q_{s,m}$	$Q_{s,m}/Q_{s,o}$	$Q_{s,m}$	$Q_{s,m}/Q_{s,o}$
Schok.	0.7	0.4	0.2	0.1	0.4	0.3
MPM	6.4	3.7	1.9	1.3	4.4	2.7
E&H	9.2	5.2	0.7	0.5	5.4	3.1
A&W	0.3	0.2	0.2	0.1	0.3	0.2
Bagnold	1.8	1.1	0.2	0.1	1.1	0.7
Smart	0.6	0.4	0.1	0.03	0.4	0.2
Cohen	1.1	0.7	0.1	0.08	0.7	0.4

Note: $Q_{s,m}$ (kg s^{-1}) is the modeled sediment transport capacity and $Q_{s,o}$ is the observed sediment flux; $Q_{s,o}$ for treated events 4 and 5 used the grab sample method; "Schok." is Schoklitsch (1943); "MPM" is Meyer-Peter and Müller (1948); "E&H" is Engelund and Hansen (1972); "A&W" is Ackers and White (1973); "Bagnold" is his 1980 equation; "Smart" is his 1984 equation; and "Cohen" is Cohen et al. (2010).

Figure 1. Downstream views of the prototype cross-section on a) 16 Jun 2003 and b) 9 Sep 2004

Note: a) was after the 1st event; b) was after events 1–3 and 5 as well as four other events. The pins are 5.2 m apart. The straw in a) was blown in from another study catchment.

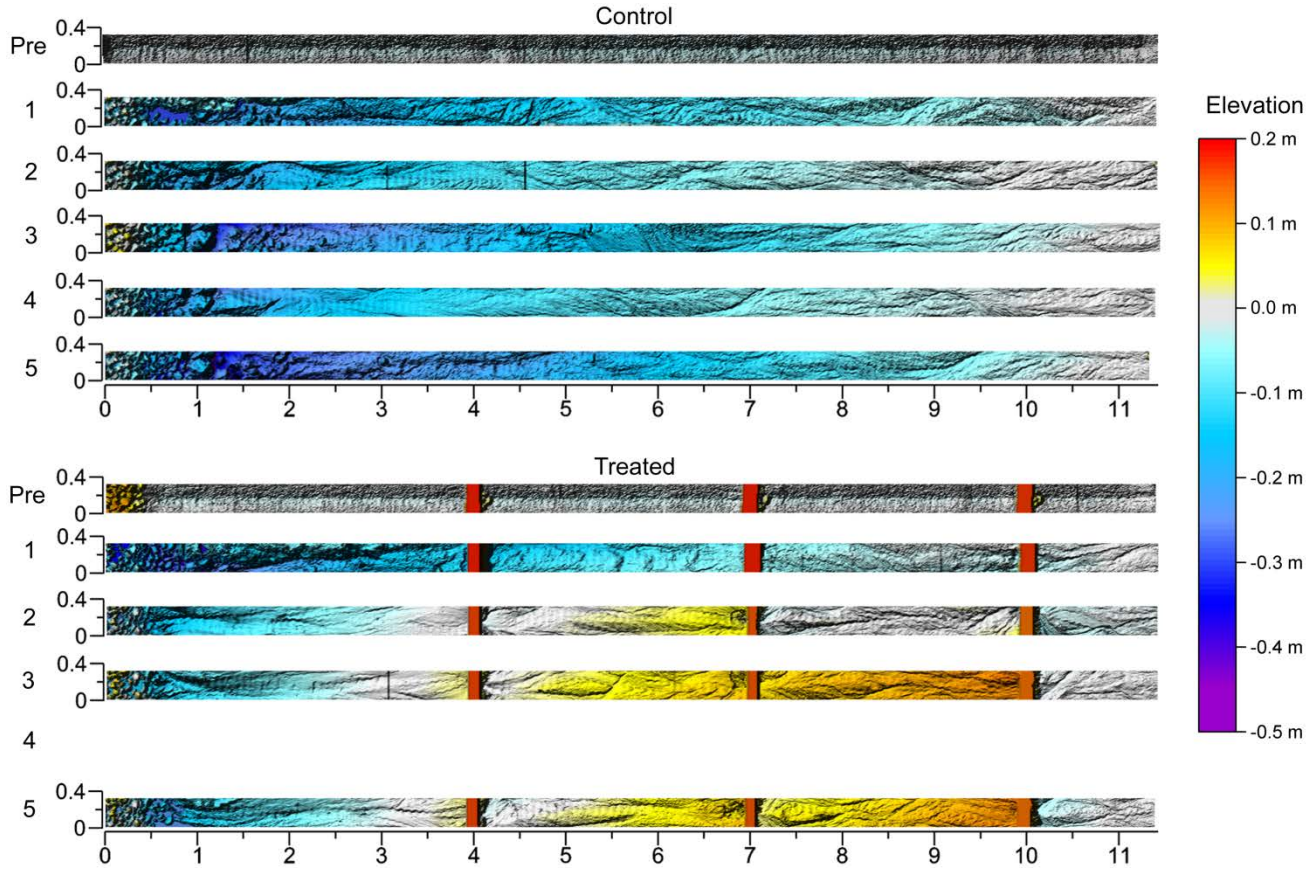

Figure 2. Bed surface elevations for control and treated events

Note: Y-distance reference is at the start of scans, approximately 0.06 m from right wall. Both axis scales are in meters. Data for fourth treated event are not available.

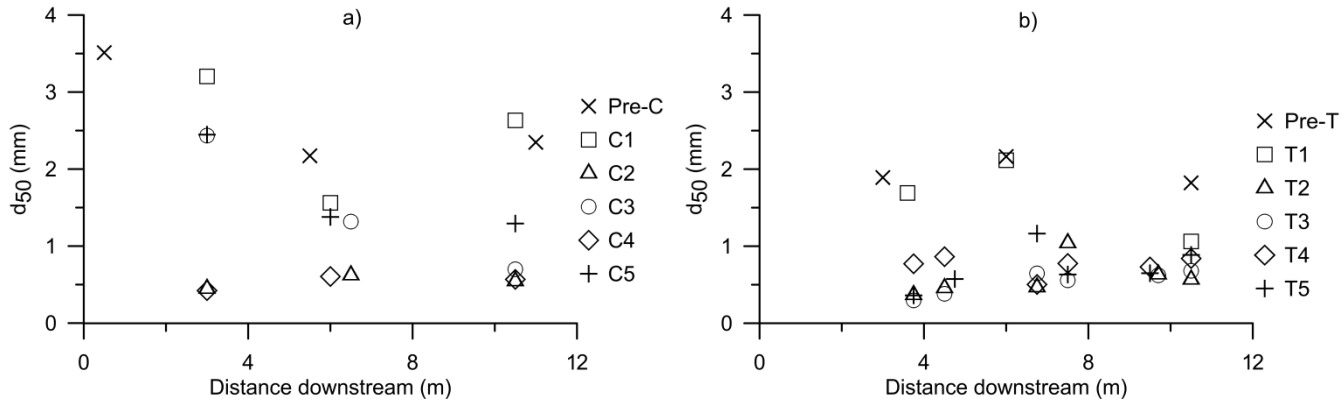

Figure 3. Mean bed d_{50} versus distance downstream for a) control events and b) treated events

Note: Pairs of points in treated events 2–5 are above and below dams. "Pre-" is prior to first event.

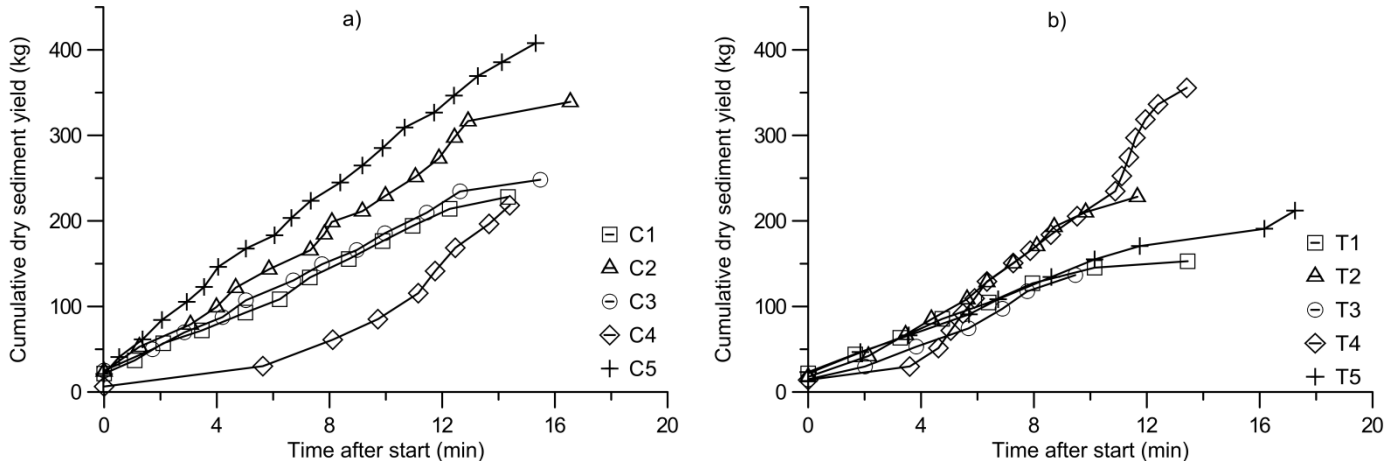

Figure 4. Cumulative dry sediment yield measured with slot sampler versus time after start of event for a) control events and b) treated events

Note: The slot sampler measured approximately 25% of the sediment yield calculated by the mass balance.

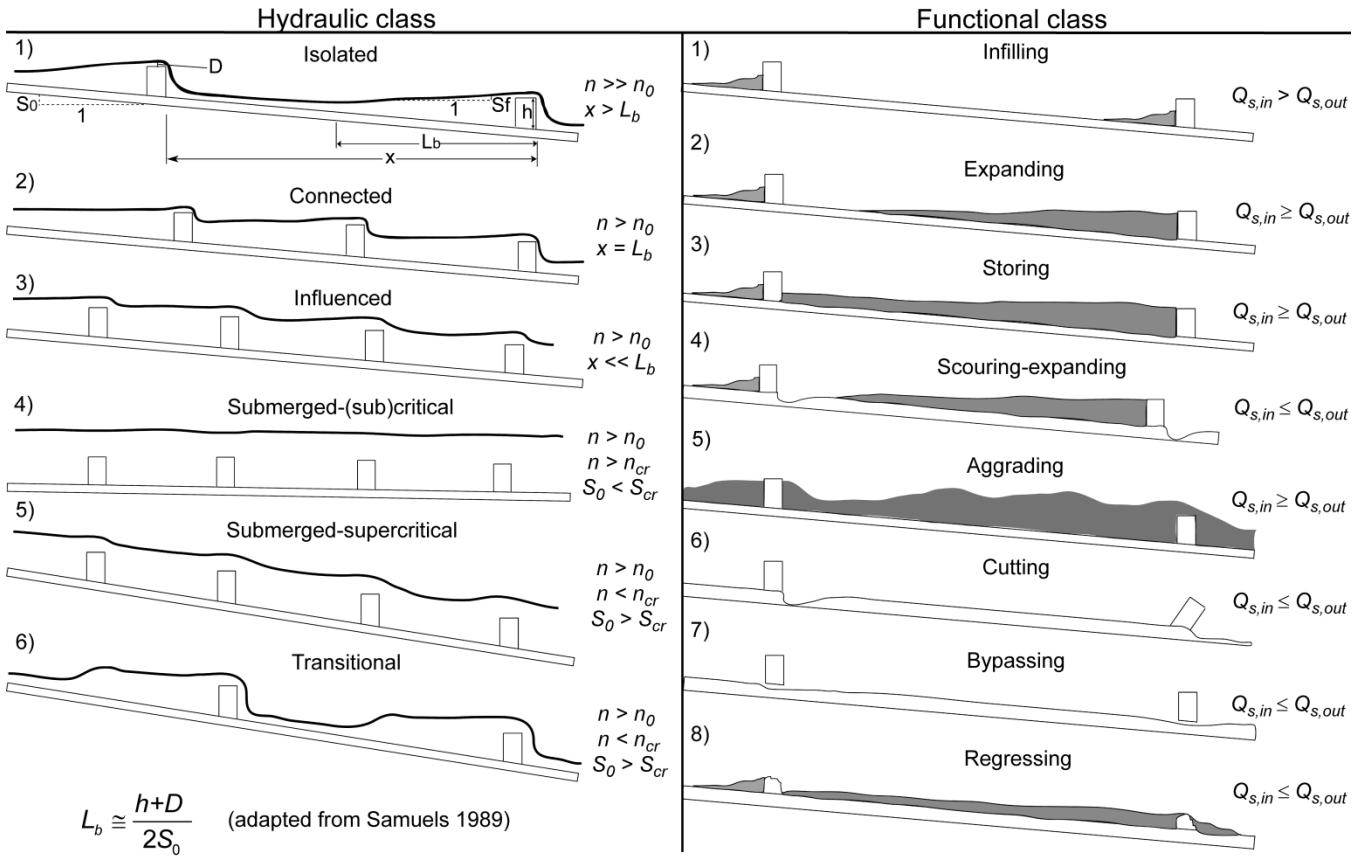

Figure 5. Check dam hydraulic and functional classification

Note: x is distance between check dams; h is check dam height; D is flow depth; S_0, S_f, *and* S_{cr} are channel, final and critical slopes, respectively; L_b is backwater length; n, n_0, and n_{cr} are Manning's n, original channel n, and critical n, respectively; and $Q_{s,in}$ and $Q_{s,out}$ are inflowing and delivered sediment fluxes, respectively.

APPENDIX 1: W. WILLOW CREEK SUMMER STORM FLOWS

Appendix 1.1: W. Willow Creek pre-fire storm flows and hydrograph statistics

Date and time of peak	Peak discharge ($m^3 s^{-1}$)	Storm runoff (m^3)	Rainfall on day of peak ($mm\ d^{-1}$)	Runoff ratio ($mm\ mm^{-1}$)	Time to peak (min)	Duration (min)	Rising limb slope ($m^3 s^{-2} \times 10^{-6}$)	Receding limb slope ($m^3 s^{-2} \times 10^{-6}$)
10 Sep 1963 14:50	0.0602	677	38.1	0.015	50	2040	20	-0.48
14 Sep 1963 0:00	0.0085	1183	25.4	0.040	180	3600	0.54	-0.02
15 Sep 1964 17:15	0.0241	4487	23.4	0.164	1695	4200	0.18	-0.027
24 Sep 1964 9:00	0.0267	5089	34.8	0.125	1980	4020	0.17	-0.049
27 Jul 1965 16:45	0.0137	316	27.9	0.010	75	1095	2.8	-0.19
29 Jul 1965 4:30	0.0346	1351	23.1	0.046	270	2880	2.0	-0.19
31 Jul 1965 14:00	0.0085	1812	8.6	0.180	240	4980	0.22	-0.013
10 Aug 1966 18:30	0.0045	1266	23.1	0.047	3206	6416	0.019	-0.0083
22Aug 1966 19:30	0.0040	1663	11.7	0.121	6930	10080	0.006	-0.0048
19 Sep 1966 15:00	0.0060	2579	10.7	0.206	12420	14400	0.008	-0.021
27 Jul 1967 18:30	0.0274	2169	32.3	0.057	1695	3825	0.26	-0.18
13 Aug 1967 5:30	0.0387	7891	25.1	0.269	2190	4100	0.19	-0.13
10 Jul 1968 11:45	0.0144	1242	24.4	0.044	15	7300	15	-0.032
3 Aug 1968 13:00	0.0205	1049	12.7	0.071	60	1995	4.5	-0.12
28 Aug 969 15:15	0.0043	149	17.3	0.007	30	1155	2.3	-0.057
29 Aug 1969 16:30	0.0122	368	31.8	0.010	390	2280	0.50	-0.10
6 Sep 1970 8:00	0.0020	243	21.6	0.010	480	3240	0.068	-0.0080
9 Sep 1970 0:00	0.0021	237	18.3	0.011	480	2387	0.054	-0.011
2 Oct 1970 22:00	0.0034	339	36.1	0.008	330	2955	0.16	-0.012
8 Aug 1971 18:00	0.0044	361	17.8	0.017	350	3050	0.19	-0.022
29 Sep 1971 23:15	0.0033	1743	47.5	0.031	630	4995	0.086	0.0036
25 Oct 1971 14:45	0.0317	4777	44.7	0.091	1050	3045	0.39	-0.079
31 Aug 1972 16:30	0.0067	591	46.2	0.011	145	3115	0.75	-0.028
3 Sep 1972 11:00	0.0024	516	13	0.034	1020	3240	0.012	-0.0064
19 Oct 1972 22:45	0.4664	40782	100.1	0.348	1455	3150	5.2	-3.0
4 Aug 1974 13:00	0.0039	301	31.2	0.008	45	3075	1.4	-0.018
8 Aug 1974 9:45	0.0018	140	8.1	0.015	405	1980	0.048	-0.010
19 Sep 1974 0:00	0.0018	205	14.2	0.012	390	3270	0.065	-0.0059
8 Sep 1975 14:10	0.0325	2258	33.3	0.058	55	2085	8.2	-0.11
31 Jul 1976 11:55	0.0028	105	9.7	0.009	20	745	1.6	-0.024
21 Aug 1977 14:50	0.0041	226	28.7	0.007	1485	2455	0.038	-0.024
5 Sep 1977 19:45	0.0049	291	31.8	0.008	245	1290	0.31	-0.041
9 Sep 1980 16:35	0.0274	418	23.9	0.015	65	570	6.2	-0.58
8 Jul 1981 13:00	0.0024	141	36.3	0.003	60	2760	0.57	-0.012
10 Jul 1981 22:00	0.0016	168	20.1	0.007	570	2130	0.019	-0.0075
8 Aug 1981 16:00	0.0028	53	19.1	0.002	960	2400	0.047	-0.029
24 Aug 1982 14:00	0.0041	44	no data	0.015	30	630	2.2	-0.063

Appendix 1.2: W. Willow Creek post-fire storm flows and hydrograph statistics

Date and time of peak	Peak discharge rate ($m^3\ s^{-1}$)	Storm runoff (m^3)	24-hr rainfall on day of peak ($mm\ d^{-1}$)	Runoff ratio ($mm\ mm^{-1}$)	Time to peak (min)	Duration (min)	Rising limb slope ($m^3\ s^{-2} \times 10^{-6}$)	Receding limb slope ($m^3\ s^{-2} \times 10^{-6}$)
26 Jul 2011 16:00	0.1950	527	8.4	0.054	85	260	38	-18
27 Jul 2011 11:55	0.2690	303	3	0.086	20	100	223	-55
30 Jul 2011 16:15	0.0380	361	8.6	0.036	35	460	17.1	-0.92
2 Aug 2011 15:10	1.4450	1428	7.9	0.154	20	135	1200	-205
3 Aug 2011 9:55	1.2200	1608	8.4	0.164	20	85	999	-290
4 Aug 2011 13:35	0.1210	121	3.6	0.029	10	25	95	-81
10 Aug 2011 14:00	1.0070	1805	11.9	0.130	15	375	1120	-46
10 Aug 2011 21:10	0.2090	495	11.9	0.036	30	215	111	-18
12 Aug 2011 18:35	0.0440	162	5.6	0.025	30	125	21	-6.2
17 Aug 2011 19:45	0.5220	542	5.1	0.091	55	165	158	-77
18 Aug 2011 12:15	0.3140	504	5.1	0.084	10	120	507	-46
19 Aug 2011 15:00	0.1210	231	2.5	0.079	30	150	64	-15
23 Aug 2011 15:50	0.2230	400	3.3	0.104	10	250	360	-15
29 Aug 2011 13:30	0.4050	582	6.4	0.078	10	230	668	-30
30 Aug 2011 13:50	0.2150	273	3.8	0.061	15	115	237	-35
1 Sep 2011 18:05	0.1660	275	4.8	0.049	10	155	267	-18
2 Sep 2011 12:15	1.1010	1410	6.9	0.175	25	170	731	-126
4 Sep 2011 15:00	0.0220	114	2.3	0.042	20	145	12	-1.7
6 Sep 2011 19:00	0.0380	117	2.5	0.040	25	95	19	-6.2
7 Sep 2011 15:05	0.8310	779	4.6	0.145	15	225	916	-65
3 Oct 2011 19:40	1.3300	2451	14.2	0.148	15	325	1470	-71
4 Oct 2011 9:35	0.1010	183	14	0.011	20	95	83	-21
4 Oct 2011 22:05	0.3800	1049	14	0.064	20	195	315	-36
7 Jul 2012 12:53	0.0120	12	10.2	0.001	11	20	12	-4.4
17 Jul 2012 11:22	0.1350	109	5.1	0.018	5	88	432	-26
8 Aug 2012 14:50	0.1700	273	14.2	0.016	18	48	156	-71
20 Aug 2012 12:43	0.7840	1529	18.3	0.071	17	105	762	-146
22 Aug 2012 13:28	1.0540	1970	17.3	0.097	36	74	483	-433
23 Aug 2012 9:00	0.2840	625	11.9	0.045	24	63	161	-88
4 Sep 2012 12:30	0.0160	90	12.2	0.006	67	133	2.9	-1.7
12 Sep 2012 8:51	0.0110	112	24.6	0.004	129	203	0.62	-0.95

APPENDIX 2: FLUME DESCRIPTION AND SEDIMENT TRANSPORT EQUATIONS

Appendix 2.1: Flume description

The width of the existing laboratory flume was reduced to 0.40 m to accommodate the sediment concentrations and the nominal capacity of the sediment feed system. The Froude scaling criterion (Hughes, 1993) and the length scale (estimated field flow width/flume width) were used to determine the design flow rates and grain sizes for each modeled event in the flume (Chapter 4: Table 2). The sediment flux for the five events was calculated from the field-estimated sediment concentration and the scaled flow rate (Chapter 4: Table 2). The minimum flow duration was established by scaling the estimated duration of each field event (2.6 to 11.6 min), but the actual durations were 14 to 20 min so that all the experimental data could be obtained during each event (Chapter 4: Table 2).

Sediment deposited during a post-fire runoff event in central Idaho was collected, screened, and used in the bed material and added to the flume supply water to attain the target incoming sediment concentrations. The screening process reduced the d_{50} of the sediment so that it more closely represented the scaled sediment sizes for the five events (Chapter 4: Table 2).

The flume width was reduced by installing a temporary plywood wall, which included a 19° angled reducing section between the head tank and the top of the test section. The plywood wall and reducing section were wrapped in polyvinylchloride sheet to simulate the roughness of the unmodified glass wall on the left side of the flume. A 0.5 m high headwall was installed at the entrance of the test section and a perforated 0.5 m tail wall was placed at the exit of the test section to contain the bed sediment. The resulting length of the test section was 11.4 m. A ramp was installed downstream of the test section to return the flow to the bed of the flume, and its slope was 29.5%. A layer of cobbles with median axes between 10 and

40 cm was placed on the metal floor of the flume, and extra cobbles were installed to a depth of 45 cm to armor the test-section entrance. The test section bed material was a blend of the screened post-fire sediment and 10 mm crushed gravel. Bed material was placed on top of the cobbles, sprayed with water to simulate a recent rainfall event, compacted to a bulk density of 1530 kg m^{-3} and 1750 kg m^{-3} in the control and treated channels, respectively, and shaped with a triangular screed with 10% side slopes. The bed was not modified during either five-event experimental sequence, but it was removed and re-built between the control and treated events.

The water supply for the flume was re-circulated from a settling pond and gravity fed from an elevated storage tank. The flow rate was controlled using a needle valve and an electromagnetic flow meter (McCrometer, Inc., Hemet, CA) on the outlet of the elevated tank. The sediment concentration of the incoming water (before the addition of sediment) was not controlled but never exceeded 1.2 g L^{-1}. The water temperature was 19°C for each event.

The screened post-fire sediment was air-dried and stored in two hoppers, and delivered to the test section using a series of conveyor belts. Depending on the sediment feed rate, one or both of the hoppers was used to supply sediment. A vibrating, Teflon coated sediment distributor was installed after the last conveyor to spread the sediment across the width of the test section. Sediment was added to the flow starting 2 to 2.1 min after runoff entered the flume, and the sediment feed continued until 0.5 min before the head tank refill pump was stopped. Water continued to flow into the test sections at low rates for several minutes after the refill pump was stopped as the water in the head tank drained down to the level of the headwall. The dry sediment feed rates ranged from 0.5 to 2.2 kg s^{-1} (Chapter 4: Table 2) and were calibrated to within +/- 0.1 kg s^{-1} prior to each event.

Twelve small straw bales (20 cm wide by 10 cm tall by 14 cm deep) were compacted and hand-tied from loose wheat straw. Three straw bale check dams, two bales wide (0.40 m) by two bales high (0.18 m), were installed with the upstream edges located at 3.95 m, 6.97 m, and 9.94 m from the entrance to the test section for the treated events. The dams were spaced to accommodate the estimated backwater lengths in the flume's channel (Napper, 2006; Samuels, 1989). The bales were placed on the bed surface and staked into the bed material using 13 mm diameter wooden dowels. Gaps between the bales and between the bales and walls of the flume were filled with rocks or wood, and the spillway for each dam was armored with 10 cm cobbles (Napper, 2006).

The slope of the flume was 8.5%, as this was near the maximum attainable using the sediment feed system and fell within the range of channel slopes observed in a field installation of straw bale check dams near the Hayman location (unpublished data). The bed slope decreased for the last four treated events, and for these events the slope was measured just upstream of the third check dam.

Appendix 2.2. Sediment transport equations

Notation:

Symbol	Meaning
A	Coefficient (Equation A.7)
C	Coefficient (Equation A.7)
d	Particle diameter (mm or m)
d_{gr}	Dimensionless grain diameter
d_{xx}	xx^{th} percentile particle size (mm or m)
d_{50}	Median particle size (mm or m)
D	Flow depth (m or cm)
F_{gr}	Dimensionless sediment mobility number
g	Gravitational acceleration (m s^{-2})
i_b	Submerged bed-load sediment transport rate (kg s^{-1} $m^{-1)}$
k	Coefficient (Equations A.7 and A.9)
K_s	Roughness coefficient ($m^{1/3}$ s^{-1})
K_r	Grain roughness ($m^{-1/6}$)
m	Coefficient (Equation A.7)
q	Unit discharge (m^2 s^{-1})
q_b	Bed-load sediment transport rate (kg s^{-1} m^{-1})
q_c	Critical unit discharge (m^2 s^{-1})
q_T	Total sediment transport rate (kg s^{-1} m^{-1})
Q	Discharge (m^3 s^{-1})
R	Hydraulic radius (m)
R_*	Shear Reynolds number
S	Slope (% or m m^{-1})
u^*	Shear velocity (m s^{-1})
V	Velocity (m s^{-1})
X	Sediment concentration, mass basis (kg kg^{-1})
α	Bed angle (°)
β	Angle of repose of the bed material (°)
γ	Specific weight of water (9795 N m^{-3})
γ_s	Specific weight of sediment (25997 N m^{-3})
θ	Dimensionless shear stress
θ_{cr}	Steep-slope non-dimensional critical shear stress
θ_{ocr}	Non-dimensional critical shear stress
ν	Kinematic viscosity (m^2 s^{-1})
ρ	Density of water (kg m^{-3})
ρ_s	Density of sediment (kg m^{-3})
τ	Shear stress (N m^{-2})
τ_c	Critical shear stress (N m^{-2})
ϕ	Non-dimensional sediment transport rate
ω	Stream power (kg m^{-3})
ω_0	Critical stream power (kg m^{-3})

Equations A.1–A.9 were derived from those described in Yang (2003).

Schoklitsch (1943):

$$q_b = 2500 S^{\frac{3}{2}} \left(q - q_c \right) \tag{A.1}$$

and

$$q_c = \frac{0.6 d_{50}^{\frac{3}{2}}}{S^{\frac{7}{6}}} \tag{A.2}$$

where q_b is bed-load transport (kg s^{-1} m^{-1}), S is channel gradient (m m^{-1}), q and q_c are unit discharge and critical unit discharge, respectively (m^2 s^{-1}), and d_{50} is the median grain sediment particle diameter (m).

Meyer-Peter and Müller (1948):

$$q_b = \left\{ 4 \rho^{-\frac{1}{3}} \left[\gamma \left(\frac{K_s}{K_r} \right)^{\frac{3}{2}} RS - 0.047 \left(\gamma_s - \gamma \right) d_{50} \right] \right\}^{\frac{3}{2}} \tag{A.3}$$

where q_b is the bed-load transport (Mg m^{-1} s^{-1}); ρ is the density of water (kg m^{-3}); γ and γ_s are the specific weights of water and sediment, respectively (kg m^{-2} s^{-2}). K_s is a roughness coefficient:

$$K_s = \left(\frac{V^2}{S R^{\frac{4}{3}}} \right)^{\frac{1}{2}} \tag{A.4}$$

where V is the flow velocity (m s^{-1}), R is the hydraulic radius (m), and S is the slope; and K_r is a grain roughness term:

$$K_r = \frac{26}{d_{90}^{\frac{1}{6}}} \tag{A.5}$$

where d_{90} is the 90th percentile sediment grain diameter (m).

Engelund and Hansen (1972):

$$q_T = 0.05\gamma_s V^2 \left[\frac{d_{50}}{g\left(\frac{\gamma_s}{\gamma}-1\right)}\right]^{\frac{1}{2}} \left[\frac{\tau}{(\gamma_s-\gamma)d_{50}}\right]^{\frac{3}{2}} \tag{A.6}$$

where q_T is total sediment transport (kg s^{-1} m^{-1}), and τ is the shear stress on the bed (kg s^{-2} m^{-1}).

Ackers and White (1973):

$$X = \frac{d}{D}\frac{\gamma_s}{\gamma}\left(\frac{u_*}{V}\right)^{-k} C\left(\frac{F_{gr}}{A}-1\right)^m \tag{A.7}$$

where X *is* total sediment concentration on a mass basis, (kg kg^{-1}), F_{gr} is the dimensionless sediment mobility number, A, C, k, and m are coefficients derived from graphical relationships (Yang, 2003: Fig. 6.6) related to the dimensionless grain diameter

$$d_{gr} = d_{50}\left[\frac{g\left(\gamma_s/\gamma-1\right)}{\nu^2}\right]^{\frac{1}{3}} \tag{A.8}$$

where ν is the kinematic viscosity (m^2 s^{-1}) and

$$F_{gr} = u_*^{\,k}\left[gd\left(\frac{\gamma_s}{\gamma}-1\right)\right]^{-\frac{1}{2}}\left[\frac{V}{\sqrt{32}\log\left(10\frac{D}{d}\right)}\right]^{1-k} \tag{A.9}$$

where u* is the shear velocity (m s^{-1}), g is gravitational acceleration (m s^{-2}), V is the velocity (m s^{-1}), and D is the flow depth (m).

Equations A.10–A.20 were derived from original sources.

Bagnold (1980):

$$i_b = (i_b)_* \left[\frac{\omega - \omega_0}{(\omega - \omega_0)_*} \right]^{\frac{3}{2}} \left(\frac{D}{D_*} \right)^{-\frac{2}{3}} \left(\frac{d_{50}}{d_{50*}} \right)^{-\frac{1}{2}} \tag{A.10}$$

where i_b is the submerged bed-load transport rate (kg s^{-1} m^{-1}) and we used d_{50} rather than the mode particle size. The stream power, ω (kg s^{-3}), is

$$\omega = \frac{\rho g Q S}{w} = \tau V \tag{A.11}$$

where ρ, g, w, τ, and V are defined above, w is the flow width (m), and Q is discharge (m^3 s^{-1}). The asterisks in Eq. A.10 indicate values derived from a point in the experiment, and we used values from the first control event.

Smart (1984):

$$\phi = 4 \left[\left(\frac{d_{90}}{d_{35}} \right)^{0.2} S^{0.6} \frac{V}{u_*} \theta^{0.5} (\theta - \theta_{cr}) \right] \tag{A.12}$$

and

$$q_{T=} \frac{\phi}{g \left(\frac{\rho_s}{\rho} - 1 \right) d_{50}} \tag{A.13}$$

where ϕ, θ, and θ_{cr} are the non-dimensional sediment transport rate, the non-dimensional shear stress, and the non-dimensional critical shear stress, respectively, and q_T is the total sediment transport rate (kg s^{-1} m^{-1}). We substituted d_{35} in place of the original d_{30}. The maximum value of our data (9.0) slightly exceeded the recommended upper limit of the ratio for non-uniform

sediment (8.5) (Smart, 1984). A steep-slope adjustment to the critical shear stress was used to calculate the non-dimensional critical shear stress (Smart, 1984),

$$\theta_{cr} = \theta_{ocr} \cos\alpha \left(1 - \frac{\tan\alpha}{\tan\beta} \right) \tag{A.14}$$

where θ_{cr} is the steep-slope non-dimensional critical shear stress, α is the bed angle in degrees and β is the angle of repose of the material (we used a value of 33°), and θ_{ocr} is the non-dimensional critical shear stress calculated from equations developed to approximate the Shields critical shear stress (Cao et al., 2006):

$$\theta_{ocr} = 0.1096 R_*^{-0.2607} \quad \text{for } R_* < 2 \tag{A.15}$$

$$\theta_{ocr} = e^{\left(-\ln R_* + 0.5003 \ln\left[1 + (0.1359 R_*)^{2.5795}\right] - 1.7148\right)} \quad \text{for } 2 < R_* < 6 \tag{A.16}$$

$$\theta_{ocr} = 0.045 \quad \text{for } R_* > 60 \tag{A.17}$$

where R_* is the shear Reynolds number

$$R_* = \frac{(gRS)^{\frac{1}{2}} d_{50}}{\nu} \tag{A.18}$$

where g, R, S, d_{50}, and ν are defined above.

Cohen et al. (2010):

$$q_b = -1.175 + 0.132\tau \tag{A.19}$$

$$q_b = -0.255 + 0.132(\tau - \tau_c) \tag{A.20}$$

where q_b is bed-load transport rate (kg $s^{-1}m^{-1}$), τ is the shear stress (N m^{-2}), and τ_c is the critical shear stress (N m^{-2}), which was calculated using Cao et al.'s (2006) approach.

References

Bagnold RA. 1980. An empirical correlation of bedload transport rates in flumes and natural rivers. Proceedings of the Royal Society of London A: Mathematical, Physical and Engineering Sciences **372** : 453–473. DOI: 10.1098/rspa.1980.0122

Cao Z, Pender G, Meng J. 2006. Explicit formulation of the Shields diagram for incipient motion of sediment. Journal of Hydraulic Engineering **132** : 1097–1099.

Cohen H, Laronne JB, Reid I. 2010. Simplicity and complexity of bed load response during flash floods in a gravel bed ephemeral river: A 10 year field study. Water Resources Research **46** : 1–14. DOI: 10.1029/2010WR009160

Hughes SA. 1993. *Physical Models and Laboratory Techniques in Coastal Engineering*. World Scientific Publishing Co, Hackensack, New Jersey

Napper C. 2006. *Burned Area Emergency Response Treatments Catalog*. *Watershed, Soil, and Air Management*, USDA Forest Service, National Technology & Development Program, Washington, D.C., 214

Samuels PG. 1989. "Backwater lengths in rivers." Proceedings of the Institution of Civil Engineers, **87**, 571–582

Smart GM. 1984. Sediment transport formula for steep channels. Journal of Hydraulic Engineering **110** : 267–276. DOI: 10.1061/(ASCE)0733-9429(1984)110:3(267)

Yang CT. 2003. Sediment transport: Theory and practice . Krieger Publishing Co.: Malabar, Florida